WELL-TESTING METHODOLOGIES FOR CHARACTERIZING HETEROGENEITIES IN ALLUVIAL-AQUIFER SYSTEMS: FIRST YEAR (8/1/91 - 7/31/92) REPORT

A research project of the
Water Resources Research Program
United States Department of the Interior
Geological Survey

by

James J. Butler, Jr. and Carl D. McElwee
Kansas Geological Survey
The University of Kansas

with

Geoffrey C. Bohling, Zafar Hyder, Wenzhi Liu,
Christine M. Mennicke, and Michael D. Orcutt
Kansas Geological Survey
The University of Kansas

December, 1992

Research supported by the U.S. Geological Survey (USGS), Department of the Interior, under USGS award number 14-08-0001-G2093. The views and conclusions contained in this document are those of the authors and should not be interpreted as necessarily representing the official policies, either expressed or implied, of the U.S. Government.

ABSTRACT

A considerable amount of research on the mechanisms of large-scale solute transport has identified the spatial distribution of hydraulic conductivity as a significant factor in determining how a plume of a conservative tracer will move in the subsurface. This report summarizes the work of the first year of a three-year research project whose objective is to assess the potential of well-testing technology for providing accurate estimates of spatial variations in hydraulic conductivity. The major thrust of the first year of this project was on the use of slug tests to describe aquifer heterogeneities. The theoretical components of this effort included the development of a time-continuous numerical model for the analysis of well-test data, an assessment of the viability of multilevel slug tests in layered aquifers, an investigation of the usefulness of observation wells in slug tests, and a study of the effective properties obtained from the analysis of slug tests performed in wells with skins of a finite radius. The field components of this work emphasized multilevel slug tests. A prototype multilevel slug-test system was tested. Test results indicated that the slug-test responses were being affected by mechanisms not accounted for in the conventional theory. A series of experiments were performed to identify the mechanisms producing the observed behavior. These experiments served as the basis for the development of new nonlinear models for the analysis of slug-test data. Additional work performed in year one included further drilling and sampling activities, modification of the KGS bladder sampler, and laboratory analysis of sampled cores.

TABLE OF CONTENTS

I. INTRODUCTION

A. RESEARCH OBJECTIVES

Over the last decade, a considerable amount of theoretical, laboratory, and field research on the mechanisms of large-scale solute transport has identified the spatial distribution of hydraulic conductivity as a significant factor in determining how a plume of a conservative tracer will move in the subsurface (e.g., Freyberg, 1986; Gelhar, 1986; Dagan, 1986; Moltyaner and Killey, 1988). Many researchers now recognize (e.g., Molz et al., 1989) that if we are to improve our predictive capabilities for subsurface transport, we must first improve our capabilities for measuring and describing conditions in the subsurface. The measurement of hydraulic conductivity in the subsurface on a scale of relevance for contaminant transport investigations, however, has proven to be a rather difficult task. Recent work at the Kansas Geological Survey and elsewhere (e.g., Streltsova, 1988; Butler and Liu, in press) has shown that conventional pumping tests provide large-scale volumetric averages of hydraulic conductivity that may be of rather limited use in transport investigations. Although multiwell tracer tests can provide information on the average interwell conductivity, these tests are rather expensive in terms of time, money, and effort. Other techniques are needed if information on conductivity variations is to be used by practicing hydrogeologists outside of the research community. The specific objective of the research described in this report is to assess the potential of advanced well-testing technology for providing more accurate estimates of spatial variations in the physical properties that control contaminant plume movement in saturated porous media. Although effective porosity is clearly an important consideration, the major emphasis of this work is on characterizing spatial variations (heterogeneities) in hydraulic conductivity.

Ideally, heterogeneities in hydraulic conductivity must be studied and characterized at several different scales in order to understand their influence on the movement of a contaminant plume. Although theoretical modeling work is an important element of any study of the influence of spatial variations in hydraulic conductivity on contaminant movement, a rigorous study of this subject must have a major field component. A field site, at which researchers at the University of Kansas can pursue work on characterizing spatial variations in aquifer properties, has been established as part of this research. The specific site of the field effort is the Geohydrologic Experimental and Monitoring Site (GEMS), which is located just north of Lawrence, Kansas on land owned by the University of Kansas Endowment

Association. Figure I.1 is a map showing the general location of GEMS and some of the major features at the site. GEMS overlies approximately 21.3 meters (70 ft) of Kansas River valley alluvium. These recent unconsolidated sediments overlie and are adjacent to materials of Pleistocene and Pennsylvanian age. A cross-sectional view of the subsurface at one of the well nests at GEMS is shown in Figure I.2. The alluvial facies assemblage at this site consists of approximately 10.6 meters (35 ft) of clay and silt overlying 10.6 meters (35 ft) of sand and gravel. The stratigraphy is a complex system of stream-channel sand and overbank deposits. The general nature of the stratigraphy would lead one to expect that a considerable degree of lateral and vertical heterogeneity in hydraulic conductivity would be found in the subsurface at GEMS. Although analyses of sampled cores do indicate considerable variability in hydraulic conductivity within the sand and gravel interval at GEMS, it is unclear how the variability at the small scale of a core translates into variability at larger scales.

In the first year of this research, the focus of the work was on the use of slug tests to describe spatial variations in hydraulic conductivity. A theoretical and field examination of the potential of multilevel slug tests for providing detailed information about conductivity variations in the vertical comprises the majority of the work in this period. However, a considerable amount of additional work was directed at increasing our knowledge of the subsurface at GEMS. This effort involved continued drilling and sampling of the alluvium, and laboratory analysis of sampled cores. These characterization efforts are directed at providing the detailed information that will allow us to better assess the quality of the estimates provided by the various well-testing approaches evaluated in this work. The ultimate goal of these characterization efforts is to describe the site in so much detail that it effectively becomes an underground laboratory at which new technology can be evaluated.

B. BRIEF OUTLINE OF REPORT

The remainder of this report is divided into four major sections, each of which is essentially a self-contained unit. Although pages are numbered consecutively throughout the report, figures, tables, and equations are labelled by section and, when warranted, subsection for the convenience of the reader.

The first section describes theoretical work directed at developing a better understanding of the information that can be obtained from slug tests in heterogeneous aquifers. A continuous-in-time numerical model, which has proven very useful for the analysis of well-test data, is first introduced. This model is then

used in a detailed study of slug tests in layered aquifers. Although the use of slug tests to describe vertical variations in hydraulic conductivity was a major focus of this study, some effort was also directed at the use of slug tests to assess lateral variations in hydraulic properties. The last two subsections of this section describe initial efforts to assess the usefulness of slug tests with observation wells and to study effective properties obtained from slug tests performed at a well with a skin. Note that these latter two subsections depend heavily on the principles of sensitivity analysis, which are introduced in Appendix B of this report.

The second section primarily describes field investigations of multilevel slug tests. A prototype multilevel slug test system, which has been developed at the KGS, is described and its use at GEMS is detailed. An extensive series of field experiments that were undertaken in order to understand the causes of anomalous behavior observed in slug-test data from wells in the sand and gravel section at GEMS are then described. The section concludes with the derivation of new models, which accounts for some of the mechanisms affecting the GEMS slug-test data, and a discussion of the applicability of these models to the GEMS data.

The third section primarily describes activities directed at increasing our knowledge of the subsurface at GEMS. Drilling and sampling activities that occurred over the last year at GEM are described in some detail. The analysis of the core samples obtained in the drilling is then described. Modifications to the procedures employed in the KGS core measurement laboratory are discussed and the results of the analyses performed in the first year of this project are reported.

The fourth section summarizes the report and briefly outlines the work planned for the second year of this project.

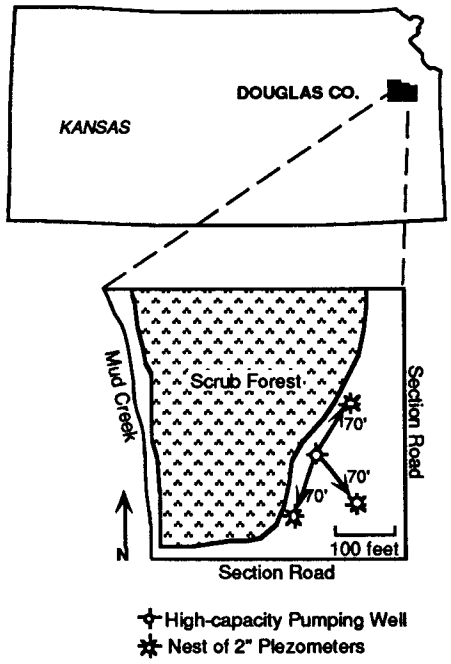

Figure I.1. - Location map for the Geohydrologic Experimental and Monitoring Site (GEMS).

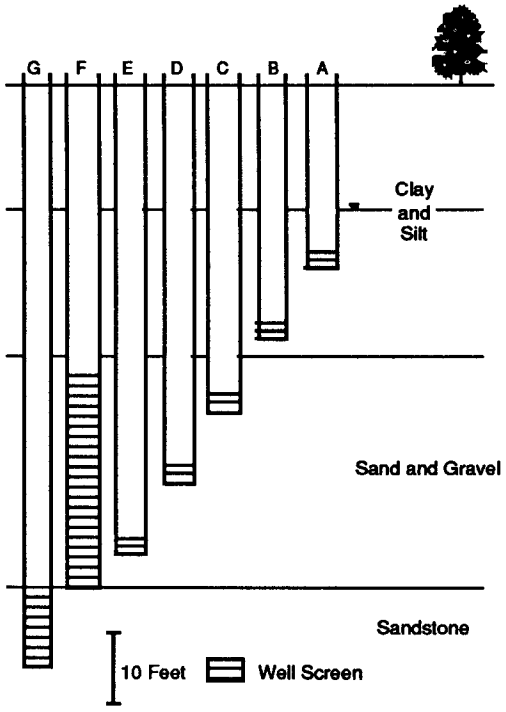

Figure I.2. Cross-sectional view of a well nestt at GEMS. Wells A-E are screened for .8 meters (2.5 ft.), well F is screened for 9.1 meters (30 ft.), and well G is screened for 1.5 meters (5 ft.).

II. THEORETICAL INVESTIGATIONS OF SLUG TESTS IN HETEROGENEOUS MEDIA

A. A CONTINUOUS-IN-TIME NUMERICAL MODEL FOR THE ANALYSIS OF WELL TESTS IN THREE-DIMENSIONAL NONUNIFORN AQUIFERS

Introduction

Analytical solutions for drawdown in response to a pressure disturbance induced at a central well are the basis of conventional well-test analysis methodology. For the most part, these solutions consider hydraulic behavior in an idealized aquifer in which flow properties are invariant in space. Aquifers in nature, however, are characterized by a considerable degree of spatial variations (heterogeneities) in flow properties. Not surprisingly, analyses based on solutions to flow in idealized uniform systems may be of limited use in assessing heterogeneities in the vicinity of the stressed well. A better understanding of these near-well heterogeneities, however, is critical if we are to improve our ability to predict the transport of contaminants in the subsurface. A component of the research in the first year of this project was therefore directed at further exploration of a numerical modeling approach that would allow the actual complexity of the geological system to be incorporated into the analysis of well-test data. This approach could then serve as a tool for both the development of insight into the role of heterogeneity in controlling well-test responses and the analysis of well tests in succeeding years of this project.

A general model for well-test analysis must allow the actual complexity of the geologic formation to be represented in the full three dimensions. Analytical solutions for well tests in simplified three-dimensional settings have been developed by a number of authors using traditional integral transform techniques (e.g., Russell and Prats, 1962; Papadopulos, 1966; Prijambodo et al., 1985; Hayashi et al., 1987; Raghavan, 1989; McElwee et al., 1990). Because of the complexities introduced by the vertical component of flow at the stressed well and within the aquifer itself, however, an exact analytical solution has yet to be derived for the general case of well testing in a three-dimensional nonuniform system. Given the limitations of the traditional analytical solution methodology, a new approach for the analysis of well-test data is considered in this work. The approach considered here is based on the idea of combining the spatial discretization used in a conventional numerical model with the Laplace transform in time used in conventional analytical models. A solution to this hybrid numerical model is obtained in Laplace space using standard

techniques of matrix algebra. A set of solutions in Laplace space is then back transformed to real space, producing a solution in real space that can be formulated in a continuous manner over a range of times. In the following discussion, the theoretical basis of this approach is explored and its implementation in this work is described.

A Time-Continuous Numerical Method

Approximate numerical methods such as the finite difference (FE) or finite element (FE) approaches have been widely used in groundwater studies for applications where analytical solutions are not feasible. These numerical approaches involve both spatial and temporal discretization of the governing equations, with the quality of the approximation dependent on the discretization strategy. The size of the time increment is often varied during the course of a simulation in order to improve computational efficiency. However, limitations on the magnitude of the initial time step and the size of the time-step acceleration factor can result in a large number of time steps being required even in cases when model output is only desired at a few points in time. In addition, if the rate of pumpage changes significantly, as in a simulation of a step-drawdown test, the time-stepping scheme must be reset to its initial values with the change in pumping rate in order to accurately simulate the system response to the new stress. Selection of the proper time increment may also present difficulties when model output is required for comparison with measured data at particular points in time. In many standard groundwater flow and transport models, it may be rather difficult to obtain a comparison between model output and measured data for the specific times at which the measurements were taken.

In order to avoid some of the problems associated with temporal discretization, a hybrid method, which combines spatial discretization with a Laplace transform in time, is employed here. The spatial discretization scheme is the same as that in a conventional finite-difference model. The resultant spatially discretized system of algebraic equations in complex space is solved using complex arithmetic for the matrix inversion. The Laplace-space solution is then inverted back into real space using an appropriate numerical inversion scheme. This procedure yields a solution that is continuous over a range of times, with the only approximation in the temporal domain being that introduced by the numerical inversion scheme.

This time-continuous method has been employed by a number of workers during the past two decades (e.g., Gurtin, 1965; Javandel and Witherspoon, 1968; Chen and Chen, 1988; Sudicky, 1989; Moridis and Reddell, 1991; Sudicky and

McLaren, 1992; Li et al., 1992). The most difficult problem associated with this method has been the inversion of the Laplace-space solution back into real space. Various methods for approximate numerical inversion, all of which involve the evaluation and summation of the transform-space function, have been developed by a number of authors (e.g., Stehfest, 1970; Crump, 1976; Talbot, 1979). One focus of the research of this project is the development of a more efficient inversion algorithm. As noted by Sudicky (1989), De Hoog et al. (1982) propose a quotient difference algorithm for increasing the rate of convergence of the summation-series approach of Crump (1976). This quotient-difference algorithm has been shown to have a significant computational advantage over other algorithms in decreasing the computations required for the analysis of well-test data (Liu and Butler, 1991). The computational savings are such that this method appears to hold considerable promise for use as a practical tool for analysis of well tests in fully three-dimensional systems. The following section describes an implementation of this method in a discrete-in-space, continuous-in-time model that has been developed for the analysis of well tests in systems where conventional analytical approaches are not viable.

The Three-Dimensional Finite Difference Time-continuous Model (3DFDTC)

The time-continuous approach can be used only if Laplace transforms exist for the governing equation together with all boundary and initial conditions. Thus, the approach described here only strictly applies to confined flow systems. The cylindrical-coordinate form of the governing equation for three-dimensional flow in a confined system is

$$\frac{1}{r}\frac{\partial}{\partial r}\left(rK_r\frac{\partial h}{\partial r}\right) + \frac{1}{r^2}\frac{\partial}{\partial \theta}\left(K_\theta\frac{\partial h}{\partial \theta}\right) + \frac{\partial}{\partial z}\left(K_z\frac{\partial h}{\partial z}\right) = S_s\frac{\partial h}{\partial t} \qquad \text{(II.A.1)}$$

where

h = drawdown, [L];

S_s = specific yield, [1/L];

K_r, K_θ, K_z = hydraulic conductivity in the radial, angular, and vertical direction, respectively, [L/T];

t = time, [T];

r = radial direction, [L];

θ = angular position, in radians;

z = vertical depth from the top of the aquifer, [L].

For the case of a pumping test in a layered aquifer, the initial and boundary conditions are defined as

$$h(r,0) = h_a,\ r < \infty \qquad \text{(II.A.2)}$$

$$h(\infty, t) = h_a,\ t \geq 0 \qquad \text{(II.A.3)}$$

$$2\pi \sum_{j=1}^{J} K_{rj} m_j \left(r \frac{\partial h}{\partial r} \right)_{r=r_w} = -\sum_{i=1}^{NP} q_i \square_i(t) \qquad \text{(II.A.4)}$$

where

$$\square_i(t) = \text{box car function} = \begin{cases} 1, & \text{if } t_{1i} \leq t \leq t_{2i},\ i = 1, 2, \cdots, NP \\ 0, & \text{elsewhere} \end{cases}$$

h_a = initial head in the aquifer, [L];
NP = number of pumping periods;
t_{1i} = starting time for pumping period i, [T];
t_{2i} = ending time for pumping period i, [T];
r_w = radius of pumping well, [L];
q_i = pumpage for pumping period i, [L^3/T];
J = total number of screened layers in the well bore;
K_{rj} = conductivity in radial direction for layer j;
m_j = depth of layer j.

The application of the Laplace transformation to equations (II.A.1) and (II.A.4), in conjunction with (II.A.2), results in:

$$\frac{1}{r}\frac{\partial}{\partial r}\left(rK_r\frac{\partial \bar{h}}{\partial r}\right) + \frac{1}{r^2}\frac{\partial}{\partial \theta}\left(K_\theta\frac{\partial \bar{h}}{\partial \theta}\right) + \frac{\partial}{\partial z}\left(K_z\frac{\partial \bar{h}}{\partial z}\right) = S_s(\bar{h}p - h_a) \qquad \text{(II.A.5)}$$

$$2\pi \sum_{j=1}^{J} K_{rj} m_j \left(r \frac{\partial \bar{h}}{\partial r} \right)_{r=r_w} = -\sum_{i=1}^{NP} q_i \frac{e^{-t_{1i}p} - e^{-t_{2i}p}}{p} \qquad \text{(II.A.6)}$$

where

p = Laplace transform variable;

$\bar{h}$ = head in Laplace space.

In order to improve the ease of radial discretization, the derivatives in the radial direction can be rewritten in a logarithmic form using the transformation $\tilde{r}=\log_e(r/r_w)$. This approach allows a discretization in the radial direction which increases exponentially when using a constant $\Delta\tilde{r}$. Thus, the form of equations (II.A.5) and (II.A.6) employed for the discretization is

$$\frac{1}{r^2}\frac{\partial}{\partial\tilde{r}}\left(K_r\frac{\partial\bar{h}}{\partial\tilde{r}}\right)+\frac{1}{r^2}\frac{\partial}{\partial\theta}\left(K_\theta\frac{\partial\bar{h}}{\partial\theta}\right)+\frac{\partial}{\partial z}\left(K_z\frac{\partial\bar{h}}{\partial z}\right)=S_s(\bar{h}p-h_a) \qquad \text{(II.A.7)}$$

$$2\pi\sum_{j=1}^{J}K_{rj}m_j\left(\frac{\partial\bar{h}}{\partial\tilde{r}}\right)_{\tilde{r}=0}=-\sum_{i=1}^{NP}q_i\frac{e^{-t_{1i}p}-e^{-t_{2i}p}}{p} \qquad \text{(II.A.8)}$$

Unlike many analytical and numerical models, which assume the radius of the well to be infinitely small, the model developed here allows the influence of well bore storage to be taken into consideration. As noted by Papadopulos and Cooper (1967), effects of well-bore storage on drawdown can be significant during early times when the majority of the water is being removed from storage inside the well bore. As time increases, the influence of well-bore storage will gradually diminish, eventually reaching a point at which the infinitely small well-bore assumption is viable.

The implementation of the well-bore storage option in the three-dimensional finite difference, time-continuous model (3DFDTC) is based on earlier work of Settari and Aziz (1974), Rushton and Chan (1977), and Butler (1986). As described by Butler (1986), the approach is based on rewriting the classical pipe flow equation (Vennard and Street, 1975) in a Darcy Law-like formulation and defining a term (involving the friction factor, the cross-sectional area of the well bore, and distance along the well bore) analogous to hydraulic conductivity. This approach allows flow inside the well bore to be governed by the porous media flow equation given by (II.A.7). Note that the initial implementation of this approach for this project produces an approximation of well-bore behavior that is equivalent to the hydrostatic head assumption employed in most analytical representations of the well bore (e.g., Papadopulos and Cooper, 1967; Cooper et al., 1967).

In the three-dimensional representation employed here, the portion of the well

bore passing through the modelled unit consists of several grid cells in the vertical. The storage coefficient is assumed to be one for the top cell of the well bore, while the storage coefficients for the remaining nodes in the well bore are set equal to the compressibility of water or zero (assuming water is incompressible). Since the radial-discretization scheme employed in the model uses logarithmic increments, the radial location (r_{min}) of the first node inside the well bore must be larger than zero (i.e. $0.0 < r_{min} < r_w$). This produces a well bore in the shape of an annular ring rather than a circle. The storage coefficient of the well-bore cells must therefore be adjusted (by a factor of $r_w^2/(r_w^2-r_{min}^2)$) to account for the decrease in well-bore cross-sectional area produced by the annular ring representation of the well bore. In addition, the traditional boundary condition at the well bore (II.A.8), which is based on the definition of radial flow along the well screen, is not used in this approach. Instead, a boundary condition at the top node of the well bore, in which the total flow out of the screened portion of the well is defined, is employed. This flow boundary condition is written as

$$2\pi K_{rJ} m_J \left(\frac{\partial h}{\partial \tilde{r}}\right)_{\tilde{r}=\log_e(\frac{r_{min}}{r_w})} = -\sum_{i=1}^{NP} q_i \frac{e^{-t_{1i}p} - e^{t_{2i}p}}{p} \qquad \text{(II.A.9)}$$

where m_J is the height of the top grid cell. Note that no-flow conditions in the radial direction are assumed at $r=r_{min}$ for the remaining nodes in the well bore. The use of (II.A.9) as a boundary condition makes this approach very appropriate for analyzing well tests in layered systems where the test well may be screened in more than one layer (as in (II.A.4) with J>1). Instead of having to define in advance the amount of water withdrawn from each layer, the model will implicitly calculate the flow out of each layer given the total flow out of the system defined by (II.A.9).

Since the representation of the well bore employed here is equivalent to the conventional hydrostatic head assumption, the hydraulic conductivity of the well bore must be defined such that the heads for all the nodes in the well bore are approximately equal. All three components of well-bore hydraulic conductivity must be at least four orders of magnitude larger than the aquifer conductivity in order to ensure negligible head loss along the well bore. In order to ensure that the majority of water will be drawn from the well bore at early times, the ratio of vertical well-bore hydraulic conductivity over its angular and radial counterparts must be large. An extensive set of experiments indicates that a ratio larger than 100 will ensure that all water will initially be drawn out of well-bore storage.

The 3DFDTC model is developed by applying a conventional central difference scheme to (II.A.7), which now represents conditions within both the aquifer and the well bore. After incorporating (II.A.9) and the Laplace transform of (II.A.3) into the finite difference scheme, the system of algebraic equations for 3DFDTC can be expressed in matrix form as

$$([A] + p[B])[\bar{h}] = -[C]\,h_a + \sum_{i=1}^{NP} q_i \frac{e^{-t_{1i}p} - e^{-t_{2i}p}}{p}[D] \qquad \text{(II.A.10)}$$

where A, B, C, and D are matrices of constant coefficients and $\bar{h}$ is a vector of unknown heads. For the sake of conciseness, (II.A.10) is rewritten in the following form:

$$[G]\,[\bar{h}] = [W] \qquad \text{(II.A.11)}$$

Both the left-hand side coefficient matrix G and the right-hand side matrix W of (II.A.11) involve the Laplace variable p, for which a value must be given before a solution in Laplace space can be obtained. The resultant solution in Laplace space can then be inverted back into real space using numerical inversion schemes such as those of Stehfest (1970) or Crump (1976). A detailed discussion of inversion algorithms with an emphasis on the method of Crump (1976) can be found in Appendix A.

The Crump algorithm approximates the inversion of a Laplace space function by means of a Fourier series that involves both sine and cosine functions. This method has a smaller error than that of a similar method presented by Dubner and Abate (1968). If the value of h at node j is desired, h_j is found using the following equation developed by Crump [1976]:

$$h_j(t) \approx \frac{e^{p_0 t}}{Tmax}\left\{\frac{\overline{h_j}(p_0)}{2} + \sum_{k=1}^{2N+1}\left[RE(\overline{h_j}(p_k))\cos\left(\frac{k\pi t}{Tmax}\right) - IM(\overline{h_j}(p_k))\sin\left(\frac{k\pi t}{Tmax}\right)\right]\right\} \qquad \text{(II.A.12)}$$

where

$\bar{h}_j(p_k)$ = solution from (II.A.11) at node j for $p = p_k$;

2Tmax = the period of the Fourier series approximating the inverse function on the interval [0, 2Tmax];

RE($\bar{h}$) = real part of $\bar{h}$;

IM($\bar{h}$) = imaginary part of $\bar{h}$;

Er = minimum relative error;

$p_k = p_0 + ik\pi/Tmax$;

$p_0 = \mu - \ln(Er/2Tmax)$, the real part of p_k;

μ = maximum real value of all the singularity points of the function in Laplace space;

$i = (-1)^{1/2}$.

Equation (II.A.12) shows that the time variable t appears only in the sine, cosine, and exponential functions. Since p_k is independent of time, we can perform the inversion over a range of times based on one set of solutions of $\bar{h}$ for one specific Tmax. The solution is thus continuous in time because once a set of $\bar{h}$ values is calculated from (II.A.11), (II.A.12) will give the desired result at any time within the range of [0, 2Tmax].

If the summation is performed as in (II.A.12), hundreds of terms (i.e. solutions of (II.A.11)) may be needed in order to obtain a solution that satisfies a given convergence criterion. Since the computational effort required for the calculation of each p-space solution of (II.A.11) is at least equal to that required for one time step in a conventional numerical model, considerable attention is paid to the convergence of the summation series given in (II.A.12). An algorithm developed by De Hoog et al. (1982) has been found to significantly accelerate the convergence of the summation series and has therefore been incorporated into the 3DFDTC model. The acceleration of the summation series is great enough that the continuous-in-time approach may often be the most computationally efficient approach for the analysis of well tests in heterogeneous formations. A detailed explanation of the De Hoog algorithm is given in Appendix A. Note that each of the solutions of (II.A.11) is independent of all the others. Thus, this approach has considerable potential for use with parallel-processing computer systems.

Discussion and Model Validation

The 3DFDTC model is considerably more flexible than its conventional analytical or numerical counterparts. Since no time-discretization scheme is employed, stability issues related to the time-stepping scheme can be ignored and a solution can be obtained directly for any specific time. Boundary conditions can also

be changed easily to adapt to different patterns of stress being placed on the test well. For example, by simply setting q_i=0.0 and changing h_a to H_0 in (II.A.10) for nodes located inside the well bore, 3DFDTC can be used to simulate a slug test with an initial head of H_0. If necessary, partial penetration and well skin effects can be accounted for by specifying the vertical position of the well screen and the radius of the skin, respectively. If there exists a symmetry in heads in either the angular or vertical direction, 3DFDTC will simulate only part of the aquifer system by assuming a no-flow condition along the plane of symmetry. Note also that 3DFDTC can be used in a one- or two-dimensional mode if heads can be assumed equal in the angular and/or vertical directions. In such cases, only one node should be used in the direction of equal heads.

In order to validate the implementation of the time-continuous approach and the well-bore approximation, 3DFDTC has been checked against many analytical solutions for both pumping and slug tests. In all cases, a comparison between the analytical results and those of 3DFDTC revealed very small differences. Four typical examples are chosen here to demonstrate the viability of the 3DFDTC model.

The first example was designed to assess the viability of the well-bore approximation employed in the model. Drawdown produced by pumping at a constant rate from a well of finite radius in a uniform aquifer is simulated. In Figure II.A.1, the simulated results for drawdown within the pumping well are compared with the analytical results of Papadopulos and Cooper (1967) for the same case. The results produced by the two approaches essentially fall on top of one another throughout the duration of the simulation. The small difference in the computed drawdown is attributed mainly to the error caused by the spatial discretization scheme employed in 3DFDTC. Further simulations have shown that by increasing the number of nodes in the radial direction, the difference between the analytical and 3DFDTC results will gradually disappear. Note that in addition to the two curves depicting well-bore storage effects, a third curve, depicting drawdown calculated by 3DFDTC when well-bore storage effects are not included, is plotted on Figure II.A.1 to illustrate the period when well-bore storage effects are important.

In the initial phases of this project, there was considerable concern about numerical problems that might accompany the well-bore approximation as a result of the dramatic change in hydraulic conductivities between the aquifer and the well bore that is required by the approach. The second example is thus chosen to illustrate the performance of 3DFDTC when adjacent hydraulic conductivities differ by many orders of magnitude. A slug test in a well surrounded by a low permeability

well skin of finite radius was simulated in order to assess model performance when a permeability contrast of ten orders of magnitude is employed. The configuration consisted of three distinct zones of differing properties: a very high permeability well bore ($K=10^7$), a low permeability skin ($K=10^{-3}$), and an aquifer of moderate permeability ($K=1$). The well was assumed screened throughout the aquifer. Figure II.A.2 illustrates a comparison of the heads simulated by 3DFDTC with the results from the analytical solution of Moench and Hsieh (1985) for a slug test in a well with a skin of finite radius. The solid line in Figure II.A.2 depicts the head at the slugged well simulated by 3DFDTC, while the dashed line displays the results of the analytical solution. As with Figure II.A.1, the two lines essentially fall on top of one another. The differences between the two curves are again mainly due to the error introduced by spatial discretization, since only a total of six nodes are placed inside the well bore and the skin.

The third example is selected to illustrate model performance when there is a strong component of vertical flow, such as might occur in multilevel slug tests. A slug test is simulated in a well that is screened for only a portion of the aquifer thickness. The aquifer is assumed to be homogeneous and isotropic with respect to flow properties. Figure II.A.3 displays a comparison of the normalized head (H/H_0) simulated by 3DFDTC with the results of the analytical solution of McElwee et al. (1990) for a slug test in a well partially penetrating the aquifer. The solid line in Figure II.A.3 depicts the head at the slugged well simulated by 3DFDTC, while the dashed line displays the results of the analytical solution. The inset provides details of the specific configuration employed for this example. As with the previous examples, 3DFDTC yields results that are essentially indistinguishable from those of the analytical solution.

The final example is selected to illustrate the advantages of this model when dealing with variable pumping rates. Figure II.A.4 includes a plot of pumping rate versus time for a well test performed by the Kansas Geological Survey in 1992 in Stanton County, Kansas. This test, which was plagued by malfunctioning generators, would be rather difficult to analyze using a conventional numerical model because of the need to refine the time-stepping scheme each time the pumping rate changed. The continuous-in-time approach is very convenient in this case, however, since the full detail of the rate variations can easily be incorporated in (II.A.9). In order to demonstrate the viability of this approach for the variable-rate pumping case, a comparison was performed between a variable-rate form of the solution of Theis (1935) and 3DFDTC. Figure II.A.4 includes the results of this comparison.

3DFDTC yields results that are quite close to those of the analytical solution. The reasons for the differences that are observed are presently the focus of additional study. Note that 17,755 different pumping rates were used in 3DFDTC for this example, allowing the pumping-rate history in all of its detail to be incorporated into the model. The inclusion of a very detailed pumping-rate history into the model may not greatly add to the total time of computation. In principle, only an increased number of terms in the summation of (II.A.10) is required. However, these initial results indicate that if the rate variations are particularly dramatic, additional terms in the summation of (II.A.12) may also be required. In order to be computationally competitive with the time-continuous approach, a conventional numerical model would have to approximate the variable-rate pumping rate with a small number of constant-rate steps, thereby introducing considerable error into the analysis.

Given the closeness of the match between the simulation results from 3DFDTC and those from the analytical solutions, it is clear that 3DFDTC can be a very useful tool for the design and analysis of well tests performed under conditions not readily represented by conventional analytical approaches. Therefore, in the following subsection of this report, 3DFDTC is used to examine the viability of multilevel slug tests in layered systems. The purpose of this numerical examination of multilevel slug tests in layered systems is to gain insight into how such tests might be designed in order to get more accurate information concerning vertical variations in the flow properties of a unit.

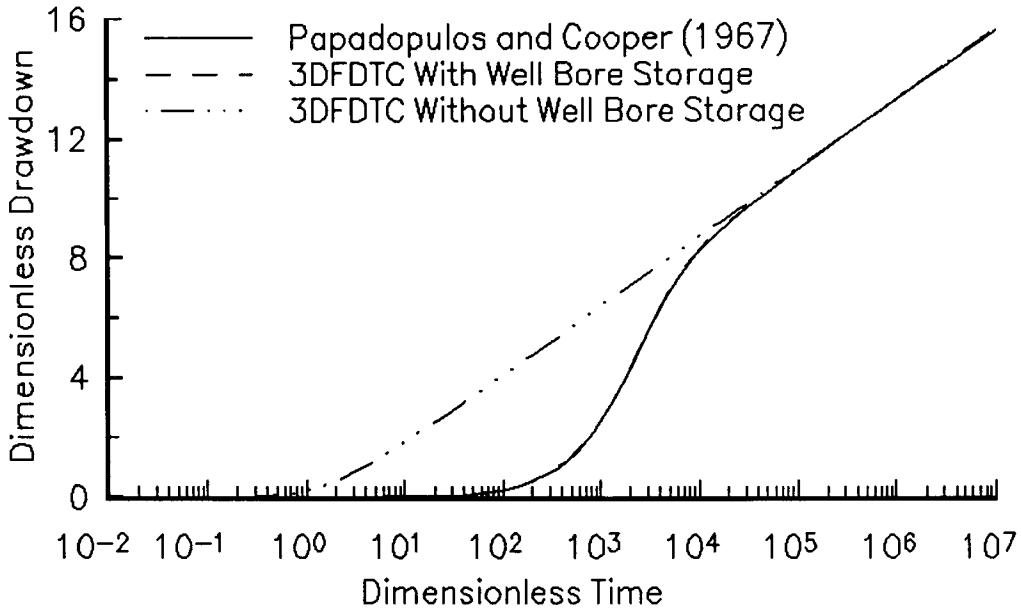

Figure II.A.1 Dimensionless drawdown ($4\pi Ts/Q$) versus time ($4Tt/Sr^2$) plot comparing the Papadopulos and Cooper (1967) solution with 3DFDTC results. (Observation well is located at r=4.6; r_w=0.167, T=1 and S=10^{-5}; 3DFDTC discretization: 3 radial nodes inside well bore, 39 nodes in the radial from r_w to 37364.15 meters and 5 nodes in vertical).

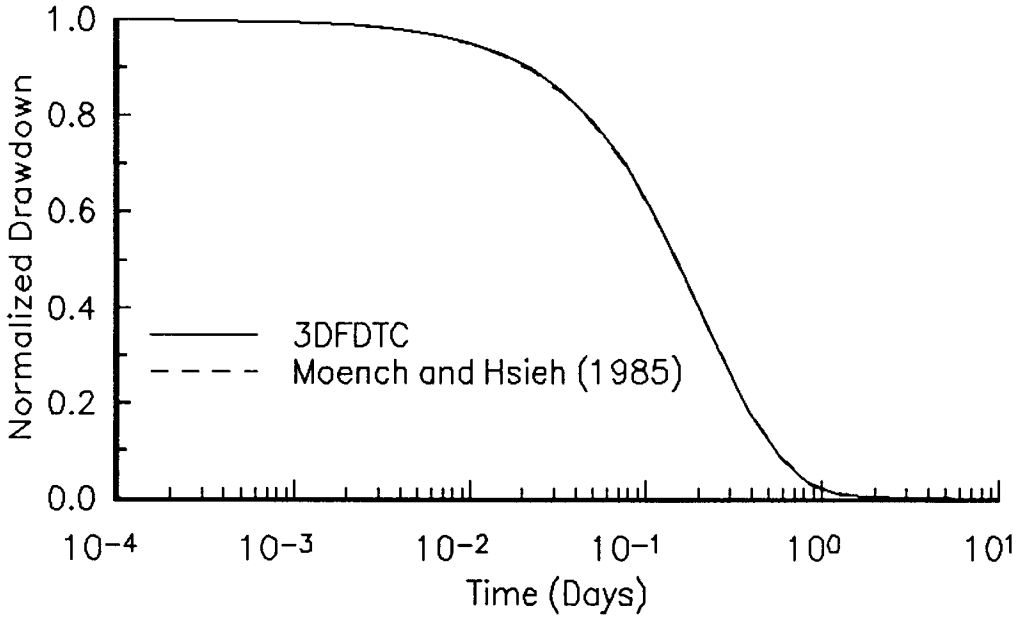

Figure II.A.2 Normalized drawdown (H/H_0) versus time plot comparing Moench and Hsieh (1985) solution with 3DFDTC results. (r_w=0.167, r_{skin}=0.333, $T_{skin}=10^{-3}$, $S_{skin}=10^{-3}$, $T_{aquifer}$=1, $S_{aquifer}=10^{-5}$; discretization as in Figure II.A.1 except that 3 of the 39 radial nodes are placed between r_w and r_{skin}).

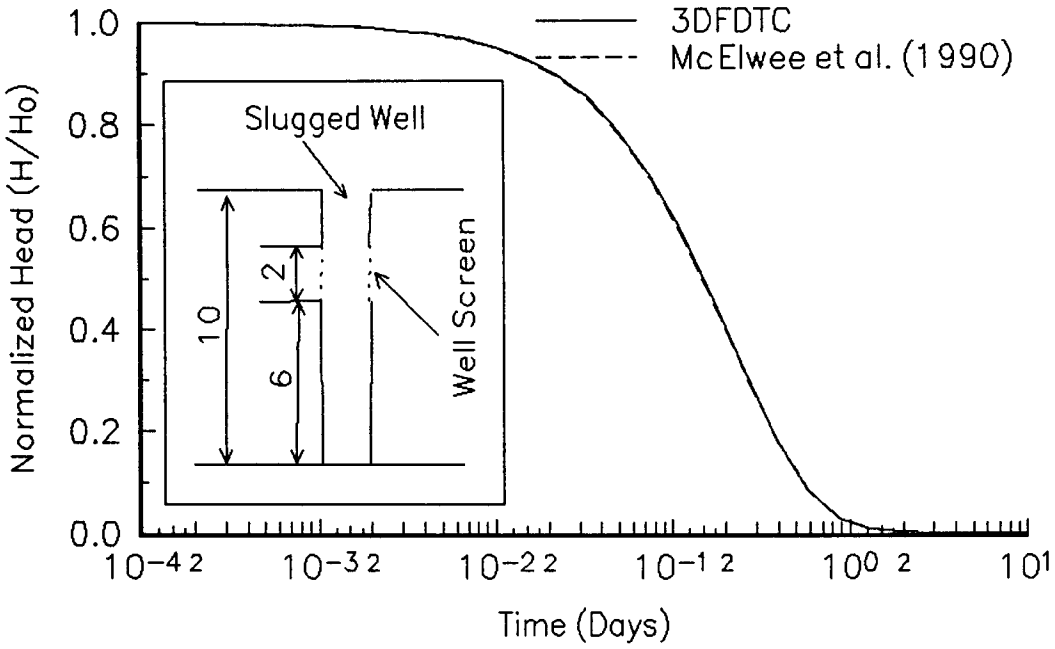

Figure II.A.3 Normalized head (H/H_0) versus time plot comparing McElwee et al. (1990) solution with 3DFDTC results. (r_w=0.167, K=0.1, S_s=10^{-6}; discretization as in Figure II.A.1).

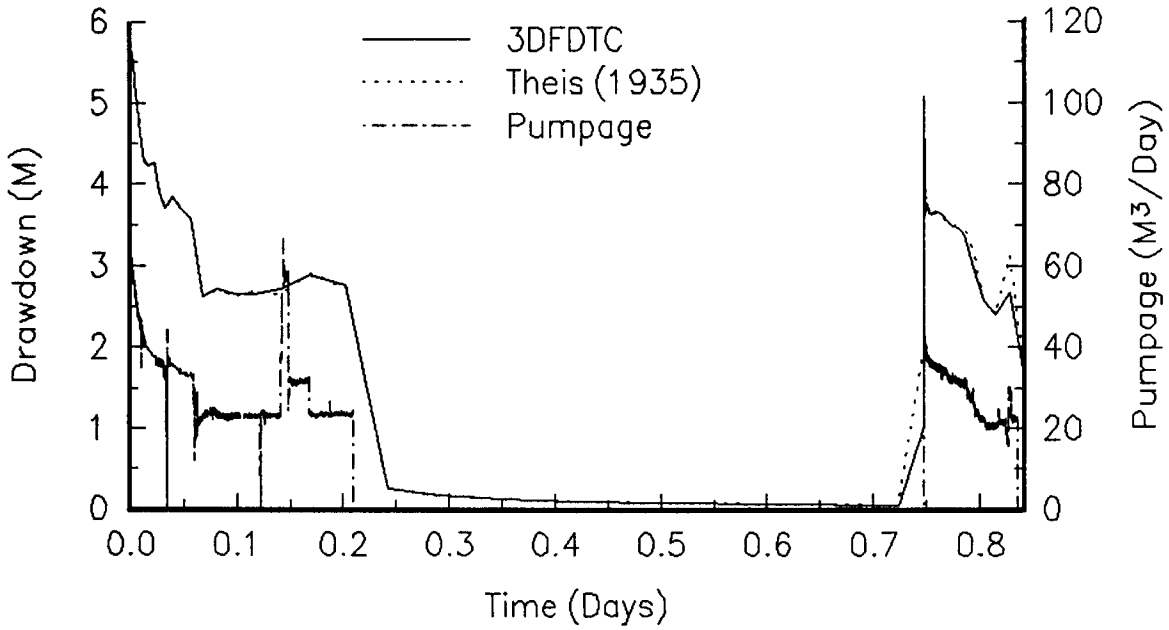

Figure II.A.4 Pumpage versus time and drawdown versus time plots comparing Theis (1935) solution with 3DFDTC results. (r=.208, T=1, S=10^{-6}, r_w=0.005; Discretization: 100 nodes from .005 to 836500 meters)

B. THE USE OF SLUG TESTS TO DESCRIBE VERTICAL VARIATIONS IN HYDRAULIC CONDUCTIVITY

Introduction

The slug test has become one of the more commonly employed techniques in applied hydrogeology. This test, which is quite simple in practice, consists of measuring the rate of recovery in a well after a near instantaneous change of water level at that well. One of the primary objectives of the first year of this project was to explore the potential of slug tests to provide information about vertical variations in hydraulic conductivity. Specifically, the aim was to assess if a series of multilevel slug tests in a well that is fully screened across the unit of interest could provide useful information about vertical variations in flow properties. In this subsection, results of a series of numerical experiments performed to assess the theoretical viability of slug tests for the purpose of describing vertical variations in conductivity are reported. In a later subsection (III.B), results of a program of field testing at GEMS are described.

Model Configuration

In order to assess the potential of slug tests for identifying vertical variations in horizontal hydraulic conductivity, an early version of the 3DFDTC model described previously was used to generate synthetic slug-test results under a number of test scenarios. The initial set of simulations was carried out using four different hypothetical cases: 1) a uniform, isotropic aquifer; 2) a uniform, anisotropic aquifer; 3) a layered, isotropic aquifer; and 4) a layered, anisotropic aquifer. The layered aquifers consist of alternating high and low conductivity layers, with the following radial (r) and vertical (z) conductivity values (units are meters/day):

	anisotropic case	isotropic case
low conductivity layer	K_r=1.; K_z=0.1	K_r=K_z=1.
high conductivity layer	K_r=10; K_z=1.	K_r=K_z=10.

The uniform aquifers are assigned the properties of the low conductivity layer. In all cases, the aquifer is 25 meters thick (with one node per meter in the vertical). The aquifer is bounded above and below by impermeable boundaries. Twenty nodes

(equal log spacing) are used in the radial direction resulting in an outer radius (constant head boundary) of 37364 m. Other model parameters are as follows:

S_s = specific storage = 1.0×10^{-5} m^{-1};

H_0 = initial head in well = 1.0 m;

r_w = well radius = 0.4 m.

Note that in this first set of simulations an unrealistically large well radius was employed. The results of this set of simulations, however, are not dependent on the radius of the test well. In later simulations, a more realistic value was employed for the test well radius.

Vertical Averaging in Fully Penetrating Slug Tests

One issue of considerable interest to hydrogeologists is the way in which aquifer properties are averaged in various types of hydraulic tests in heterogeneous systems (e.g., Butler and Liu, 1991; Desbarats, 1992; Harvey, 1992). In the initial phase of this work, the manner in which vertical variations in hydraulic conductivity are averaged in a slug test performed over the entire screened interval in a fully penetrating well (fully penetrating slug test) was explored. Figure II.B.1 displays the results of several simulations of slug tests in aquifers with the same thickness-weighted average of layer conductivities, but with different patterns of conductivity variations. Results are shown for the analytical solution of Cooper, Bredehoeft, and Papadopulos (CBP) (Cooper et al., 1967) for a slug test in a uniform, isotropic aquifer with K_r= 4.6, and for four numerical simulations. The numerical simulations include a uniform, anisotropic aquifer case with K_r=4.6, K_z=0.46, and three other simulations of layered aquifers with alternating bands of the properties K_{low} and K_{high} (anisotropic case of table on previous page). The layering schemes are shown in Figure II.B.2. All three layering schemes have a thickness weighted average K_r of 4.6 (15 units of K_r=1.0 and 10 units of K_r=10.0).

As shown in Figure II.B.1A, the numerically simulated heads at the slugged well are essentially identical in the uniform and all three layered cases. All four plots of the numerically simulated heads fall just slightly below the heads computed from the analytical solution as a result of the discretization error discussed in the previous subsection. Clearly, slug tests over the entire screened interval in fully penetrating wells can provide little information about vertical variations in conductivity when the slugged well is the measurement location. In all cases, the computed conductivity will be a thickness-weighted arithmetic average of the horizontal conductivities of the individual layers. Note that this result is an extension

of the work of Karasaki (1986), who found the same result for slug tests in layered aquifers in which there is no vertical flow between layers. Thus, the vertical averaging in fully penetrating slug tests is independent of the degree of vertical flow between layers.

The previous discussion has focussed on using the slugged well as the measurement location. Figure II.B.1B shows the responses at an observation well at a distance from the stressed well in the same set of slug-test simulations. The observation well is screened opposite vertical node 13 (the middle of the aquifer) at a radial distance of 3.7 meters from the center of the slugged well. Note than even though the observation well occurs in a low-conductivity zone in all three layering schemes, the observation-well responses are different in all three cases. Thus, the response at partially penetrating observation wells is a function of the particular layering scheme in the tested unit. This result clearly demonstrates the potential of observation wells to provide information about conductivity variations using fully penetrating slug tests. In a later subsection of this report (II.C), the general issue of the use of observation wells in slug tests is explored in more detail.

Although fully penetrating slug tests can provide some information about vertical variations in conductivity when observation wells are employed, the need for observation wells somewhat limits the applicability of the technique. Another approach for gaining information about vertical variations in flow properties is the multilevel slug test (e.g., Dagan, 1978; Braester and Thunvik, 1984; Hayashi et al., 1987; Melville et al., 1991), in which a series of slug tests are performed at different levels in the screened interval of a single well while using packers to isolate the test zone. An extensive series of numerical simulations was performed in this work in order to assess the potential of multilevel slug tests for providing information about vertical variations in hydraulic conductivity.

Multilevel Slug Tests

The simulations of multilevel slug tests performed here all employ a well fully screened across the aquifer with the slug tests being carried out in a limited interval that is isolated by packers above and below the test zone (straddle packer arrangement). A separate packer above the screened section prevents movement of water from the cased region of the well into screened intervals other than the test zone. Note that this configuration is the same as that used in the KGS multilevel slug test system employed in the field testing discussed in a later subsection (III.A). The nodes representing the slugged interval are assigned an initial head of 1.0, while

the remaining nodes in the model (including those in the screened section of the well outside the straddle packer) are assigned an initial head of 0. The slugged interval is assigned a specific storage equal to the inverse of its length, so that the storage coefficient for the slugged interval equals 1.0. The open sections of the wellbore outside the straddle packer are assigned a value for specific storage that corresponds to the compressibility of water.

An initial series of simulations was performed in order to assess the dependence of slug-test results on the length of the slugged interval and on proximity to the upper and lower impermeable boundaries. For this initial set of simulations, the results were analyzed using the CBP analytical solution incorporated in an automated well-test analysis package, SUPRPUMP, developed at the Kansas Geological Survey (Bohling and McElwee, 1992). Figure II.B.3 presents the results of a series of simulations investigating the effects of the length of the test interval on slug tests in the uniform aquifers described earlier. In these simulations, the slugged interval is centered on vertical node 13 and the length of the interval is gradually increased symmetrically about that node. Results are presented in terms of the vertical position of the top node of the slugged interval. Note that the conductivity values determined using the automated analysis package can only be considered apparent conductivities, since the true flow field contains a significant vertical flow component, while the CBP analytical solution assumes strictly horizontal flow.

Figure II.B.3 clearly demonstrates that the analysis of multilevel slug tests under the assumption of negligible vertical flow can result in a significant overestimation of the horizontal hydraulic conductivity. The vertical component of flow allows the effect of the pressure disturbance at the slugged well to be dissipated more rapidly than it would be under purely horizontal flow conditions. Figure II.B.3 also demonstrates that the apparent K_r approaches the true K_r value as the length of the slugged interval approaches the thickness of the aquifer. However, there is a slight discrepancy between the true and apparent values even for the fully penetrating case. Additional simulations have shown that this difference is due to the discretization error resulting from the fairly coarse discretization scheme employed in the radial direction. Note that the overestimation of K_r is worse under isotropic conditions than under anisotropic conditions as a result of the flow being increasingly constrained to the horizontal plane as the ratio of vertical to hydraulic conductivity decreases.

Figure II.B.4 presents the results of simulations designed to examine the effects of impermeable boundaries on slug-test results. A series of simulations was

performed in the uniform aquifer configurations described earlier using a three-node slugged interval (Figure II.B.4A) and a one-node slugged interval (Figure II.B.4B), with the center node of the slugged interval being progressively moved from node 2 (in the three-node slugged interval case) or node 1 (in the one-node interval case) to node 13. The difference in magnitude in apparent K_r between the two plots is a result of the increased importance of vertical flow in the shorter slugged interval. In both cases, the boundary effects are fairly similar. As the slugged interval approaches the boundary, the vertical flow out of the slugged interval is constrained, resulting in a smaller overestimation of K_r.

Figure II.B.5 presents the results from a series of simulations similar to those shown in Figure II.B.4 performed in layered aquifers. Note that again a greater overestimation of K_r occurs in the isotropic case than in the anisotropic case. Although use of a one-node slugged interval results in a greater overestimation of K_r, it does allow for clearer definition of the boundaries between layers of contrasting conductivity. Also note that results in Figure II.B.5 are presented in terms of the ratio of apparent K_r to true K_r, so that uniform and layered cases may be readily compared. In this investigation, the true K_r is taken to be the thickness-weighted average of the model K_r values over the length of the slugged interval.

Up to this point, the simulated slug-test data have been analyzed using the CBP model, which is clearly an overly simplified representation of the flow system. Two issues of some importance are 1) will the nature of the fit of the CBP model to the data indicate that an inappropriate model is being employed, and 2) will different divergences from the model assumptions produce different types of model misfits. Figure II.B.6 presents the observed and CBP best-fit head values for four of the simulations included in Figure II.B.5. Figure II.B.6A shows the results for a three-node slugged interval centered at vertical nodes 7 and 12 in the layered, anisotropic aquifer, while Figure II.B.6B shows the results for a one-node slugged interval at the same positions. The CBP model heads consistently fall below the observed heads early in the test and above the observed heads later in the test. This systematic lack of fit is the result of neglecting the vertical component of flow. Unfortunately, a very similar lack of fit results from the presence of a positive well skin (low conductivity zone surrounding the well) in a homogeneous aquifer (see subsection II.D). Thus, skin effects and the effects of partial penetration may be difficult to discriminate in practice.

Given that analyses of slug-test responses using the CBP model do provide at least a gross picture of vertical variations in conductivity, it is reasonable to assume

that analyzing the slug-test data with a more appropriate model, i.e. one that accounts for the partial penetration effects seen with multilevel slug tests, would reduce or remove the problem of overestimation of K_r due to neglect of the vertical component of flow. Two other models were considered here for use in the analysis of multilevel slug-test data. McElwee et al. (1990) have developed an analytical solution for slug tests in partially penetrating wells with skins, which can be readily configured to analyze data from multilevel slug tests in homogeneous, anisotropic aquifers. Unfortunately, this solution, which is based on the application of both Fourier and Laplace integral transforms, is so computationally intensive that it cannot presently be used for the analysis of large amounts of field data. Ongoing work is directed at improving the computational efficiency of this model.

Hvorslev (1951) developed a model for the analysis of slug tests performed in a screened interval of finite length in a uniform, vertically unbounded, medium with a vertical to horizontal anisotropy in hydraulic conductivity. A major assumption of the Hvorslev approach is that the specific storage of the aquifer can be ignored. McElwee et al. (1989), in a theoretical analysis of slug tests in confined aquifers, have shown that the head response at the slugged well is relatively insensitive to the specific storage of the unit, indicating that this assumption of Hvorslev may be acceptable in many cases. Figure II.B.7 shows the results of Hvorslev analyses of the same simulated multilevel slug tests employed in Figure II.B.5. Note that the Hvorslev model requires the use of a "shape factor", which is related to the geometry of the well intake region. The shape factor used here is that for Case 8 described in Hvorslev (1951). The Hvorslev function for this case is in the form of a two-parameter (K_r and anisotropy ratio) model. Unfortunately, the two parameters are perfectly correlated, so they cannot be estimated independently. For the analyses presented in Figure II.B.7, three different values of the anisotropy ratio are employed. The true value of the ratio of horizontal to vertical conductivity is 10. As shown in Figure II.B.7, the resulting overestimation or underestimation of K_r is not strongly influenced by the improper specification of the anisotropy ratio. The correlation between the two parameters is also apparent, since the estimated hydraulic conductivity changes by a multiplicative constant for all analyses as a result of using a different value for the anisotropy ratio. Note that Dagan (1978) and Widdowson et al. (1990) have developed techniques for the analysis of multilevel slug tests that are based on a series of graphs/charts developed from simulation of slug tests under conditions similar to those considered by Hvorslev (1951). These techniques were not considered sufficiently different from the approach of Hvorslev

to merit further consideration in this work.

Figure II.B.8 displays the Hvorslev model fits for the same intervals as shown in Figure II.B.6 for the CBP analyses. The plots are for the case in which the true anisotropy ratio is used. The fitted results, however, would be essentially identical for all values of anisotropy ratio, due to the perfect correlation between the model parameters. Specifying a different anisotropy ratio would result in the same optimal fit (measured in terms of the sum of squared head deviations) for a different value of K_r. Comparing Figures II.B.7 and II.B.8 to Figures II.B.5 and II.B.6 reveals that, in this case, use of the Hvorslev model improves the estimates of K_r and provides a better fit to the observed data. The improved fit is attributed to the fact that the Hvorslev model accounts for the vertical flow component, while the CBP model does not. The Hvorslev model, however, must be used with caution due to its neglect of storage effects on slug-test responses (Chirlin, 1989), its poor performance in the presence of a well skin (see subsection II.D), and its increasing error in wells with small ratios of screen length to well radius (Hvorslev, 1951). Note that the Hvorslev analyses were not performed in the conventional fashion in this work. The optimal conductivity was determined here using a nonlinear regression algorithm to minimize the sum of the squared differences between the actual observed heads and the model-predicted heads. A conventional Hvorslev analysis is performed by minimizing the sum squared deviation between log-transformed head values, using that portion of the data that appear to fall on a straight line on a log-head versus arithmetic-time plot. The conclusions of this work, however, are not dependent on the fitting criterion. Given the closeness of the Hvorslev calculated parameters to the actual model values, the Hvorslev model was used for the analysis of simulated slug-test data for the remainder of this work.

Dependence of Multilevel Slug Test Results on Layer Thickness and Skin Permeability

The simulations described above showed that multilevel slug tests will indicate the existence of layers of differing conductivity to some degree and that the Hvorslev model is the most appropriate model at present for the analysis of the test data. Further work, however, is needed to explore the dependence of multilevel slug-test results on layer thickness and to assess how a well skin will influence test results. A series of simulations designed to address these issues is described here.

For this series of simulations, the configuration consisted of an aquifer made up of layers of two distinct materials (denoted here as A and B). The model

parameters are as follows:

$S_{SA} = S_{SB} = 1x10^{-5}\ m^{-1}$;

$H_0 = 1.0$ m;

$r_w = 0.05$ m;

$K_A = 2x10^{-5}$ m/sec;

$K_B = 2x10^{-4}$ m/sec.

In this series of simulations, a model grid of 20 nodes in the radial and 48-96 nodes in the vertical directions was employed. The number of nodes in the vertical varied depending on the screen length used in the particular scenario (Case 1 of Table II.B.1 employed 50 nodes (1.0 m spacing), Cases 2-6 employed 48 nodes (.312 m spacing), and Cases 7-8 employed 96 nodes (.156 m spacing)). Note that a series of simulations was performed in order to check on the error introduced by the various vertical discretization schemes. The discretization schemes employed in Cases 2-8 were found to introduce an error of less than 2% to the calculated parameters, while the scheme employed in Case 1 was found to introduce an error of less than 5%. These errors were considered acceptable for the purposes of this work. Equality of heads in the angular direction was assumed, so no additional nodes in the angular direction were required.

The initial scenario examined in this series of simulations (see Table II.B.1 for details of all examined scenarios) consisted of an isotropic aquifer of material A in the center of which is located a single isotropic layer of material B. The purpose of this first set of simulations was to examine how layer thickness impacts the conductivity calculated from a slug test. Seven different thicknesses were used for the B layer, which, in all cases, was symmetrically located about the center of the aquifer (total thickness of 50 meters). Note that a test interval of four meters was assumed.

Figure II.B.9 displays plots of conductivity versus depth to the top of the test interval for each of the different thicknesses of layer B. An important point to note is that even when the test interval lies completely within layer B, the calculated conductivity may underestimate the layer conductivity as a result of the influence of the lower conductivity material adjoining layer B. Only in very thick layers (i.e. layer thicknesses of 20 and 30 meters) is the influence of adjacent material negligible. Note that conductivities calculated for intervals in which layer B was thinner than the slugged interval (layer thicknesses 1 and 2) underestimated layer conductivity as a result of the vertical averaging discussed previously.

The results depicted in Figure II.B.9 were determined for the ideal case in

which formation layering extends to the well screen. Often, however, well drilling and development creates a near-well zone (well skin) of properties differing from those of the formation in which the well is screened. If the well skin is less permeable than the formation, the vertical flow out of the test interval will be suppressed as shown by McElwee et al. (1990). In addition, the calculated conductivity will be a function of both skin conductivity and formation conductivity. As discussed in subsection II.D, this function is heavily weighted towards the skin conductivity when a low conductivity skin exists and the Hvorslev model is used for the data analysis. Thus, a low conductivity skin can cause the magnitude of the vertical variations in conductivity to be underestimated.

A well skin may be of higher permeability than the formation as a result of voids forming along the well screen during well emplacement or of well development activities. A high conductivity skin can serve as a conduit for additional vertical flow. A second set of simulations was run using a configuration similar to that used in Figure II.B.9 except that a well skin of .11 m in radius with a conductivity of $5x10^{-4}$ m/sec was added to the system. The skin was assumed isotropic and to have the same specific storage as the formation as a whole. Figure II.B.10 displays the results of this series of simulations for five of the seven layering schemes examined in Figure II.B.9. Note that in all cases the existence of a high conductivity skin causes the calculated conductivities to increase as a result of the increased vertical flow. The increase is greatest for the thicker layers since the vertical flow moving along the well skin will be in contact with the higher conductivity layer for a longer time. Thus, the spread between the conductivities calculated for the different layers increases with the addition of a high permeability well skin. An additional set of simulations was performed to examine the effect of increasing skin conductivity an order of magnitude to $5x10^{-3}$ m/sec. Although not shown here, the results of these simulations indicate that the calculated conductivities continue to increase in a manner similar to the pattern shown in Figure II.B.10.

Two additional series of simulations were performed in configurations similar to that employed in Figure II.B.9 in order to examine the effects of formation anisotropy and a lower specific storage. The addition of anisotropy (vertical conductivity lower than horizontal conductivity) into the configuration produced results similar to those described previously, i.e. vertical flow was suppressed causing a decrease in the calculated conductivity. In addition, the suppression of vertical flow caused the influence of adjoining lower conductivity layers to be diminished, resulting in the layer B conductivities calculated for the different layering configurations to be

more similar. The analyses described in this paragraph were performed assuming isotropic layers. This is a reasonable assumption since in most situations one will not know what degree of anisotropy is appropriate. As discussed earlier, the anisotropy ratio and the horizontal conductivity are perfectly correlated in the Hvorslev model. Thus, uncertainty will be introduced into the parameter estimates due to the uncertainty concerning anisotropy.

Unlike the anisotropic case, a lower specific storage resulted in the pressure disturbance induced by the slug test to spread out more rapidly in all directions, causing the influence of adjoining lower conductivity layers to be increased. The increased influence of adjoining lower conductivity layers produced considerably lower values for the calculated layer B conductivities. Thus, the specific storage can have a considerable influence on the calculated conductivity in layered systems. This is in contrast to the work of McElwee et al. (1989) for slug tests in homogeneous systems, which showed that specific storage had relatively little influence on conductivity estimates obtained from heads at the slugged well in a homogeneous aquifer.

An important objective of this theoretical analysis was to assess under what conditions vertical variations in conductivity will be suppressed or completely hidden during multilevel slug tests. As discussed earlier, the existence of a low conductivity skin can cause the effect of layering to be suppressed. A large number of additional simulations were performed to better assess the conditions under which vertical variations may be suppressed. Results from a small subset of these simulations are described here (see Table II.B.1 for a description of all the scenarios examined here and Table II.B.2 for a summary of results from the simulations described below).

It was shown previously that fully penetrating slug tests in a layered aquifer will yield a hydraulic conductivity that is a thickness-weighted average of the layer conductivities. No indication of layering will be evident from the head response at the slugged well. An obvious question of importance for multilevel slug tests is how much will layering be suppressed when the screen length is larger than the average layer thickness. Figure II.B.11 displays the results of a series of simulations of slug tests in a layered aquifer consisting of alternating layers of A and B. Each layer is 2.5 m. in thickness. The screen length used in the simulation is 5.0 m. As shown in Figure II.B.11, the vertical variations in conductivity are strongly suppressed in this case. The difference between the calculated layer conductivities is 11% of the actual difference. The results shown in Figure II.B.11 are for the ideal case of periodic variations with the screen extending over one complete cycle of variations.

Additional simulations indicate that the actual degree of suppression of vertical variations will depend on the screen length, the pattern of the variations, and the aspect ratio. McElwee et al. (1990) describe how a decrease in aspect ratio (screen length/r_w) promotes partial penetration effects, i.e. vertical flow out either end of the well screen. Those authors show that for the well radius used in this simulation, partial penetration effects should be rather small for screens greater than about 5 meters in length, a result that is in agreement with Figure II.B.11. Even when partial penetration effects are greater, however, relatively little information about vertical variations in conductivity can be gained when the screen length is several times larger than layer thickness. Thus, if one is interested in characterizing the detailed nature of the conductivity variations in a formation with multilevel slug tests, the screen length must be on the order of the layer thickness or less.

Even when the screen length is on the order of the layer thickness or less, there is still the possibility that other effects could serve to dampen the variations observed through multilevel slug tests. A very extensive set of simulations was performed to assess whether layer thickness and/or a low or high conductivity skin would serve to dampen the conductivity variations.

Figure II.B.12 displays results for a series of multilevel slug tests performed using a 2.5 m. screen in a layered aquifer consisting of alternating layers (each 2.5 m. in thickness) of A and B. Note that the calculated conductivity for layer B is less than the actual conductivity due to the suppression of vertical flow by the adjoining layers of material A in a manner similar to that seen in Figure II.B.9. This results in the conductivity variations being somewhat dampened (difference between the calculated layer conductivities is 86% of the actual conductivity difference). Figure II.B.13 displays analogous results for the case of layers of .15 m. in thickness and a screen of .15 m. in length. In this case, the effect of the adjoining lower conductivity layers is even greater (calculated conductivity difference is 46% of actual) as a result of the greater proportion of vertical flow that occurs as the aspect ratio decreases. Note that although the addition of anisotropy ($K_r > K_z$) to this configuration does serve to decrease vertical flow, further simulations indicate that this actually results in the conductivity variations being further suppressed because the calculated conductivities for the high permeability layers decrease more than the conductivities calculated for the low permeability layers.

Earlier it was stated without supporting simulation results that a low permeability skin can cause the magnitude of the vertical variations in conductivity to be suppressed. A series of simulations was performed to get an understanding of

the degree of suppression that occurs with a low permeability skin (cases 6C and 7F of Table II.B.1). Table II.B.2 summarizes the results of these simulations. In both cases, the suppression of the vertical variations is almost complete (calculated conductivity difference is 2.9% and 1.7%, respectively, of actual). In addition to the shrinking of the range, the calculated conductivities are much lower than under the no-skin condition as a result of the heavy weighting of the low permeability skin in the parameter estimates (see subsection II.D). Note that the calculated conductivities are considerably lower in case 7F as result of the greater influence of vertical flow with smaller aspect ratios. In this case, the vertical flow is being suppressed producing lower calculated conductivities.

Although the simulation results displayed in Figure II.B.10 do not indicate that vertical variations in conductivity are dampened by the existence of a high conductivity skin, a further series of simulations was performed to assess the role of a high permeability skin in the configurations employed in Figures II.B.12 and II.B.13. Figure II.B.14 displays the results of simulations in which a high conductivity skin ($K=1x10^{-3}$ m/sec) of .11 m. in radius is added to the configuration employed in Figure II.B.12. As in Figure II.B.10, the addition of a highly conductive skin causes an increase in the calculated conductivities. In this case, the difference between the conductivities calculated for the two layers is slightly larger than the difference calculated for the no skin case. As layer thickness decreases, however, the effect of a high conductivity skin changes. Figure II.B.15 displays the results of simulations in which the same high conductivity skin is added to the configuration employed in Figure II.B.13. In this case, the layers are thin enough that when the screen is opposite a layer of material A, substantial amounts of water flow vertically along the well skin and into the layers of material B. This results in a great increase in the conductivity calculated for layers of material A and a dramatic decrease in the calculated difference between layer conductivities (calculated difference is 20% of actual difference). Thus, a highly conductive skin in an aquifer consisting of thin layers can cause multilevel slug tests to be of rather limited effectiveness in describing the vertical variations in hydraulic conductivity.

Given that a highly conductive skin can limit the effectiveness of multilevel slug tests, a series of additional simulations was performed in order to assess if well-construction measures could be taken to reduce the effect of a conductive skin. One possibility suitable to wells where the sand pack is the high conductivity skin would be to place very thin layers (1-2 cm) of low conductivity material (e.g., bentonite pellets) in the sand pack at relatively frequent intervals. These layers would serve

to decrease the vertical movement of water in the sand pack but would have very little impact on the horizontal movement of water. This scheme was evaluated here by simulating slug tests in wells with high conductivity skins in which an anisotropy in conductivity was assumed for the skin. Figure II.B.16 presents the results of a series of simulations in which anisotropy ratios (K_h/K_v) of 1, 2, and 10 were employed (K_h remaining constant, K_v decreasing). As shown in the figure, increases in the anisotropy ratio cause the range of the calculated conductivities to increase and the estimated values to decrease towards the no skin case. Thus, these results indicate that if a well is to be used for multilevel slug tests, periodic thin layers of low conductivity material in the sand pack would be useful in mitigating the effect of a high conductivity skin. Unfortunately, in uncased wells in consolidated rock, such an approach would not be possible making it difficult to remove the effect of a high conductivity skin (e.g., near-well zone of drilling-induced fractures) in such situations.

All of the simulations described above were performed assuming either that the packers were quite long (greater than 2 meters) or that the well was cased everywhere in the unit except at the test interval (infinite packer). This was done in order to remove any effects due to the circumvention of the packers from the results. However, in field applications of multilevel slug tests, packer circumvention is a very real concern. Thus, a series of additional simulations was performed in order to assess the effect of packer length on multilevel slug tests. In the 3DFDTC model used in this work, packers are simulated as no-flow boundaries in the well bore, so there is no restriction on the length of the modelled packer. Four configurations were employed in this analysis (Cases 8a-8d of Table II.B.1) in order to allow the effects of packer length to be evaluated in homogeneous and layered situations, both with and without a high conductivity skin. Figure II.B.17 presents the results of this series of simulations in the form of a plot of packer length versus the difference between the estimated conductivity using a packer of a certain length and the estimated conductivity using an infinite packer normalized by the infinite packer estimate. Note that a dramatic decrease in this difference is seen in all cases with an increase in packer length. This plot also indicates that a highly conductive skin will exacerbate packer circumvention problems. In all cases, however, these results demonstrate that the relationships derived in this work are essentially the same as would be obtained using a packer of .75-1.5 meters in length, which is the length range of many commercially available packers. Note, however, that these results are dependent on the thickness of the high conductivity skin. In cases where very thick

skins are suspected, longer packers or a number of packers in series should be employed.

As stated earlier, the Hvorslev model was employed to calculate K_r values from simulated slug-test data. One final issue to be addressed is that of the quality of the fits of the Hvorslev model to the simulated data. Figure II.B.18 displays a typical plot from the last series of simulations reported on here. As shown in the figure, the Hvorslev model provides a relatively good fit to the simulated data. This fit was characteristic of all the cases examined here.

The results discussed in this section are taken from a subset of the simulations performed for this project. Tables II.B.1 and II.B.2 summarize all the scenarios examined in this work.

Summary

The results of this modeling investigation of the viability of slug tests for the purpose of describing vertical variations in hydraulic conductivity can be summarized as follows:

1) Slug tests performed in a screened interval that passes through the entire aquifer will yield a thickness weighted average of layer conductivities. The response at the slugged well will show no indication of layering. Observation wells must be employed if fully penetrating slug tests are going to provide any information about vertical variations in hydraulic conductivity;

2) In multilevel slug tests, when the screen length is considerably greater than the layer thickness and the aspect ratio (screen length/r_w) is large, a slug test will yield an approximate thickness weighted average of the layers intersecting the screen. As the aspect ratio decreases, the properties of layers outside of the screened interval will influence the calculated conductivity as a result of the increased vertical flow;

3) Analysis of multilevel slug-test data with the CBP model (Cooper et al., 1967) can lead to a considerable overestimation of the radial hydraulic conductivity and also produces a systematic lack of fit between predicted and observed responses;

4) The model of Hvorslev (1951) appears to be the best present approach for analyzing multilevel slug-test data. This approach provides more reasonable estimates and a much better fit than the CBP model;

5) Even when the screened interval is less than the layer thickness, considerable error can be introduced into the description of vertical variations in hydraulic conductivity as a result of the influence of layers adjoining the tested layer.

The magnitude of the influence of the adjoining layers will depend on the layer conductivities, the specific storage and anisotropy ratio of the tested layer, skin conductivity, and the aspect ratio;

6) A low conductivity skin will make it difficult to describe vertical variations in hydraulic conductivity because the conductivity calculated from the slug-test data will be strongly influenced by the conductivity of the skin;

7) A high conductivity skin will make it difficult to describe vertical variations in hydraulic conductivity when the screened interval and the layer thickness are both small. In this case, a large amount of vertical flow can occur along the skin, making it difficult to detect the existence of layers of low conductivity. Emplacing thin low conductivity layers in the sand pack can decrease vertical flow and allow a more accurate description of the conductivity variations;

8) Experimental simulations showed that packer circumvention should not be a major problem when packers of .75 meters or longer are employed. Packer circumvention is of greatest concern in the case of a thick, high permeability skin. Vertical flow can be suppressed by placing thin low conductivity layers in the sand pack.

In summary, multilevel slug tests can provide considerable information about vertical variations in hydraulic conductivity under the right conditions. The best conditions would be thick layers using test intervals considerably smaller than the layer thickness. However, even in these conditions, well skins can dramatically decrease the effectiveness of the approach. Attention must be given to well construction and development in order to minimize the impact of a well skin on multilevel slug tests.

Note that the results discussed in this subsection were based on a series of simulations performed in perfectly stratified aquifers, i.e. layering is continuous throughout the entire model domain. Many aquifers, however, consist of a series of discontinuous layers. Further work is required to assess the effect of layer discontinuity on the results described here.

Table II.B.1 - Summary of layered-aquifer slug-test scenarios.

Scenario	K_S (10^{-3}m/s)	K_H/K_V	r_s (m)	l_s (m)	l_y (m)	Note
1	-	1	-	4	1*	1*
1A	0.5	1	0.11	4	1A*	1A*
1B	5	1	0.11	4	1B*	1B*
1C	-	1	-	4	1C*	1C*
2	-	1	-	5	2.5	2*
2A	-	1	-	0.6	0.30	2*
2B	-	1	-	7.5	2.5	2*
2C				3.75	2.5	2*
2D				0.30	0.15	2*
3	-	1	-	2.5	2.5	2*
3A	1	1	0.11	2.5	2.5	2*
3B	-	2	-	2.5	2.5	2*
4	-	1	-	1.25	2.5	2*
4A	1	1	0.11	1.25	2.5	2*
4B	-	2	-	1.25	2.5	2*
4C	1	1	0.11	1.25	2.5	2*
4D	-	1	-	1.25	2.5	2*,3*
5	-	1	-	1.25	1.25	2*
5A	1	1	0.11	1.25	1.25	2*
6	-	1	-	0.3	0.3	2*
6A	1	1	0.11	0.3	0.3	2*
6B	1	1	0.22	0.3	0.3	2*
6C	0.01	1	0.11	0.30	0.30	2*
7	-	1	-	0.15	0.15	2*
7A	1	1	0.11	0.15	0.15	2*
7B	-	2	-	0.15	0.15	2*
7C	-	10	-	0.15	0.15	2*
7D	1	1	0.11	0.15	0.15	2*,4*

7E	1	1	0.11	0.15	0.15	2*,5*
7F	0.01	1	0.11	0.15	0.15	2*
8A	-	1	-	0.15	-	6*
8B	-	1	-	0.15	0.15	2*
8C	1	1	0.11	0.15	-	6*
8D	1	1	0.11	0.15	0.15	2*

Note: Specific storage is 1×10^{-5} m^{-1} if not specified otherwise. $K_A = 2 \times 10^{-5}$ m/s and $K_B = 2 \times 10^{-4}$ m/s for all scenarios. r_s = radius of skin, l_s = length of screen, and l_y = layer thickness.

1*: Single layers of B located symmetrically about the center of aquifer A. Simulations performed for B layers of 1, 2, 4, 6, 10, 20, and 30 m in thickness.

1A*: Scenario same as 1 with skin.

1B*: Scenario same as 1 with higher permeability skin.

1C*: Scenario same as 1 with lower specific storage (1×10^{-7} m^{-1}).

2*: Alternating layers of A and B.

3*: Initial Head is 10 m.

4*: $K_{H(skin)}/K_{V(skin)} = 2$.

5*: $K_{H(skin)}/K_{V(skin)} = 10$.

6*: Single homogeneous unit with properties of layer B.

Scenario	Computed difference between layer conductivities (10^{-4} m/s)	% of actual range (actual range = 1.8×10^{-4} m/s)
2	1.308-1.106 = 0.202	11.22
2A	1.156-0.914 = 0.242	13.44
2B	1.492-0.889 = 0.603	33.48
2C	1.332-0.925 = 0.407	22.61
3	1.783-0.244 = 1.539	85.50
3A	2.113-0.538 = 1.575	87.50
3B	1.695-0.259 = 1.436	79.78
4	1.857-0.244 = 1.613	89.63
4A	2.296-0.510 = 1.786	99.22
4B	1.727-0.219 = 1.508	83.87
4C	3.122-1.209 = 1.913	106.30
4D	1.857-0.244 = 1.613	89.63
5	1.627-0.280 = 1.347	74.83
5A	2.006-0.648 = 1.358	75.44
6	1.301-0.258 = 1.043	57.94
6A	2.106-1.346 = 0.760	42.22
6B	3.531-3.172 = 0.359	19.94
6C	0.232-0.180 = 0.052	2.89
7	1.077-0.245 = 0.832	46.22
7A	2.240-1.887 = 0.353	19.61
7B	0.952-0.202 = 0.750	41.67
7C	0.741-0.135 = 0.606	33.67
7D	1.829-1.360 = 0.469	26.06
7E	1.451-0.667 = 0.784	43.54
7F	0.165-0.135 = 0.03	1.67

Table II.B.2 - Summary of slug-test simulations in configuration consisting of alternating layers of A and B. Results are given in terms of the difference between the computed conductivities for the two layers. See Table II.B.1 for description of each scenario.

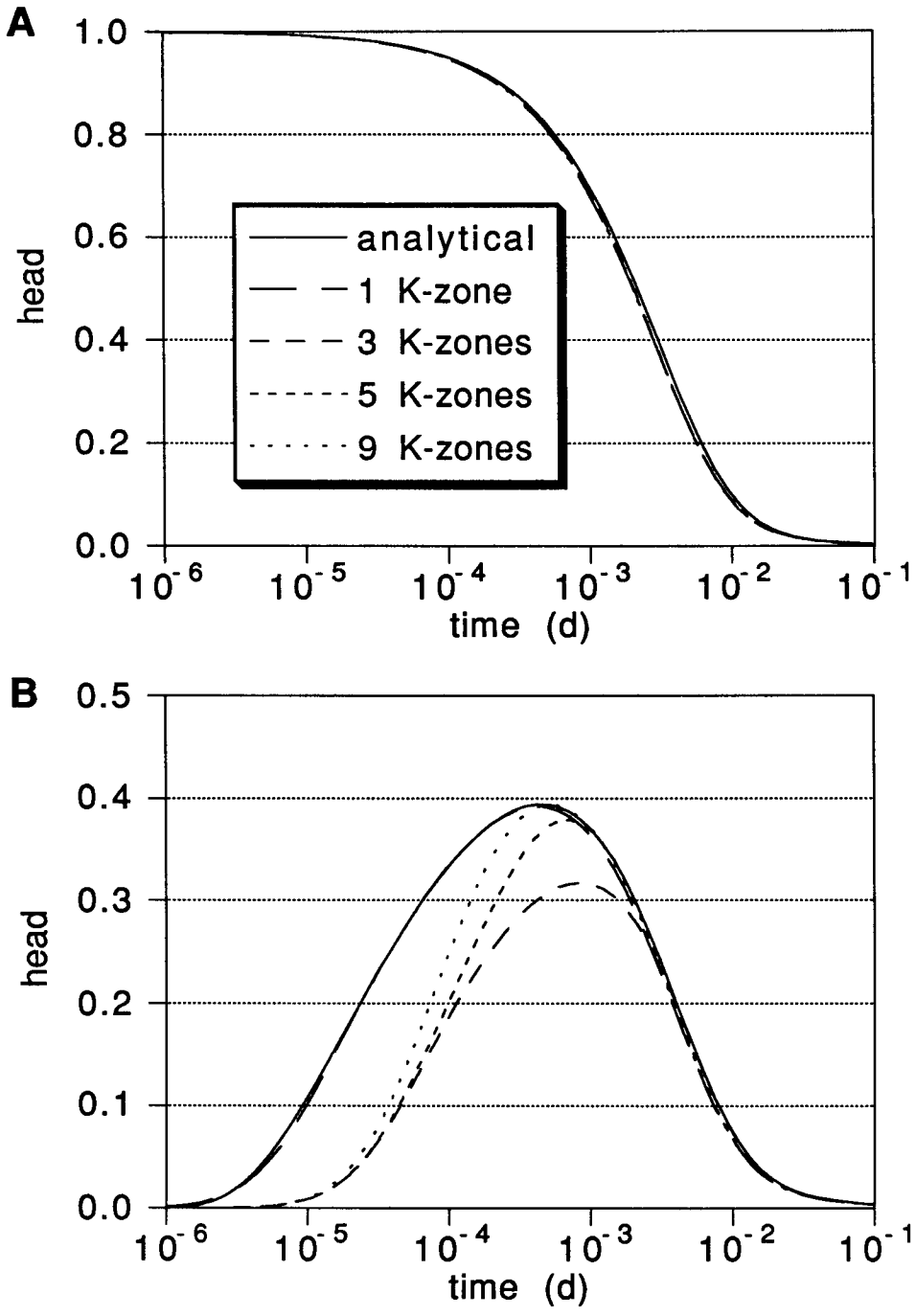

Figure II.B.1: Effects of variable layering on fully-penetrating slug test results at (A) the slugged well and (B) an observation well located at vertical node 13 and 3.7 meters radial distance from the slugged well. Layering schemes are shown in Figure II.B.2.

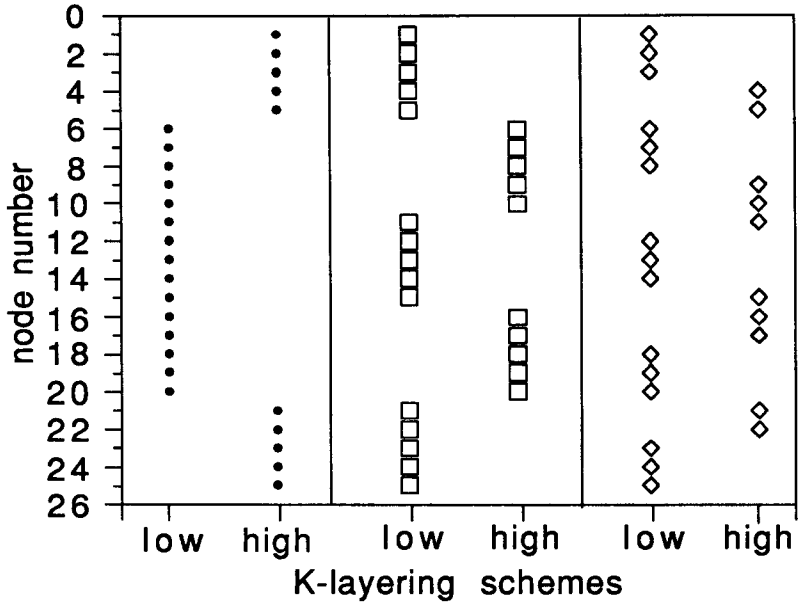

Figure II.B.2: Layering schemes employed for results shown in Figure II.B.1. Low and high hydraulic conductivities are those for the layered, anisotropic aquifer.

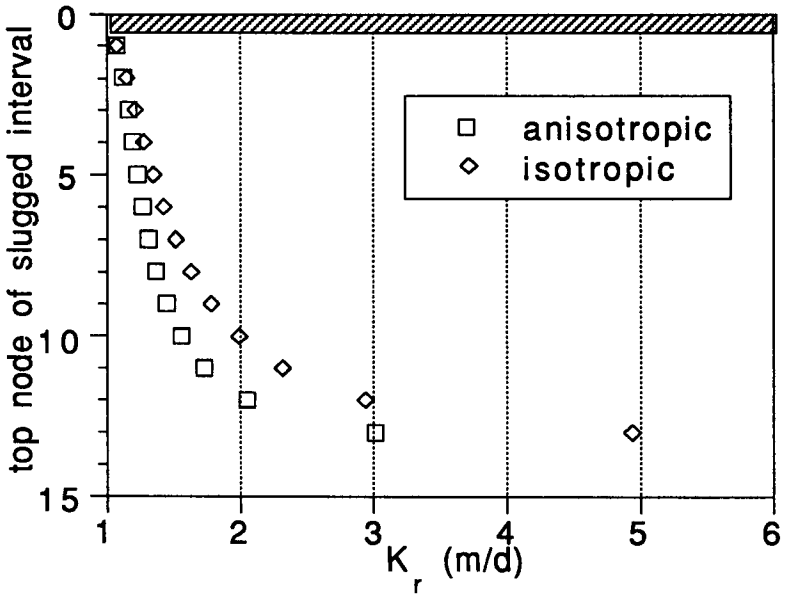

Figure II.B.3: Effects of slugged interval length in a uniform aquifer. Slugged interval is centered at vertical node 13 and its length increases symetrically up to the full thickness of the aquifer (25 nodes).

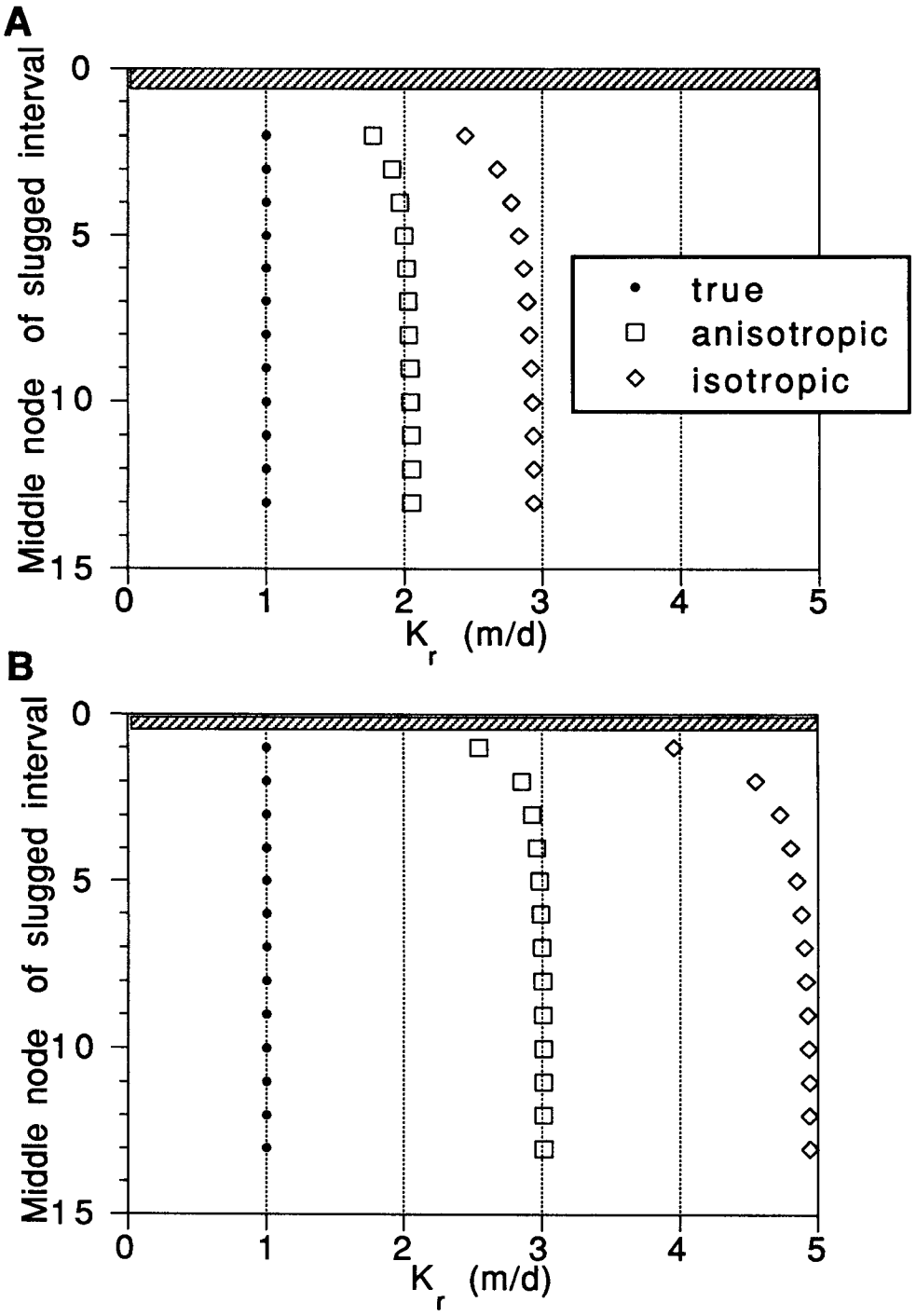

Figure II.B.4: Boundary effects in the uniform aquifers using (A) a three-node slugged interval and (B) a one-node slugged interval.

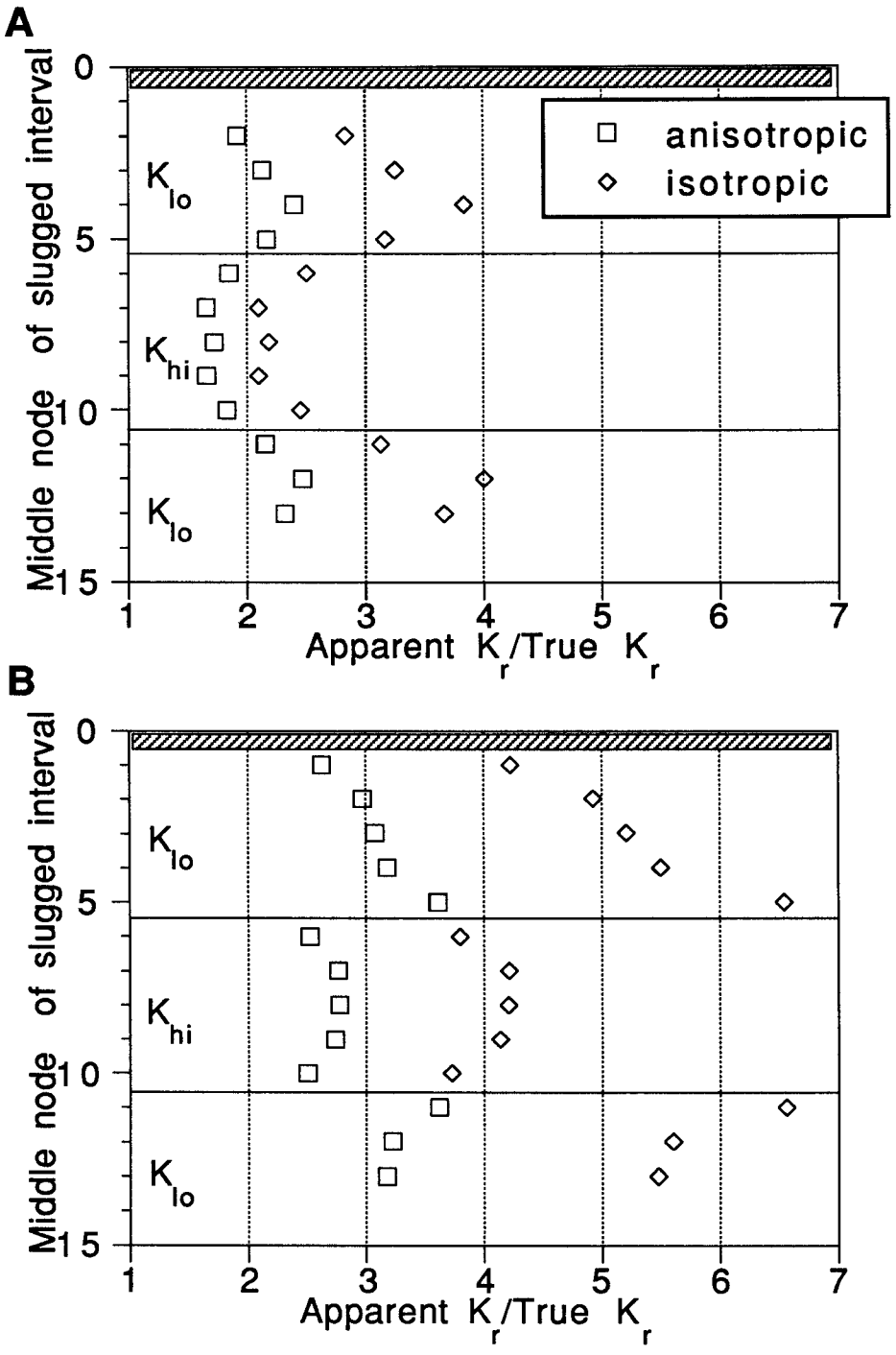

Figure II.B.5: Results of CBP analyses of multilevel slug test results using (A) a three-node slugged interval and (B) a one-node slugged interval in the layered aquifers.

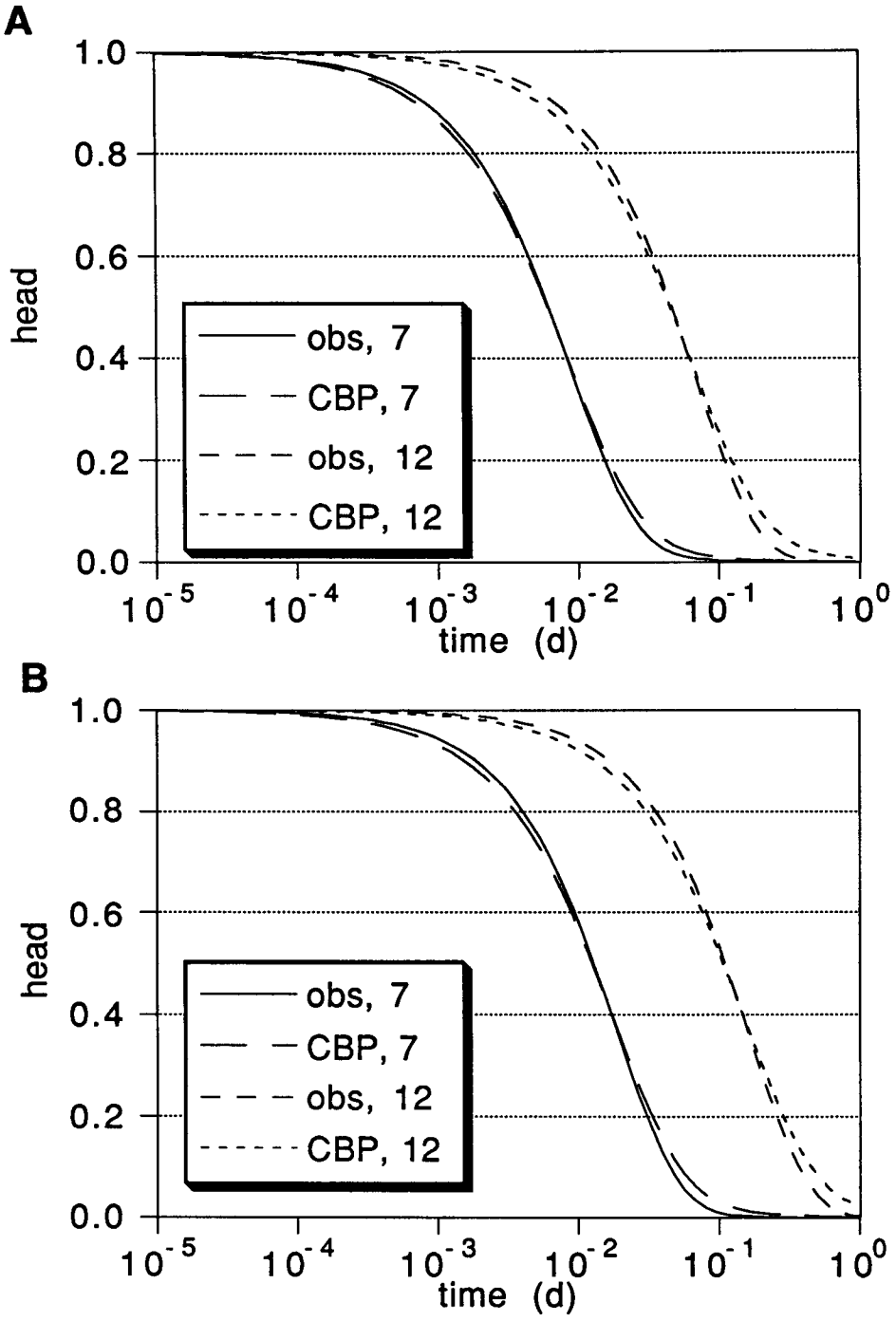

Figure II.B.6: Observed (obs) and CBP best-fit heads at vertical nodes 7 and 12 of layered, anisotropic aquifer using (A) a three-node slugged interval and (B) a one-node slugged interval.

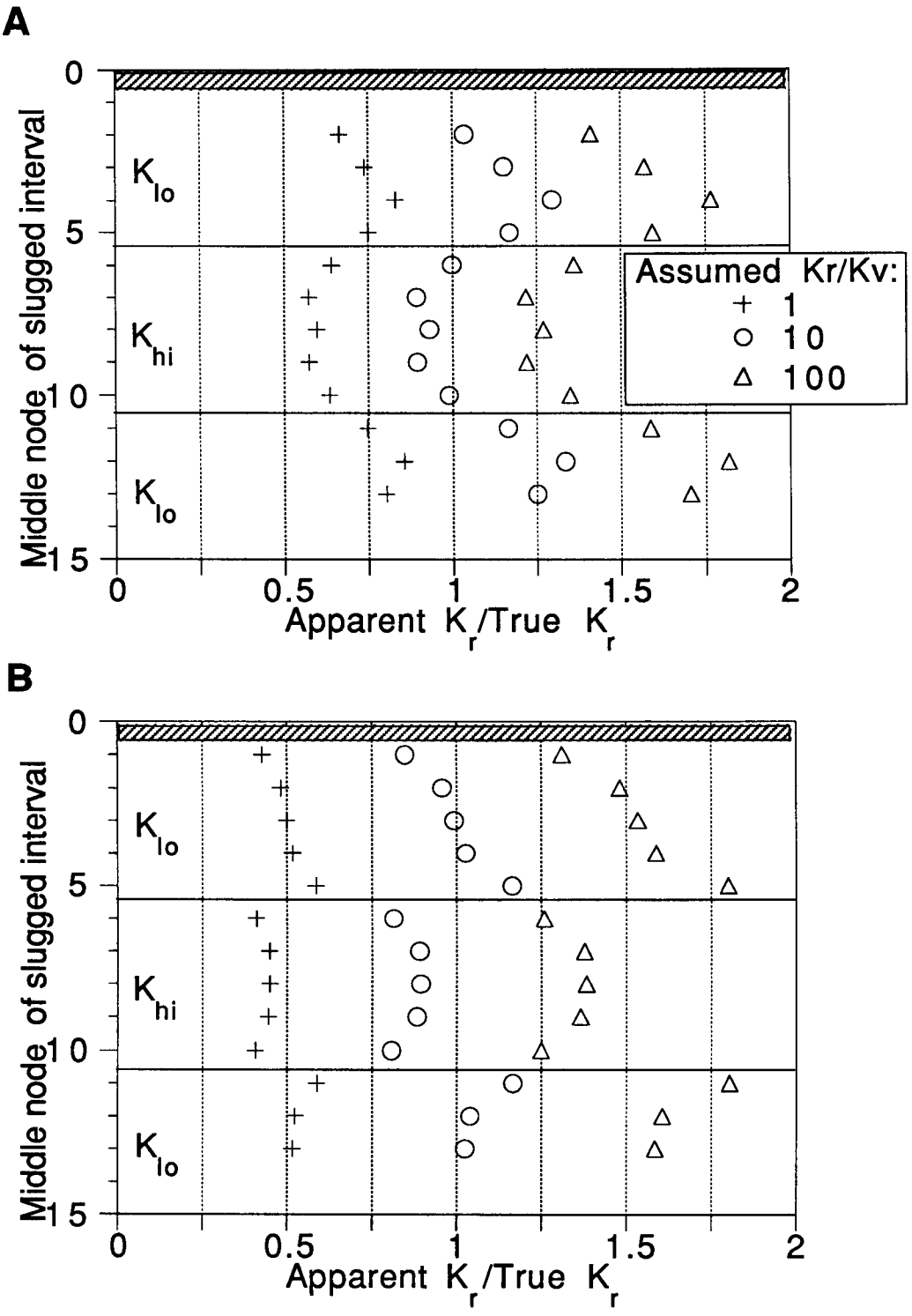

Figure II.B.7: Results of Hvorslev anlyses of multilevel slug tests using (A) a three-node slugged interval and (B) a one-node slugged interval in the layered aquifers.

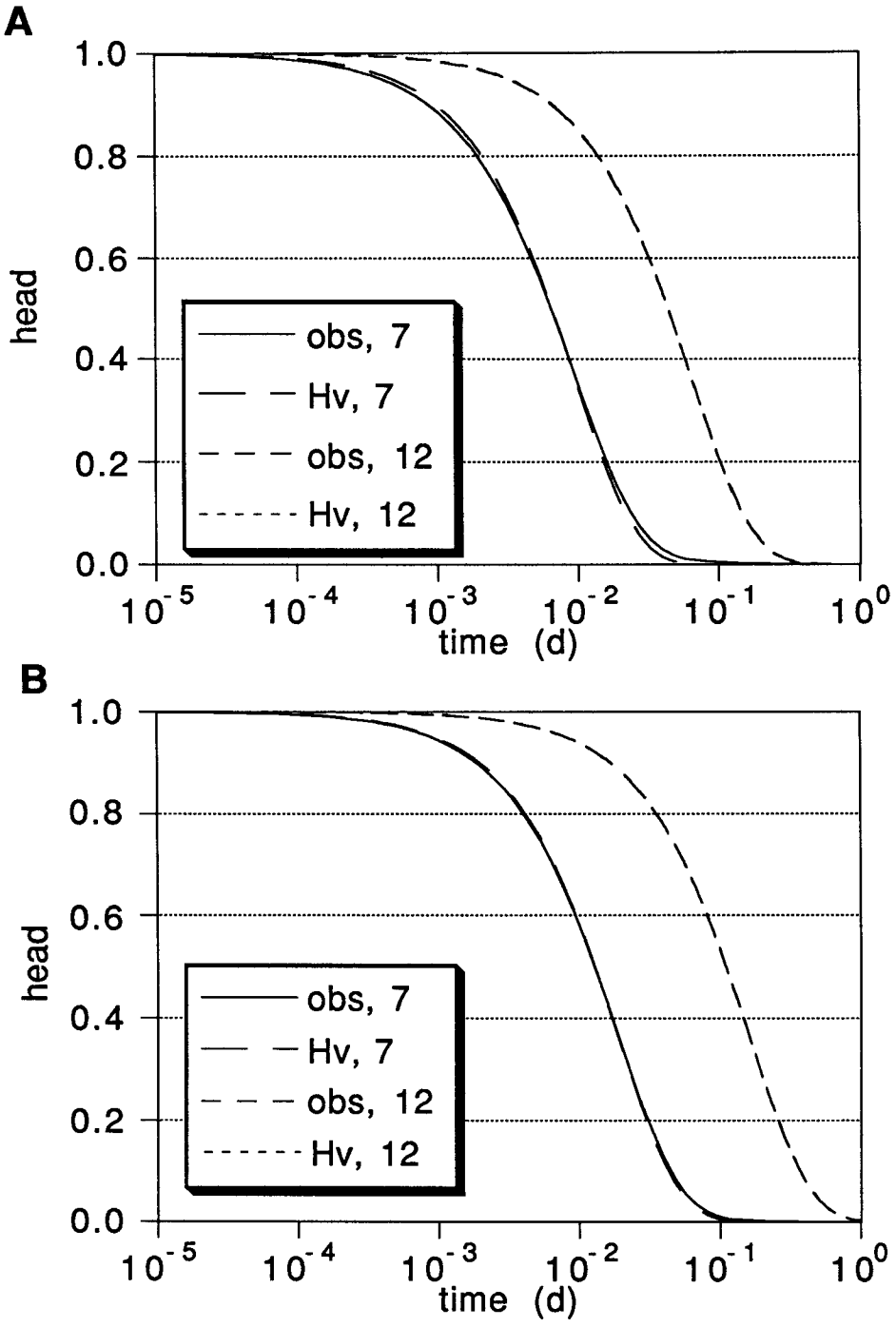

Figure II.B.8: Observed (obs) and Hvorslev (Hv) best-fit heads at vertical nodes 7 and 12 of layered, anisotropic aquifer using (A) a three-node slugged interval and (B) a one-node slugged interval.

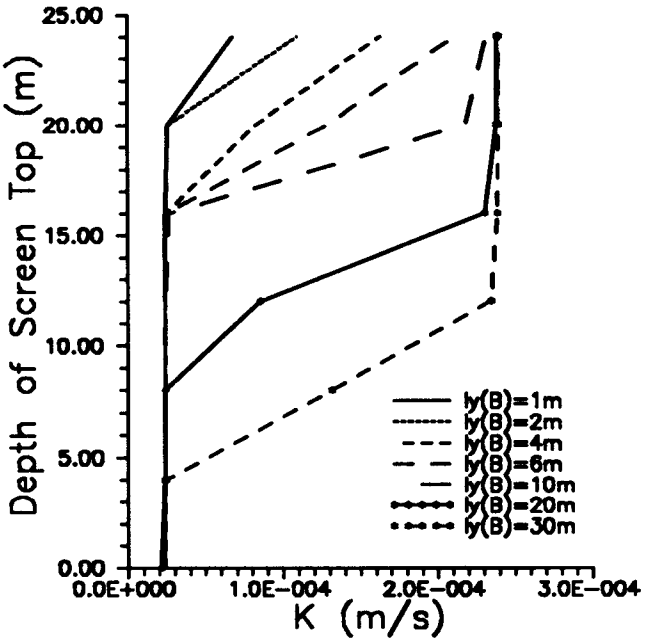

Figure II.B.9. Conductivity versus depth plot for Scenario 1 of Table II.B.1 (ly(B) = thickness of layer B)

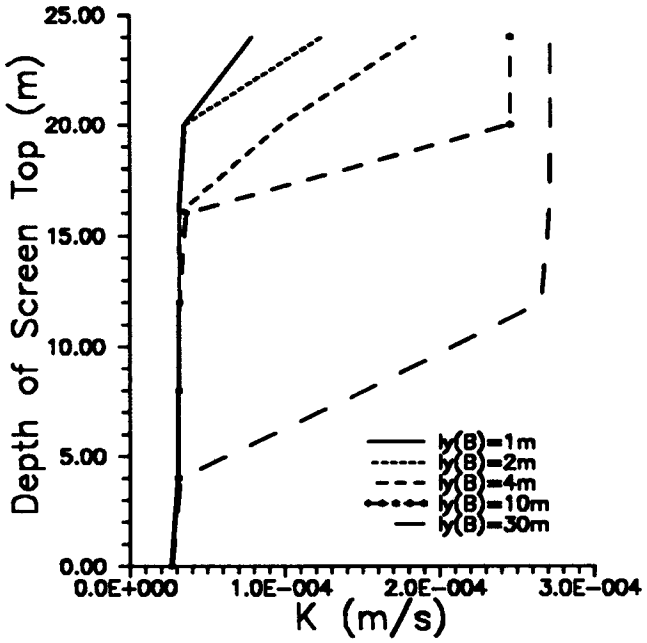

Figure II.B.10. Conductivity versus depth plot for Scenario 1A of Table II.B.1 (ly(B) = thickness of layer B)

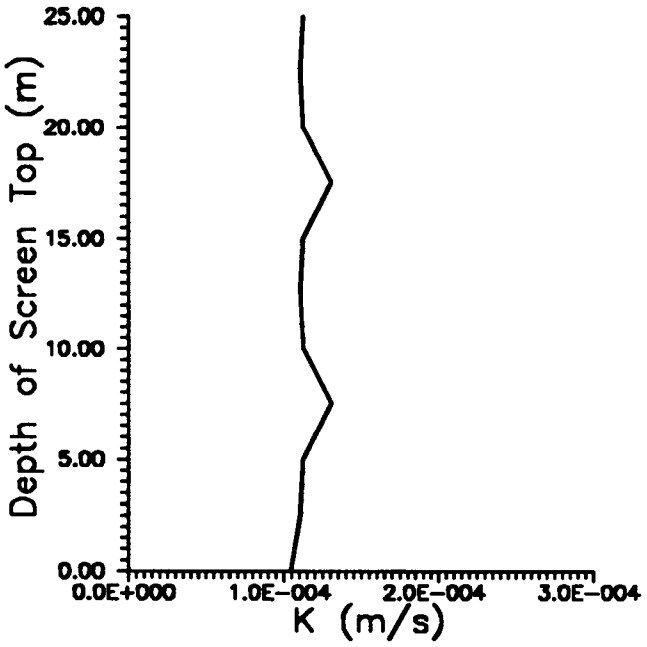

Figure II.B.11. Conductivity versus depth plot for Scenario 2 of Table II.B.1

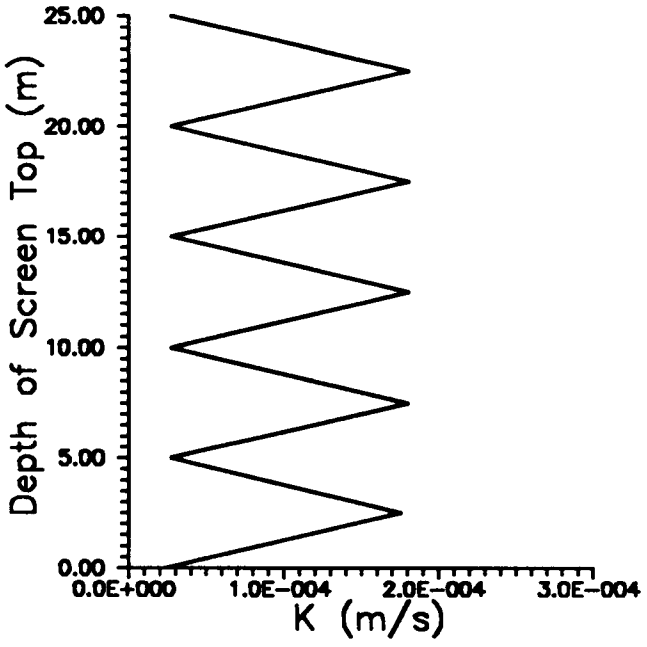

Figure II.B.12 - Conductivity versus depth plot for Scenario 3 of Table II.B.1

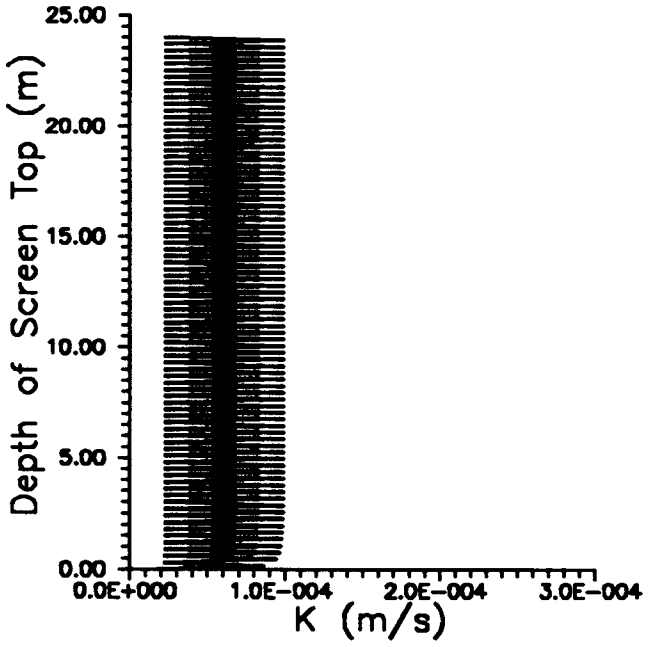

Figure II.B.13 - Conductivity versus depth plot for Scenario 7 of Table II.B.1

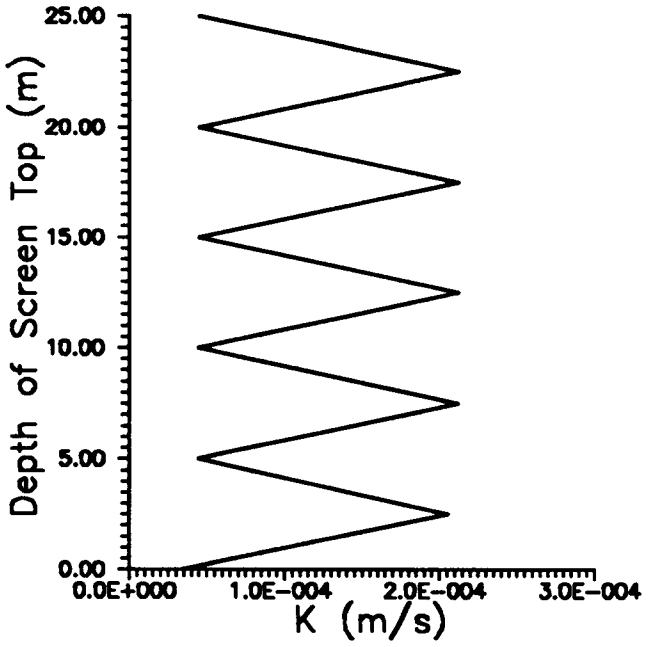

Figure II.B.14 - Conductivity versus depth plot for Scenario 3A of Table II.B.1

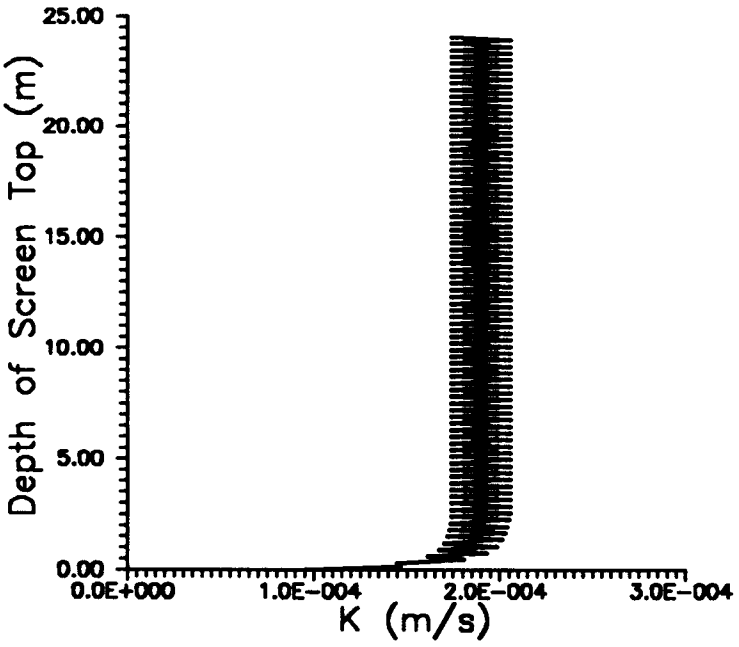

Figure II.B.15 - Conductivity versus depth plot for Scenario 7A of Table II.B.1

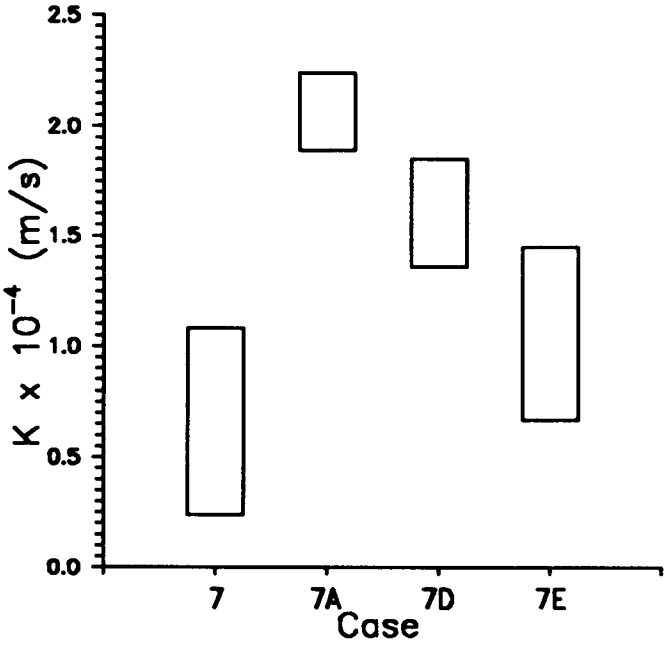

Figure II.B.16 - Plot depicting the range of calculated conductivities for the high permeability skin case. Cases 7A, 7D, and 7E display results for increasing anisotropy within the skin ($K_h > K_v$).

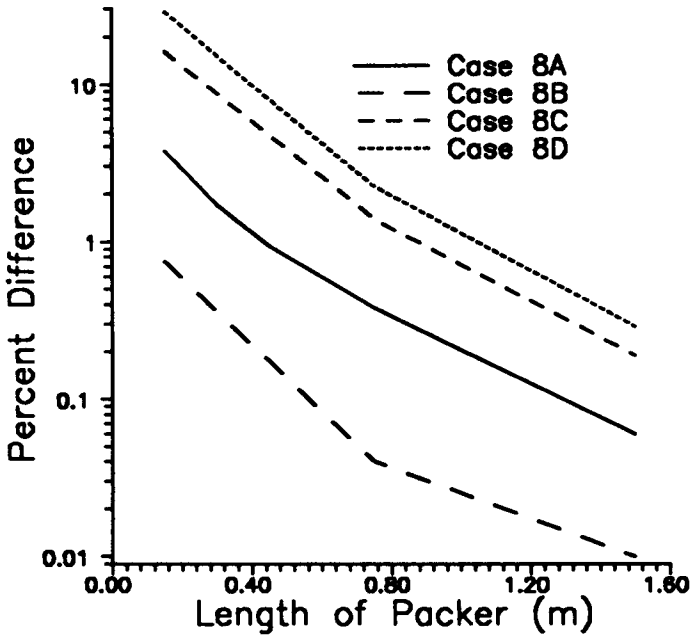

Figure II.B.17 - Packer length versus normalized difference plot for Cases 8A-8D of Table II.B.1.

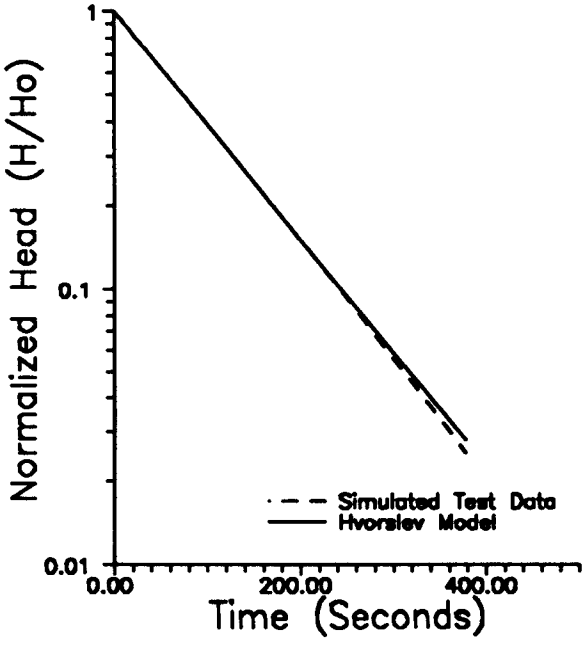

Figure II.B.18 - Plot showing the results of the Hvorslev analysis applied to simulated test data from Scenario 7A

C. SLUG TESTS WITH OBSERVATION WELLS

Introduction

The common methods for the analysis of slug-test data are based on analytical solutions to a partial differential equation describing the flow of groundwater in response to an instantaneous slug of water at a central well. Cooper et al. (1967) developed a rigorous solution for the case of the transient head response due to a slug test in a fully penetrating well in a confined aquifer. McElwee et al. (1989) performed a sensitivity analysis of slug tests using the Cooper et al. solution to represent system behavior. They showed how a slug test could be designed to yield reasonably accurate estimates of the aquifer transmissivity through appropriate selection of the number and times of measurements. As demonstrated in that work and as also shown by Cooper et al. (1967), the head response at the central well during a slug test is not very sensitive to the storage coefficient. In this section, an investigation of the radial dependence of the analytical solution of Cooper et al. (1967) is undertaken. The results of this investigation show that the use of one or more observation wells (i.e. wells other than the central well at which the slug was introduced) can vastly improve the parameter estimates, particularly the estimate of the storage coefficient.

Analytical Solution of Cooper et al. (1967)

The analytical solution of Cooper et al. (1967) can be written as

$$H(\alpha, \beta, H_0, r/r_s) = \frac{2H_0}{\pi} \int_0^\infty \frac{e^{-\beta u^2/\alpha}}{\Delta(u)} F(u, \alpha, r/r_s)\, du \quad \textbf{(II.C.1)}$$

where

$$F(u, \alpha, r/r_s) = [J_0(u\frac{r}{r_s})\,[uY_0(u) - 2\alpha Y_1(u)] - Y_0(u\frac{r}{r_s})\,[uJ_0(u) - 2\alpha J_1(u)]];$$

$$\Delta(u) = [uJ_0(u) - 2\alpha J_1(u)]^2 + [uY_0(u) - 2\alpha Y_1(u)]^2;$$

$$\beta = Tt/r_c^2;$$

J_i, Y_i = Bessel functions of the first and second kind, respectively, of order i;

$$\alpha = \frac{r_s^2}{r_c^2} S;$$

r_s, r_c = radius of the screen and casing, respectively;
H_0 = initial head displacement.

Equation (II.C.1) shows that slug-test responses can be expressed as a function of four parameters: α, a parameter related to screen and casing radii and the storage coefficient; β, a dimensionless time involving transmissivity and the casing radius; H_0, the initial head displacement; and r/r_s, the distance to an observation well divided by the screen radius. In the following discussion, this solution is employed to examine the sensitivity of slug-test responses to model and aquifer parameters, with an emphasis on the dependence of the sensitivity coefficients on the r/r_s ratio. Introductory material on sensitivity analysis can be found in Appendix B of this report.

Sensitivity to H_0

Figure II.C.1 depicts the sensitivity of slug-test responses to H_0 versus time for observation wells located at various radial distances from the stressed well. The maximum sensitivity occurs at $r=r_s$ (Figures II.C.1 and II.C.3) and decreases with time and radial distance. Figure II.C.1 shows that an observation well will respond in time with a bell-shaped curve whose maximum amplitude decays with distance from the slugged well. At $175r_s$, the maximum amplitude has fallen to about .01 H_0 for $\alpha = 10^{-3}$ (see Figure II.C.2). As shown in Figures II.C.2 and II.C.4, smaller values of α will result in larger responses in space and time. Figures II.C.3 and II.C.4 clearly show how the area of influence of a slug test spreads with time.

Sensitivity to Transmissivity

Figures II.C.5-8 illustrate the dependence of the sensitivity to transmissivity on time, distance, and α. As shown by Figures II.C.5 and II.C.6, the normalized sensitivity has both positive and negative lobes except when observations from the stressed well ($r=r_s$) are considered. Figures II.C.7 and II.C.8 show that the sensitivity decays rapidly with increasing r. Figures II.C.6 and II.C.8 illustrate the dependence on α. The maximum amplitude of the sensitivity appears to vary inversely with α (Figure II.C.6), although this dependence is somewhat weakened at the central well (Figure II.C.8). As noted previously, the smaller the value for α, the greater the area

of influence of the slug test.

Sensitivity to Storage

Figures II.C.9-12 illustrate the dependence of the sensitivity to storage on time, distance, and α. The maximum sensitivity does not occur at the central well, but rather at a distance of about 5 screen radii from the central well for $\alpha=10^{-3}$ (Figures II.C.9 and II.C.11). Figure II.C.10 shows that, for a given radial location, the maximum amplitude of the sensitivity is inversely proportional to α and occurs at earlier times with smaller values of α. Figure II.C.11 shows that the normalized sensitivity plot widens and decays with increasing time. The dependence relationships depicted in Figure II.C.12 again show that the signal propagates much farther from the well for smaller values of α.

Correlation of Sensitivity to Transmissivity and Storage

Figure II.C.13 depicts plots of the sensitivity coefficients for transmissivity and storage for measurements taken at the stressed well. Except for the large difference in amplitudes, the curves are extremely similar. This plot indicates that the head measurements at the stressed well are much more sensitive to transmissivity than to storage. The limited sensitivity to storage that does exist is highly correlated with the sensitivity to transmissivity. Thus, the storage estimate obtained from a slug test using data from the stressed well will be unreliable because of the ill-conditioned nature of the sensitivity summation matrix (see Appendix B).

Figure II.C.14 depicts plots of the sensitivity coefficients for transmissivity and storage for measurements taken at a well located at ten screen radii from the stressed well. This figure shows that the sensitivity plots are similar in amplitude but much different in shape when measurements from an observation well are used. This plot indicates that the correlation between transmissivity and storage is dramatically reduced by using data from an observation well in a slug test. The much lower correlation produces a much better conditioned sensitivity summation matrix, leading to a more reliable estimate for the storage coefficient.

Theoretical Example

From previous permeameter analyses and long-term pumping tests, we have obtained estimates for the average hydraulic properties at GEMS (K=91.29 m/day; T=973.8 m^2/day; S=.00063). We can use these parameter estimates to simulate a hypothetical slug test with observation wells at GEMS. We assume that the stressed

well is .102 m in diameter and that observation wells are located 1.52 and 3.05 meters from the stressed well. All wells are assumed to fully penetrate the 10.6 meter thick sand and gravel interval. Measurements at the observation wells are assumed to have been taken below packers isolating the screen from the open casing. The simulated data are rounded to the nearest .03 meters and then analyzed using SUPRPUMP, a well-test analysis program developed at the Kansas Geological Survey (Bohling and McElwee, 1992). The results are given below for analyses using three different data sets: 1) data from the stressed well only; 2) data from the stressed well and one observation well; and 3) data from the stressed well and both observation wells.

	Data Set 1	Data Set 2	Data Set 3
Range of T	951.1-1070.1	965.8-985.9	968.5-987.2
Range of S ($x10^{-3}$)	.178-.722	.616-.666	.609-.648
Correlation	.98	.54	.44
rms deviation	.026	.026	.025
Remarks	Trouble converging	Converged rapidly	

Note that although the addition of the observation well data does not greatly improve the model fit (root-mean-square (rms) deviation ($\sqrt{s^2}$ of Appendix B) changes little), the width of the parameter ranges and the magnitude of the correlation are significantly decreased. The decrease in the parameter correlation results in the parameter estimation problem being much better behaved, which is reflected in the rapid convergence of the least-squares iterative procedure. Note that the parameter ranges are based on approximate confidence intervals calculated using the estimated standard error defined in Appendix B.

Results From Slug Tests in the Dakota Aquifer

A program of well testing is being carried out by the Kansas Geological Survey as part of a regional study of the Dakota aquifer in Kansas. At one site in

Lincoln County, Kansas, two wells (.102 and .051 meters in diameter), screened over similar intervals, are located 6.46 meters apart. A series of slug tests was carried out at this site to illustrate some of the concepts discussed in this section. These tests consisted of introducing a slug at the larger of the two wells and measuring the responses both at the stressed well and at the observation well. Measurements from the observation well were taken using a transducer placed below a packer located just above the top of the screen. The packer enabled effects associated with wellbore storage at the observation well to be kept very small. Three different data sets were used in the analysis of the test responses: 1) data from the stressed well only; 2) data from the observation well only; and 3) data from both the stressed well and the observation well. The results of these three analyses are

	Data Set 1	Data Set 2	Data Set 3
T (m^2/day)	6.98	8.07	8.26
S	$.20 \times 10^{-3}$	$.51 \times 10^{-4}$	$.52 \times 10^{-4}$
Correlation	.99	.27	.49
rms Deviation	.0024	.0030	.0040

Figure II.C.15 shows the field measurements and fitted model results for the analysis using the third data set. Although the actual parameter values for this site are not known, the results of the sensitivity analysis and the previous theoretical example indicate that the parameters from the second and third data sets are probably more representative of conditions at the site than the parameters from the first data set. Note that the dramatic decrease in correlation seen when data from an observation well were employed would make the [A] matrix of equation (B4) much better conditioned.

The results of the theoretical and field examples clearly show that use of observation wells can greatly improve the reliability of parameters obtained from slug tests. Although it may not be practical to install observation wells solely for use in a slug test, the density of pre-existing monitoring wells at many sites is such that this technique can be readily employed. Generally, the observation well must be fairly close (less than ten meters) to the stressed well in order that the signal can be

discerned from background noise. The storage coefficient must be quite small in order to see the effects of the slug test at greater distances from the stressed well. As described above, the observation well can be packed off in order to remove the lagging and damping of the signal that occurs due to wellbore storage at the observation well. If a packer is not employed, an analytical solution that incorporates wellbore storage at the observation well must be employed in the data analysis (e.g., Novakowski, 1989).

Figure II.C.1.

Variation of u'_{H_e} With Time For Various r/r_e

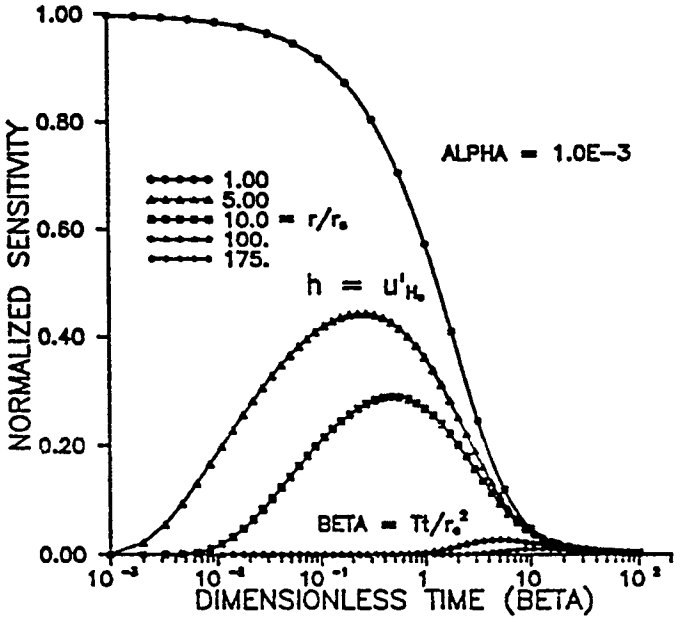

Figure II.C.2.

Variation of u'_{H_e} With Time For Various Alpha

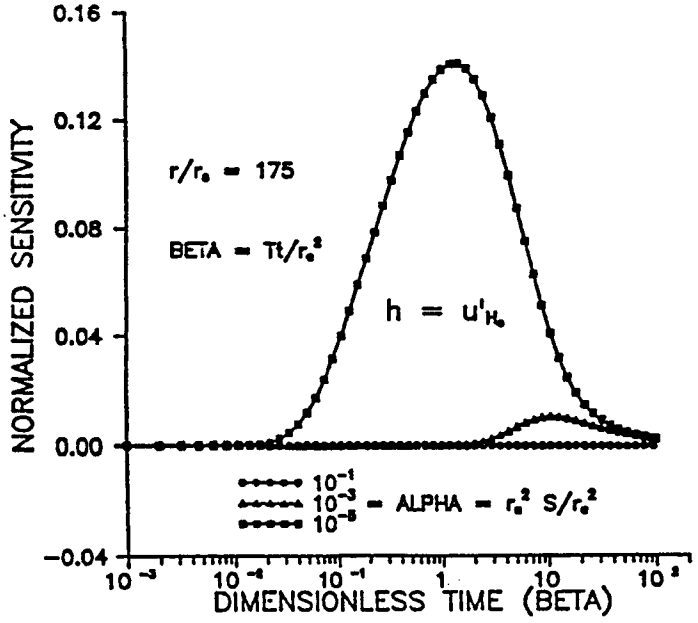

Figure II.C.3.
Variation of u'_{H_o} With Distance For Various Times

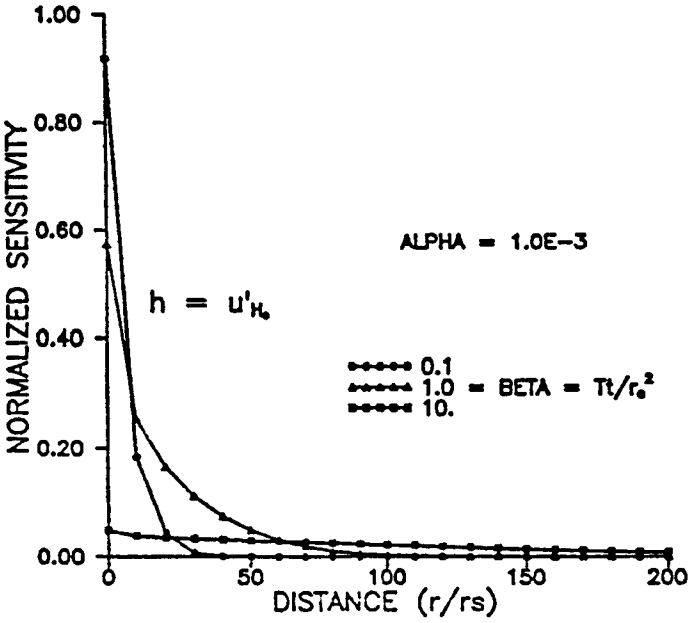

Figure II.C.4.
Variation of u'_{H_o} With Distance For Various Alpha

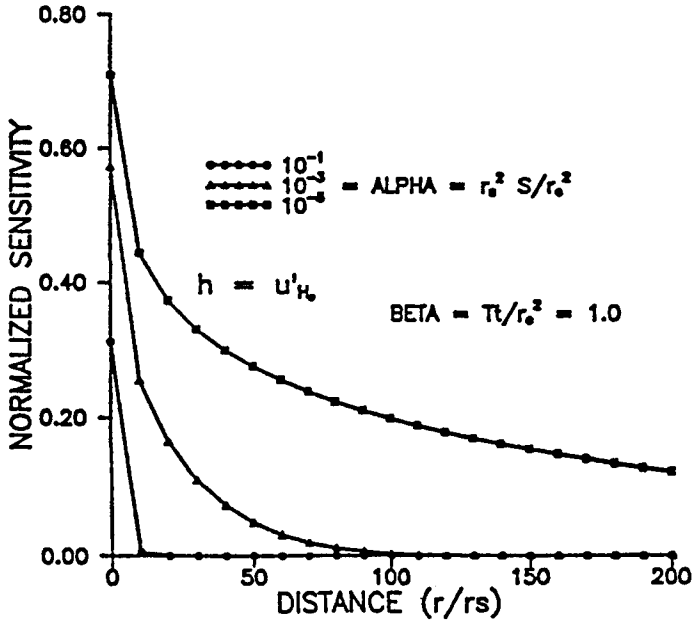

Figure II.C.5.

Variation of u'_T With Time For Various r/r_o

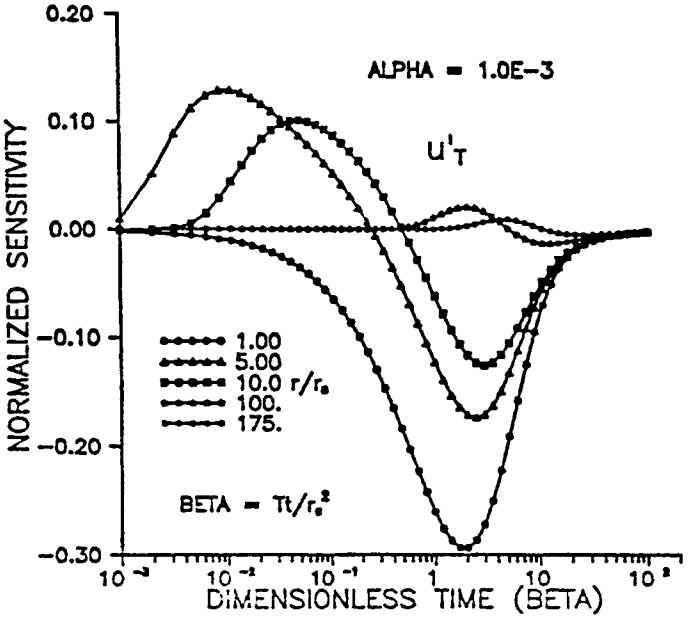

Figure II.C.6.

Variation of u'_T With Time For Various Alpha

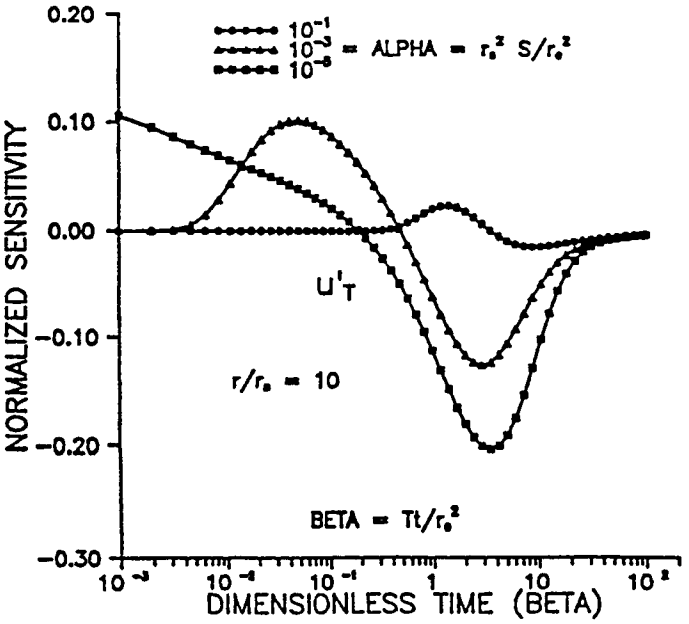

Figure II.C.7.
Variation of u'_T With Distance For Various Times

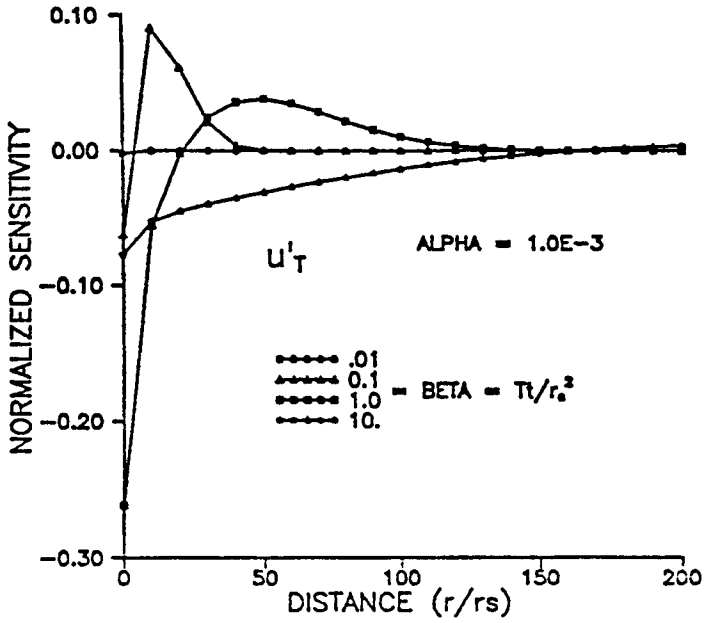

Figure II.C.8.
Variation of u'_T With Distance For Various Alpha

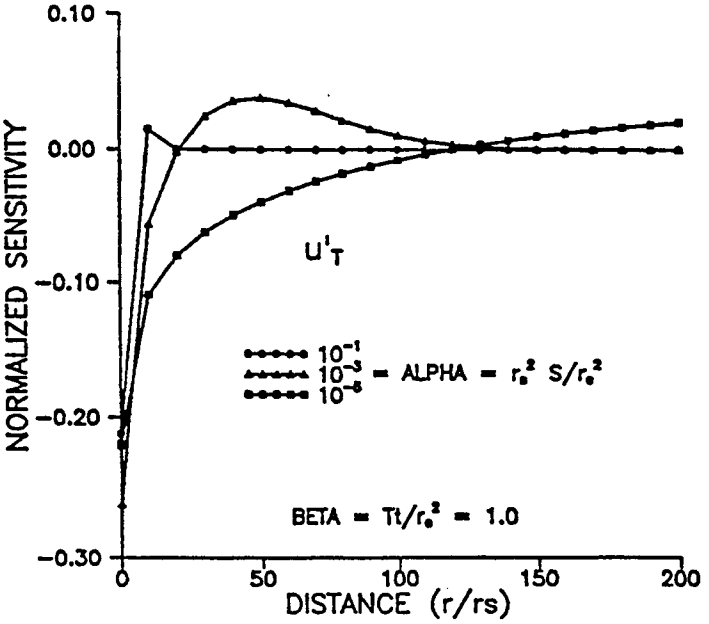

Figure II.C.9.
Variation of u's With Time For Various r/r_s

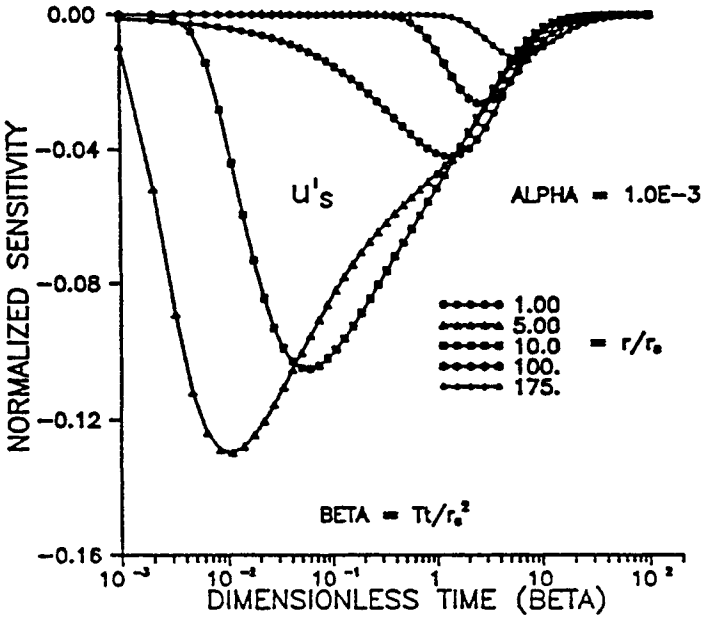

Figure II.C.10.
Variation of u's With Time For Various Alpha

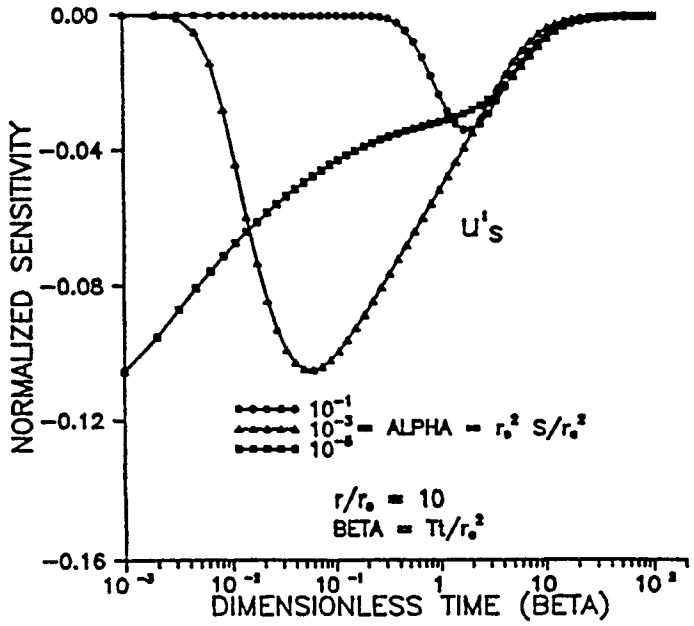

Figure II.C.11
Variation of u's With Distance For Various Times

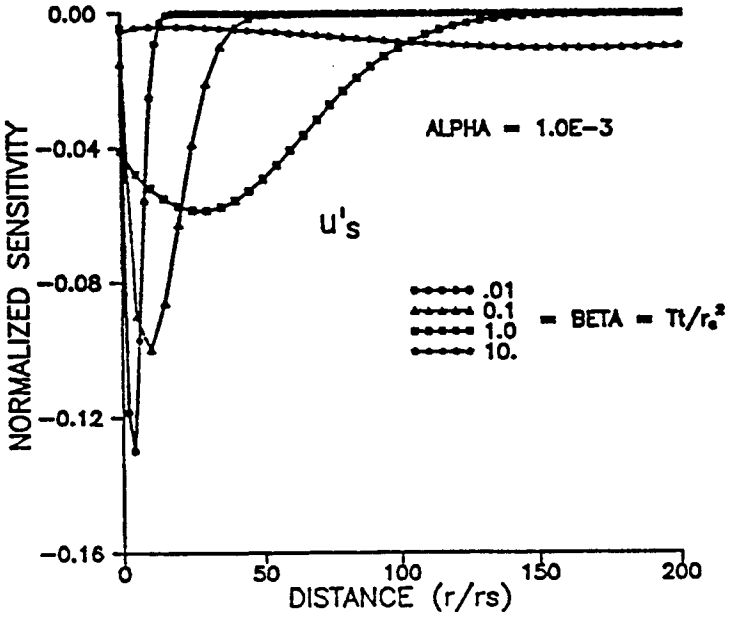

Figure II.C.12.
Variation of u's With Distance For Various Alpha

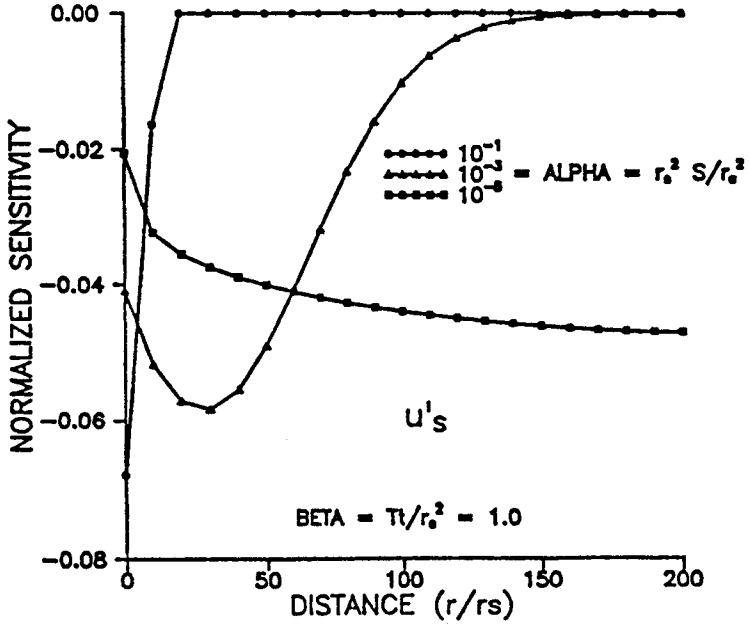

Figure II.C.13
Comparison of Sensitivities at the Screen Radius

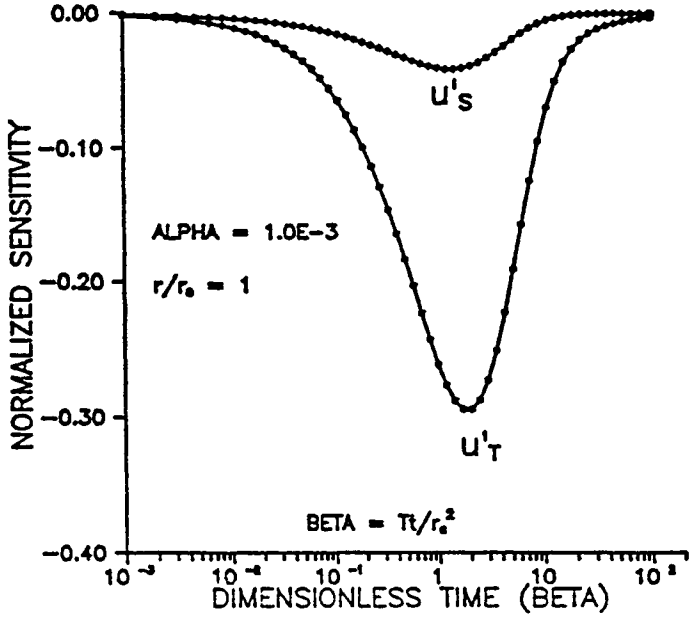

Figure II.C.14.
Comparison of Sensitivities at 10 Screen Radii

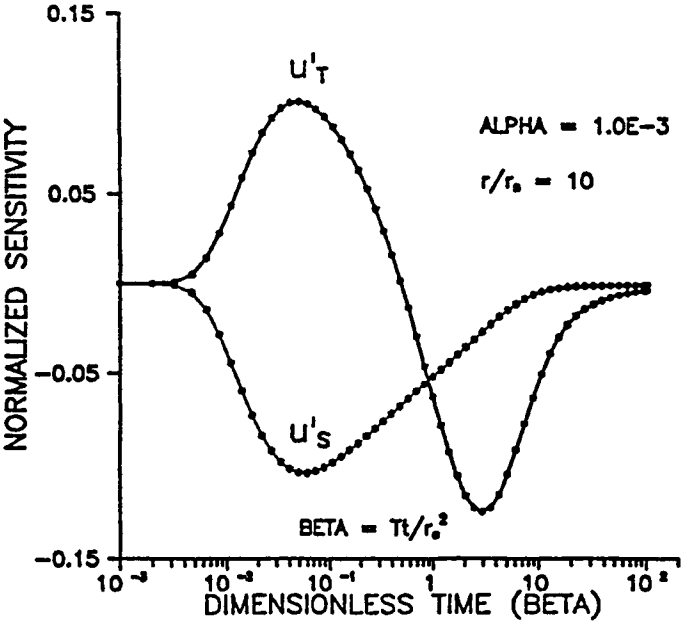

Figure II.C.15
Dakota Aquifer Test, Lincoln County Kansas

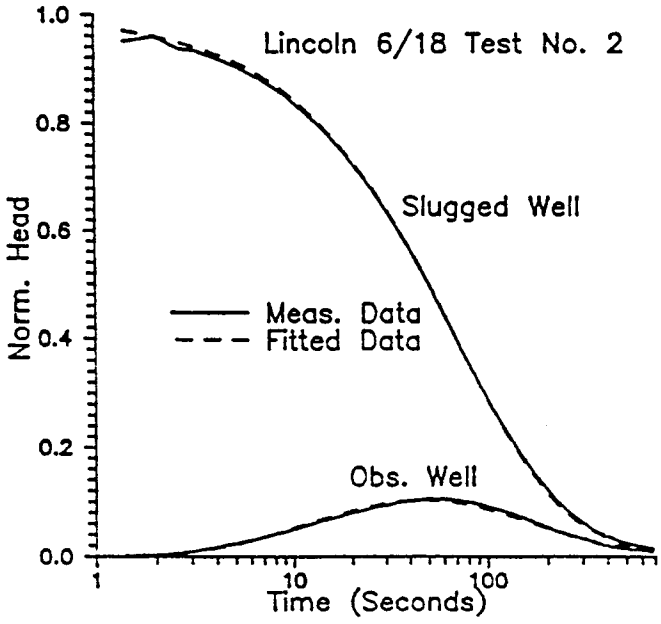

D. SLUG TESTS IN THE PRESENCE OF A WELL SKIN

Introduction

Conventional methods for analysis of slug-test data are based on a series of assumptions about the formation being tested. One of the more important of these assumptions is that the formation is homogeneous in the vicinity of the stressed well. In natural systems, however, there is often a near-well zone of disturbance (well skin) created during well drilling or development activities that has differing properties than the formation as a whole. The issue of how to analyze slug-test data from a well with a skin is one of considerable importance. In this section, an investigation of various approaches for analyzing data from a slug test in a well with a skin is undertaken. The results of this investigation show that it may be very difficult to accurately estimate formation properties from a slug test in the presence of a low permeability well skin.

Model for Slug Tests in the Presence of a Well Skin

Figure II.D.1 depicts the configuration of interest here. A slug test is being performed in a well that is screened for the full width of a perfectly confined aquifer (b). In the immediate vicinity of the well, there is a well skin of radius R_S. The well skin extends through the full thickness of the aquifer and has transmissive (T_1) and storage (S_1) properties that may be different from those of the aquifer (T_2 and S_2). Note that the well may have a screen (r_w) of different radius than the casing (r_c). The change in water level due to the introduction of the slug is denoted by H_0.

Moench and Hsieh (1985) have proposed a mathematical model to describe head responses to a slug test in this configuration. The mathematical model is defined by the following partial differential equations and auxiliary conditions:

Governing equations:

$$\frac{\partial^2 H_1}{\partial r^2} + \frac{1}{r}\frac{\partial H_1}{\partial r} = \frac{S_1}{T_1}\frac{\partial H_1}{\partial t}, \quad r \le R_s \qquad \text{(II.D.1)}$$

$$\frac{\partial^2 H_2}{\partial r^2} + \frac{1}{r}\frac{\partial H_2}{\partial r} = \frac{S_2}{T_2}\frac{\partial H_2}{\partial t}, \quad r \ge R_s \qquad \text{(II.D.2)}$$

Initial conditions:

$$H_1(r,0) = H_2(r,0) = 0, \quad r > r_w \qquad \textbf{(II.D.3)}$$

$$H_1(r_w,0) = H_0 \qquad \textbf{(II.D.4)}$$

Boundary conditions:

$$\pi r_c^2 \left(\frac{\partial H_1}{\partial t}\right)_{r_w} = \left(2\pi T_1 \frac{\partial H_1}{\partial r}\right)_{r_w} \qquad \textbf{(II.D.5)}$$

$$H_1(R_s,t) = H_2(R_s,t) \qquad \textbf{(II.D.6)}$$

$$T_1 \left(\frac{\partial H_1}{\partial r}\right)_{R_s} = T_2 \left(\frac{\partial H_2}{\partial r}\right)_{R_s} \qquad \textbf{(II.D.7)}$$

$$H_2(\infty,t) = 0 \qquad \textbf{(II.D.8)}$$

Note that two conditions (equations (II.D.6) and (II.D.7)) are required in order to ensure continuity of flow across the boundary between the well skin and the aquifer.

Equations (II.D.1)-(II.D.8) describe the flow conditions of interest here. Moench and Hsieh (1985) present an analytical solution for the functions H_1 and H_2 that satisfy these conditions. Their solution is used here to assess the sensitivity of the head response to various model parameters.

Sensitivity to T_1 and T_2

Figures II.D.2 and II.D.3 depict the sensitivity of head at the stressed well to the transmissivity of the skin and the aquifer. Figure II.D.2 shows the sensitivity

coefficients (see Appendix B for an introduction to sensitivity coefficients) for the case when the transmissivities of the skin and aquifer are equal, while Figure II.D.3 illustrates conditions when the skin transmissivity is an order of magnitude smaller than that of the aquifer. In both cases, the plots of the sensitivity coefficients for T_1 and T_2 are very similar in shape, although the plot for T_2 is slightly shifted towards larger times. Note that the maximum amplitude of the sensitivity plots is inversely proportional to the transmissivity. The lower sensitivity for T_2 displayed in Figure II.D.3, coupled with the similarity in the shape of the two sensitivity plots (correlation between the two sensitivity coefficients is large), indicates that it is going to be very difficult to accurately estimate T_2 using the measured heads. The small sensitivity to T_2 and the large correlation with T_1 will result in the sensitivity summation matrix being poorly conditioned and an unreliable T_2 estimate (see Appendix B). Note that at observation points other than the stressed well there is some difference in shape between the sensitivity coefficients for T_1 and T_2. The amplitude of the sensitivities, however, decays rapidly, making it difficult to utilize these differences. Also note that the sensitivities displayed in Figures II.D.2 and II.D.3 were computed assuming a skin radius equal to ten times the well radius. Although not shown here, the head response at the slugged well is rather insensitive to the storage properties of both the skin and the aquifer. McElwee et al. (1989) and Section II.C of this report discuss the sensitivity of slug-test responses to the storage coefficient in more detail. As discussed in those reports, it is very difficult to obtain a reliable estimate of the storage properties of a system using head measurements from the slugged well.

Effect of Varying the Skin Radius

Figures II.D.4 and II.D.5 show how slug-test responses change with variations in the skin radius. Regardless of the location of the observation point, increasing the skin radius shifts the head response curve to larger dimensionless times when $T_1 < T_2$. Figure II.D.4 shows the normalized head in the slugged well for various skin radii, while Figure II.D.5 is a similar plot for an observation well located at 100 well radii away from the slugged well. Note that the response in the observation well declines with increasing skin radius for $T_1 < T_2$, as would be expected.

Correlation Between T_1 and R_s

Figure II.D.6 depicts sensitivity of head at the stressed well to the transmissivity of the skin and to the skin radius. Note that the sensitivity to the skin radius is smaller than that to the skin transmissivity and of an opposite sign. The

shape of the two sensitivity plots is very similar, however, so the absolute magnitude of the correlation between the two sensitivity coefficients is very large. As discussed earlier, a large correlation between two sensitivity coefficients can make it very difficult to reliably estimate one or both of those two parameters. There may be many pairs of values of T_1 and R_s that give equally good results. In some instances, the approximate value of the skin radius may be known based on the diameter of the hole created by the drilling equipment. In such cases, the skin radius can be assumed known and not estimated in the fitting process.

Analyzing a Slug Test at a Well With a Skin Using a Uniform Aquifer Model

Usually it is not known in advance whether the well being tested has a skin, so slug-test data are normally initially analyzed using a model that assumes that the aquifer is uniform. A commonly used uniform aquifer model for slug tests is that of Cooper et al. (1967) (henceforth designated the C-B-P model). An important issue to consider is the nature of the effective transmissivity estimated using this model when a well skin is present. Figure II.D.7 displays a plot of simulated data computed using the Moench and Hsieh (1985) model and the best-fit curve to the data obtained with the C-B-P model. Note that the fitting was performed using SUPRPUMP, a well-test analysis package developed at the Kansas Geological Survey (Bohling and McElwee, 1992). This figure shows a systematic deviation between the simulated data and the model fit for the case of $T_1 < T_2$. This deviation consists of the simulated data lying above the C-B-P model curve at early times and below the C-B-P model curve at late times.

The effective transmissivity calculated from the C-B-P model must be some sort of average of the skin and aquifer transmissivities. We have found that the following empirical equation can provide reasonable estimates of the effective transmissivity from a C-B-P analysis:

$$\frac{1}{T_{eff}} = \left[\frac{\ln(R_s/r_w)}{T_1} + \frac{\ln(r_{eff}/r_w) - \ln(R_s/r_w)}{T_2}\right] \quad \textbf{(II.D.9)}$$

where

$r_{eff}/r_w = [C/S]^{.5}$, $1 \le C \le 2$;

r_{eff} = effective radius of influence of the slug test;

C = empirical coefficient;

S = storage coefficient.

Although the effective parameter obtained from this equation is heavily weighted by T_1, the lowest value of transmissivity (whether it is in the aquifer or the skin) will be the dominant factor in determining the effective transmissivity. Note that the storage coefficient is assumed to be the same in the skin and the aquifer for this empirical equation. Also note that, as expected, the effective transmissivity is independent of the height of the initial slug.

A series of slug-test simulations were run using the Moench and Hsieh (1985) model and the simulated data were analyzed using the C-B-P model. The effective transmissivities estimated from the C-B-P model were then compared to the effective transmissivities estimated from the empirical equation. Table II.D.1 lists the results of this exercise. Note that a constant storage coefficient of .001 was used in all of the simulations and the head data were assumed to come from an observation well 100 well radii from the stressed well. These results demonstrate the viability of the empirical expression given in equation (II.D.9).

Analyzing a Slug Test at a Well With a Skin Using the Moench and Hsieh Model

If there is a systematic deviation between the measured data from a slug test and the best-fit CBP curve such as shown in Figure II.D.7, one possible explanation would be the existence of a low permeability well skin. The Moench and Hsieh (1985) model could be employed to analyze the test data in this situation. However, the results of the previously discussed sensitivity analysis indicate that there is considerable correlation between several of the parameters of this model. Thus, it is unclear how effective the model will be in estimating system parameters.

A theoretical investigation of the viability of the Moench and Hsieh model for the analysis of slug-test data was undertaken as part of this work. A slug test in a well with a low permeability skin was simulated with the Moench and Hsieh model assuming four observation wells at varying distances from the stressed well (r/r_w = 1, 25, 50, 100). Fifty- six time measurements between .01 and 1000. units of dimensionless time ($\beta = T_2 t / r_w^2$) were simulated. The data from all four wells were analyzed simultaneously with the Moench and Hsieh model assuming that the skin and aquifer transmissivities and the skin radius were unknown. The analysis was performed using the SUPRPUMP well-test analysis package (Bohling and McElwee, 1992). Table II.D.2 displays the result of the analysis and additional diagnostic output from SUPRPUMP. Note that the approximate 95% confidence intervals

indicate that T_1 and T_2 can be determined to within 40%, while the skin radius estimate is very unreliable (a physically unrealistic negative skin radius arises from the use of approximate confidence intervals). The underlying reasons for these results are revealed by looking at the diagnostic output from SUPRPUMP displayed in Table II.D.2. The sensitivity summation matrix indicates that the simulated data are much more sensitive to T_1 than the other parameters. Note the large correlation between T_1 and R_s shown by the sensitivity correlation matrix. The high degree of correlation between these two parameters and the large difference in the sensitivity of the simulated data to the model parameters results in very broad confidence intervals for the skin radius and a very large parameter correlation between the skin transmissivity and the skin radius. Note that the correlation between the two transmissivities is smaller than might have been expected from Figures II.D.2 and II.D.3 because of the use of data from observation points other than at the stressed well. Also note that these results are based on simulated data that have been truncated to the nearest .025 H_0. One would expect considerably worse results when the noise that will be found in actual applications is added to the truncated measurements employed here.

GEMS Field Application

Figures II.D.8 and II.D.9 display results of an analysis of a slug test performed at a well at GEMS that was suspected of having a low permeability well skin. Figure II.D.8 depicts the results of an application of the C-B-P model to the measured data. Note that there is a systematic deviation between the fitted model and the measured data that is similar to that seen in the theoretical example. Figure II.D.9 depicts the results of an application of the Moench and Hsieh model to the measured data. Note that although the fit is considerably better, convergence of the parameter estimation procedure was very difficult to achieve. The estimation procedure was very sensitive to the number of parameters being fit and the initial values of these parameters. In many cases, convergence could not be achieved due to the poorly conditioned sensitivity summation matrix. The sensitivity of the measured data to S_1 and S_2 was very low, so the best results were obtained by considering these parameters as known and setting them to reasonable values. Since R_s was highly correlated with T_1, it was considered known and set to .101 m, a value consistent with the diameter of the hole that is created by drilling with auger flights of the size used at GEMS. Table II.D.3 provides the results of the analysis and additional diagnostic output from SUPRPUMP. Note that the estimated conductivities must be considered

rather approximate because of the possible error introduced by considering R_s known when the data were actually fairly sensitive to this parameter. Also note that although the correlation between the sensitivity coefficients for the two conductivities is quite large, the magnitudes of the summed sensitivities are much closer than for the examples illustrated in Figures II.D.2 and II.D.3. The primary reason for this is that the estimate for the skin thickness used for GEMS well #04 is considerably smaller than that used in the previous examples. It is of interest to note that substitution of the parameters obtained with the Moench and Hsieh model into the empirical equation (assuming C=2 because of the low permeability skin) produced an effective transmissivity of .16 m/day, a value somewhat lower than the effective transmissivity estimated by the C-B-P model (.40 m/day). Given the uncertainty associated with the estimated parameters from the Moench and Hsieh model, however, the agreement between the two effective transmissivities must be considered quite good.

This field example coupled with the results of the theoretical simulation indicate that it can be very difficult to estimate system parameters using data from a slug test performed at a well with a skin. Unless one has additional information about the skin radius or the skin transmissivity, the parameters may be rather unreliable. One possible approach for getting a prior estimate of skin transmissivity would be to initially analyze the data with the Hvorslev model (Hvorslev, 1951). As Butler et al. (1990) point out, the hydraulic conductivity estimated from the Hvorslev technique will be very close to the conductivity of the skin due to the nature of the assumptions incorporated in the Hvorslev model. The skin conductivity could thus be considered as known and set to the Hvorslev estimate. One could then solve for the skin radius and aquifer transmissivity. Although further work needs to be done to fully assess this approach, it is of interest to note that a Hvorslev analysis of the field data yielded a hydraulic conductivity of .36 m/day, a value quite similar to the skin conductivity estimated by the Moench and Hsieh model (.34 m/day).

Table II.D.1

Effective Transmissivities in the Presence of a Skin

T_1	T_2	R_s/r_w	T_{CBP}	C (emp.)	T_{eff}
0.1	1.0	5	.205	2	.208
0.1	1.0	10	.155	2	.155
0.1	1.0	20	.126	2	.124
1.0	0.1	5	.175	1	.172
1.0	0.1	10	.260	1	.250
1.0	0.1	20	.456	1	.456

TABLE II.D.2
SUPRPUMP OUTPUT
THREE PARAMETER FIT

The estimated root-mean-squared residual is .2500E-01

The parameter values with approximate 95% confidence intervals are:

Parameter	Value	Lower Bound	Upper Bound
TRANSMISS. OF AQUIFER	1.000	.6227	1.377
TRANSMISS. OF SKIN	.1000	.5668E-01	.1433
SKIN RADIUS	10.00	-1.459	21.46

For the following arrays:
Col-Row 1 represents TRANSMISSIVITY OF AQUIFER (T2)
Col-Row 2 represents TRANSMISSIVITY OF SKIN (T1)
Col-Row 3 represents SKIN RADIUS (Rs)

Raw crossproducts matrix of normalized sensitivities:

	1	2	3	
1	.2357E-01	.8306E-01	-.3155E-01	| This matrix shows that
2	.8306E-01	1.093	-.4113	| T1 has the highest
3	-.3155E-01	-.4113	.1566	| sensitivity by far.

The reciprocal condition number of the
sensitivity crossproducts matrix is .1079E-02

Sensitivity correlation matrix:

	1	2	3	
1	1.000	.5174	-.5192	
2	.5174	1.000	-.9940	-------Very high correlation
3	-.5192	-.9940	1.000	between T1 and Rs.

Covariance matrix of normalized parameter variations:

	1	2	3
1	.3630E-01	-.6035E-03	.5727E-02
2	-.6035E-03	.4787E-01	.1256
3	.5727E-02	.1256	.3349

Parameter correlation matrix:

	1	2	3	
1	1.000	-.1448E-01	.5194E-01	
2	-.1448E-01	1.000	.9918	--------Very high correlation
3	.5194E-01	.9918	1.000	between T1 and Rs.

TABLE II.D.3
SUPRPUMP OUTPUT
GEMS WELL #04 ANALYSIS

The root mean squared residual is .3837E-02

The parameter values with approximate 95% confidence intervals are:

Parameter	Value	Lower Bound	Upper Bound
HY. COND. OF AQUIFER	1.23	1.10	1.36
HY. COND. OF SKIN	0.34	0.30	0.37

For the following arrays:
Col-Row 1 represents HY. COND. OF AQUIFER
Col-Row 2 represents HY. COND. OF SKIN

Raw crossproducts matrix of normalized sensitivities:

	1	2
1	.3073	.3013
2	.3013	.3644

The reciprocal condition number of the
sensitivity crossproducts matrix is .4993E-01

Sensitivity correlation matrix:

	1	2
1	1.000	.9003
2	.9003	1.000

Covariance matrix of normalized parameter variations:

	1	2
1	.2721E-02	-.2250E-02
2	-.2250E-02	.2294E-02

Parameter correlation matrix:

	1	2
1	1.000	-.9003
2	-.9003	1.000

Figure II.D.1. Schematic of a slug test in a well with a skin.

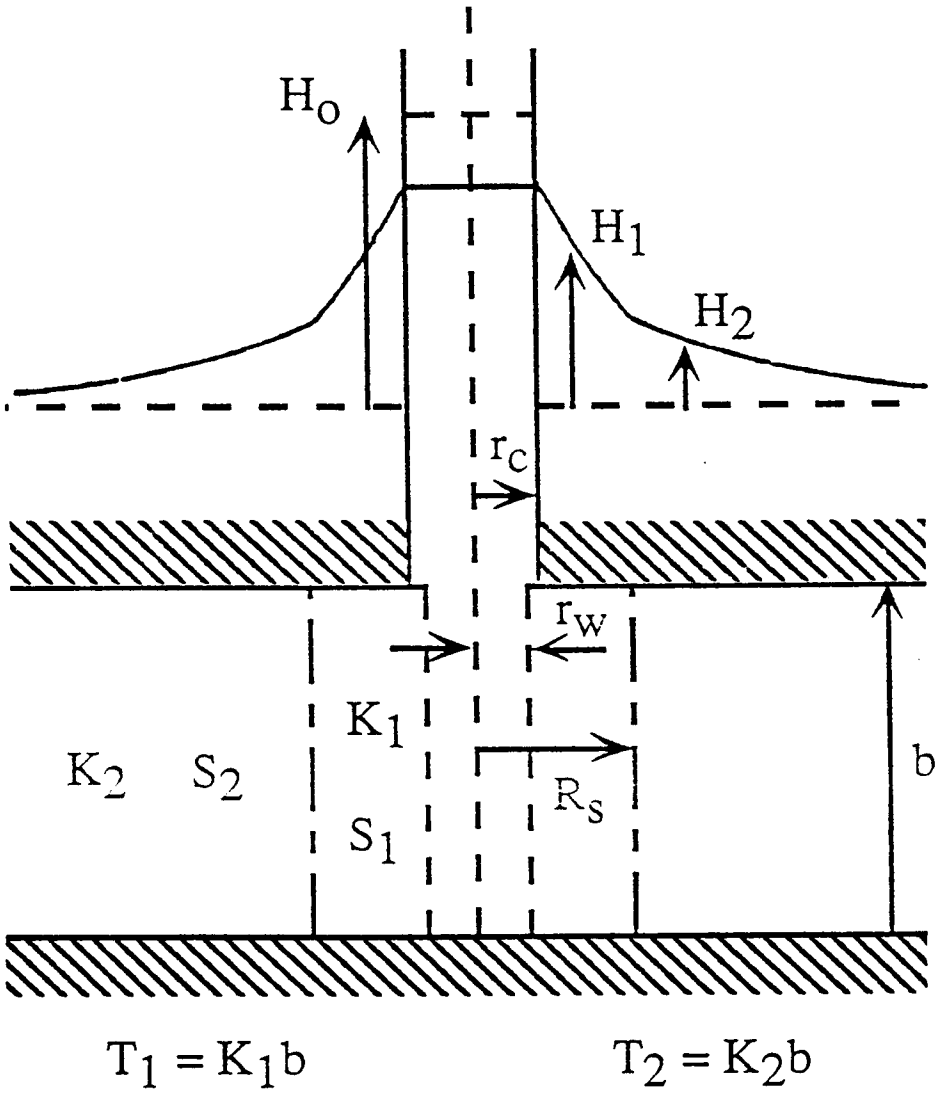

Figure II.D.2.

Variation of u'_T With Time at the Slugged Well

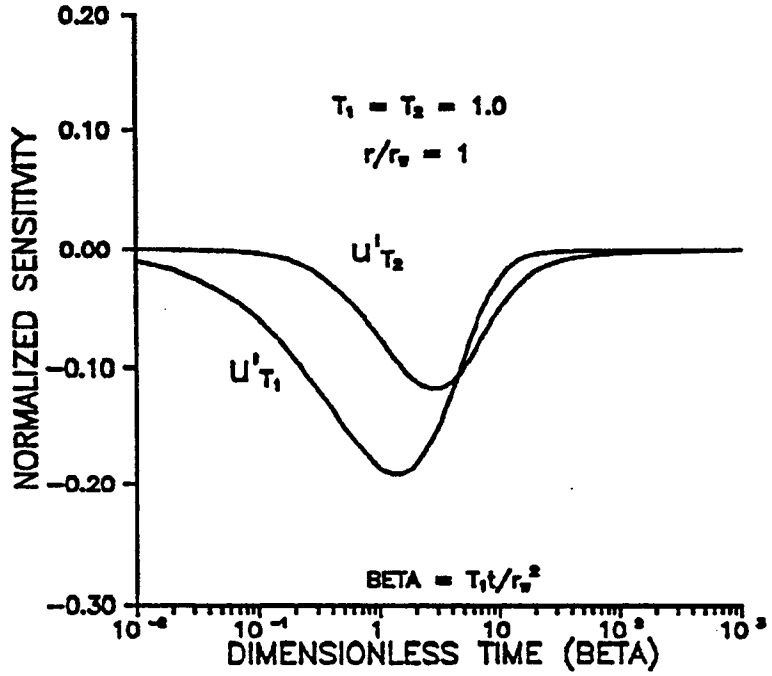

Figure II.D.3.

Variation of u'_T With Time at the Slugged Well

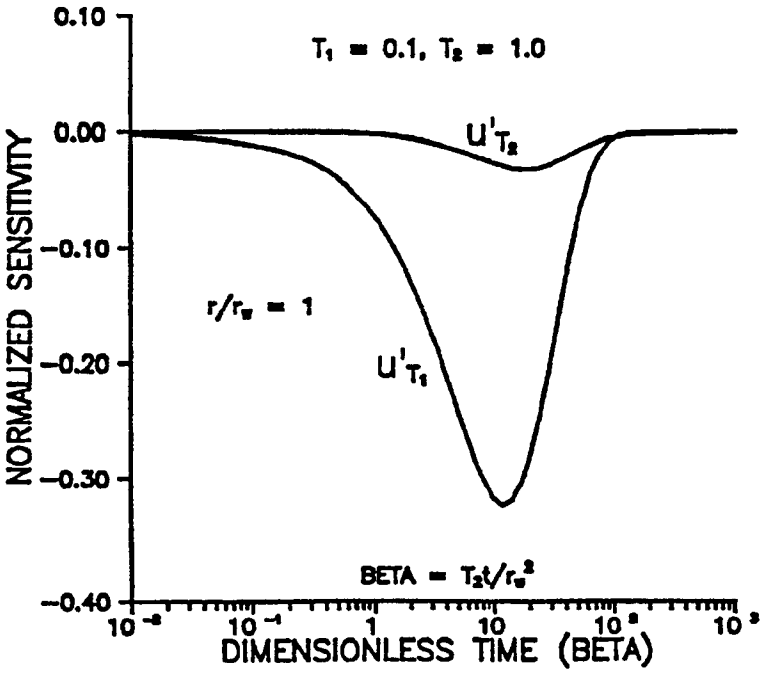

Figure II.D.4.

Variation of Head in Slugged Well With Skin Radius

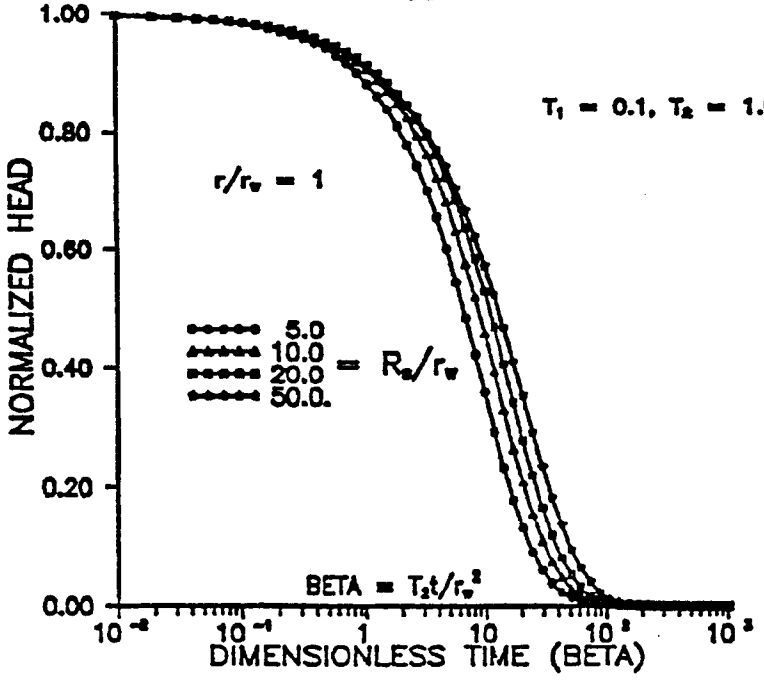

Figure II.D.5.

Variation of Head in Obs. Well With Skin Radius

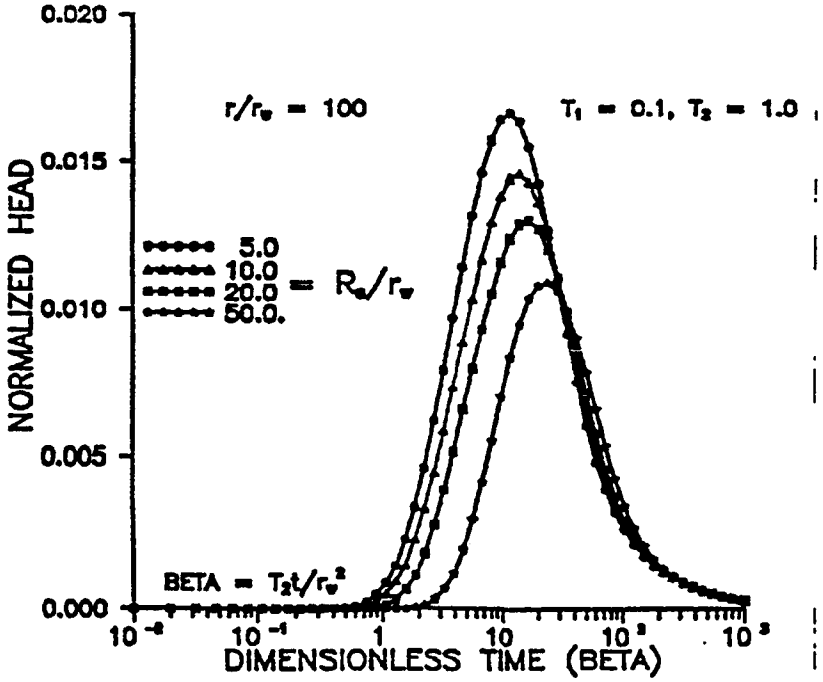

Figure II.D.6.

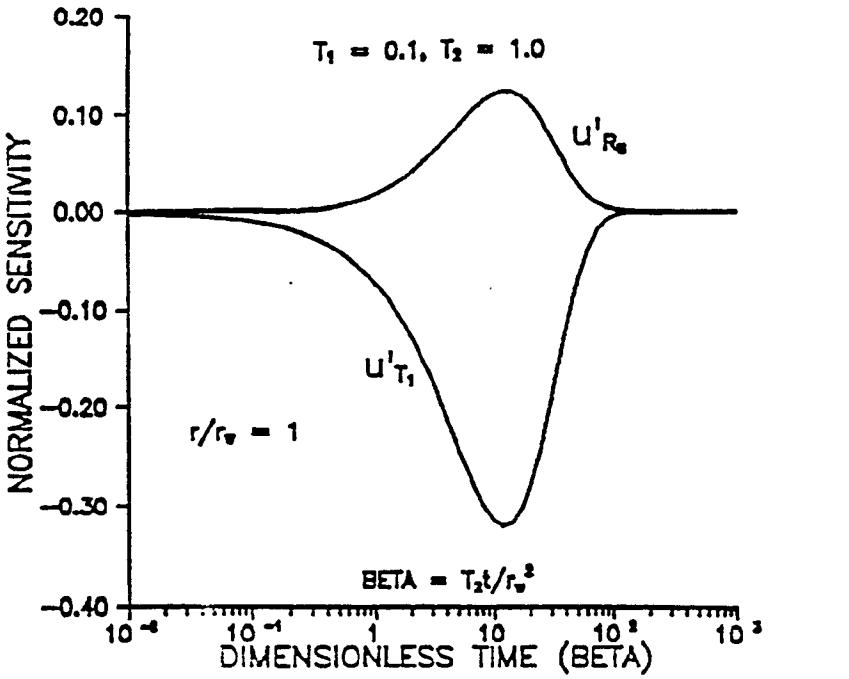

Figure II.D.7.

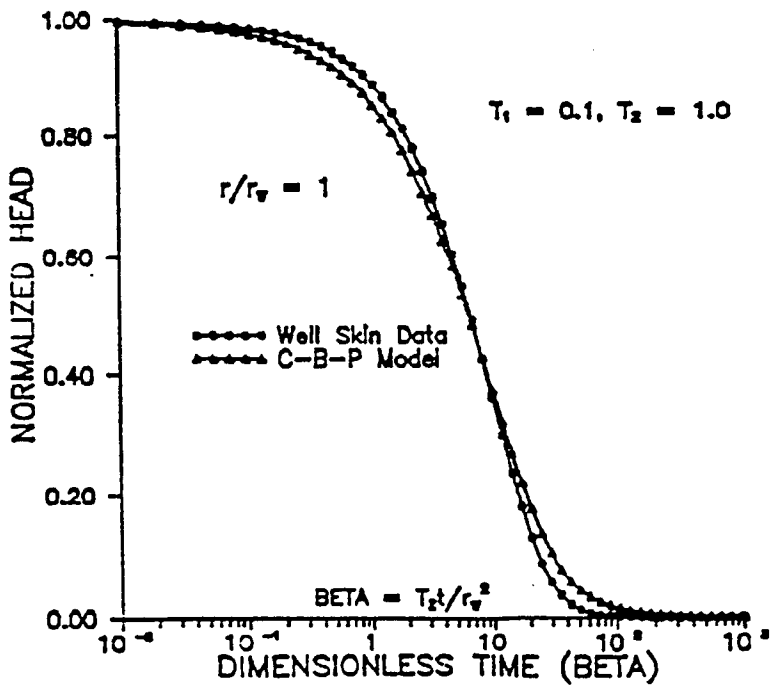

Figure II.D.8.

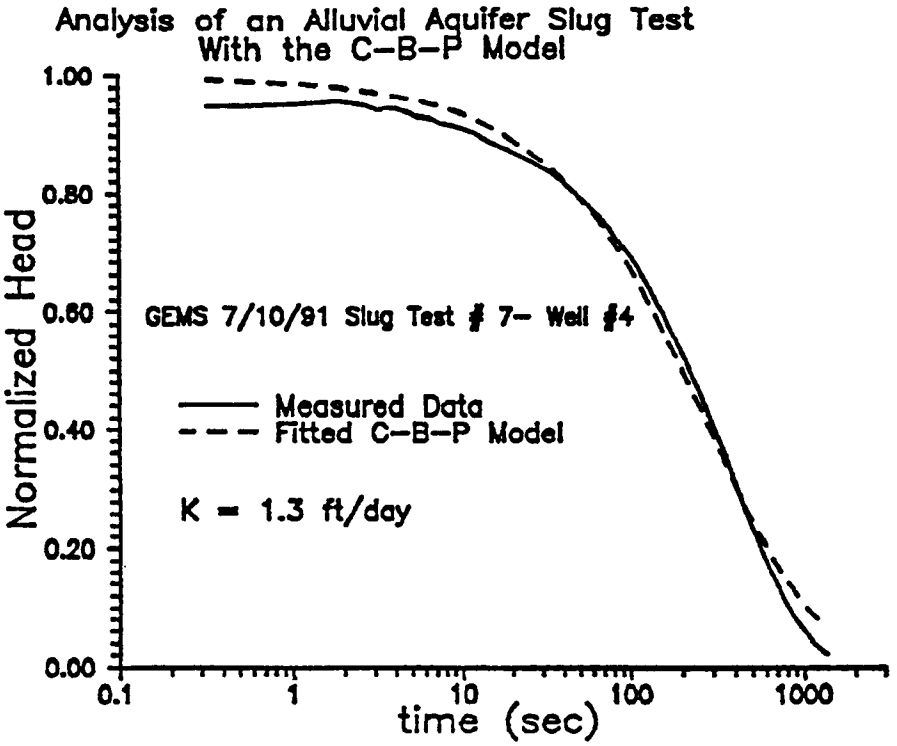

Figure II.D.9.

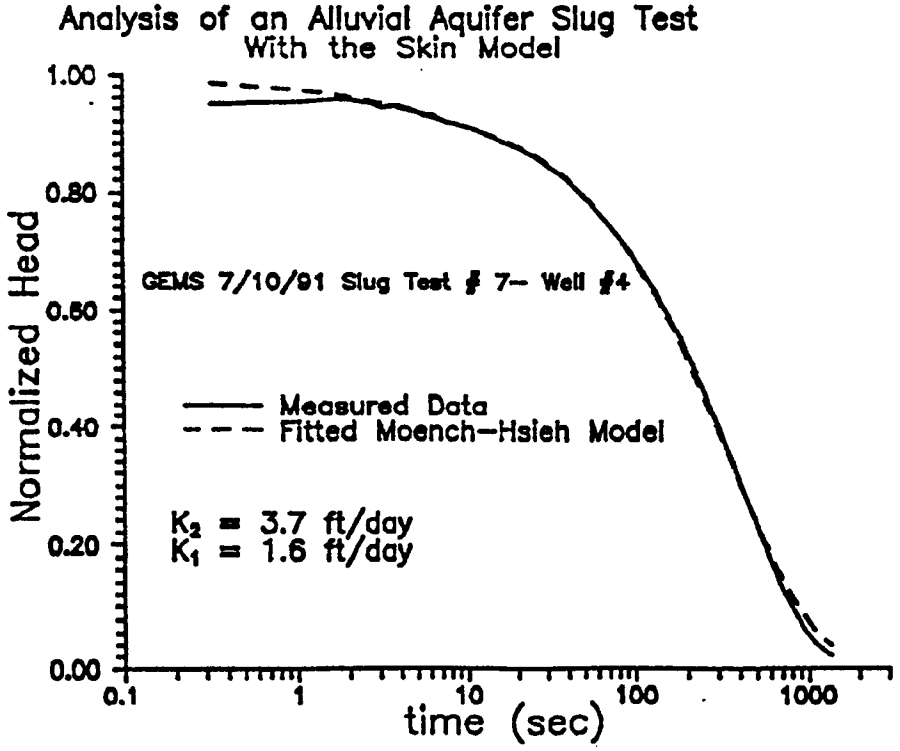

III. FIELD INVESTIGATIONS OF MULTILEVEL SLUG TESTS

A. KGS MULTILEVEL SLUG-TEST SYSTEM

In 1989, a slug-test system was developed at the KGS for the purpose of performing slug tests in wells of small diameters (.05 m ID) located in highly permeable alluvial units (McElwee and Butler, 1989). This equipment served as the basis of a multilevel slug test system that is being developed for the research described in this report. A prototype straddle-packer system for multilevel slug tests has been constructed at the KGS. The prototype system consists of two packers (each approx. .67 m in length when fully inflated) that are used to seal off the test interval from the adjacent screen. A section of .025 m ID PVC (SCH 40) pipe is connected to the central flow-through pipe of the top packer of the pair. A series of sections of the .025 m ID PVC pipe runs to a third packer located above the top of the screened interval. This pipe allows the pressure pulse initiating a slug test to be confined to the straddle-packer interval. The central flow-through pipe of the middle packer is closed off prior to testing. A slug test is initiated by adding or removing water to the casing above the third packer and then opening the central flow-through pipe in the middle packer. As with the original KGS slug-test system (McElwee and Butler, 1989), the central flow-through pipe is opened by the mechanical lowering of a plug attached to pump rods. Note that other initiation mechanisms, such as via pneumatic means (e.g., Orient et al., 1987) or water displacement using a solid object of a known volume, could also be employed with this system. Although the test interval can be up to several meters in length, it cannot be less than .29 m in the present configuration.

After the completion of testing at one level, the packers are deflated and the string of packers and pipes is moved until the straddle-packer interval is opposite the next zone to be tested. The string can be moved until the top of the third packer is raised above the static water level or lowered below the top of the screen. At that point, a section of PVC pipe must be either removed or added, respectively, to the pipe string connecting the straddle packer to the top packer before testing can be continued. In this manner, a series of multilevel slug tests can be readily performed across the entire screened interval of a well in a relatively short period of time. At shallow depths the string of packers and pipes can be lifted manually, while at deeper depths a special tripod and winch arrangement that was constructed during the first year of this project is employed. Note that the packers used in this system were

designed and constructed at the KGS. Commercially available packers for use in .05 m ID wells have central flow-through pipes that are .0125 m ID or smaller. Packers with larger flow-through pipes (.025 m and .019 m) were designed in an effort to ensure that the parameters estimated from the response data would be reflective of properties in the aquifer, and not the diameter of the flow-through pipe.

As stated above, slug tests are initiated by adding or removing water from the cased section of the well above the third packer. In all cases, pressure transducers (PS7000 and PS9000 series, Instrumentation Northwest, Inc.) placed above the third packer are employed to monitor water-level responses in the slugged well. During the field season, the transducers are calibrated in the laboratory on a monthly to bimonthly basis using the equipment described in subsection IV.B. Between laboratory calibrations, transducer functioning is checked in the field by measuring the height of the column of water above the transducer using an electric tape (Model 101 flat tape water meter, Solinst Canada Ltd.). The transducers are connected to one of two types of data acquisition devices: a datalogger (21X datalogger, Campbell Scientific, Inc.), or a data acquisition card (PC/IEEE 488 General Purpose Interface Board, IOtech, Inc.). Note that the data-acquisition card has been placed in the expansion chassis of a 20 MHZ laptop computer (NBA 386 SX, Chaplet Systems USA, Inc.).

In the following subsection, the use of this equipment in an initial series of multilevel slug tests at GEMS is described.

B. MULTILEVEL SLUG TESTS AT GEMS

Multilevel Tests at GEMS 2-5

The prototype KGS multilevel slug-test system was employed in a series of multilevel slug tests at GEMS. GEMS well 2-5 (depth = 20.67 m, screen length = 9.14 m), which is screened essentially through the entire sand and gravel section at the site, was used for these tests. An initial series of tests was run in which the slug consisted of the volume of water required to raise water levels 3.07 meters in the cased section of the well (H_0=3.07 m). As shown in Figure III.B.1, the slug-test responses measured at the different depths were very similar. Note that Table III.B.1 lists the depths corresponding to each test interval. Although the variation in the hydraulic conductivity values calculated from the core samples taken from a nearby well (GEMS 2-6) at these same depths was not large (Butler et al., 1991), greater variation in the conductivity estimated from the slug tests was expected. Therefore, the decision was made to repeat the series of slug tests using H_0's of different magnitudes to see if greater discrimination between test zones would be possible using a different H_0. Figure III.B.2 shows a plot for slug tests over the same intervals as Figure III.B.1 using a H_0 of approximately 1.65 m. A comparison of the two figures shows that, although there is little difference between tests using the same H_0, there is a considerable difference between tests using different H_0's. Normalized plots of the slug-test responses from a series of tests in the third test interval using differing H_0's are presented in Figure III.B.3. Note the dramatic dependence of the slug-test responses on magnitude of H_0. Dependence relationships of this form were seen in all the tested intervals. Table III.B.1 summarizes the parameters calculated from the slug-test responses for a subset of the tested intervals. In all cases, the higher the H_0, the lower the calculated conductivity. The inverse relationship between the magnitude of H_0 and the calculated conductivity does not appear to require a threshold value for H_0. Experiments have shown that differences in H_0 as small as .03 meters will still produce conductivity differences in the direction predicted from this relationship. Thus, the small difference in H_0 that exists between the slug tests shown on Figure III.B.1 or Figure III.B.2 could largely explain the differences displayed on those plots. Note that when special care was taken to ensure that the same volume was used for the slug in repeat tests at a given interval, the plots of the responses for the repeat tests coincided.

It is important to note that the theory from which the conventional

methodology used for slug-test analysis (e.g., the CBP or Hvorslev models) was developed holds that the slug-test responses should be independent of H_0. In other words, plots of slug-test responses from tests using differing H_0's normalized by the H_0 used in each test should coincide. Clearly, the multilevel slug tests at GEMS are being affected by processes not considered in the standard theory. It is doubtful, however, that these additional processes are solely responsible for the smaller than expected variation seen in the vertical. Based on the simulation results described in subsection II.B, we suspect that the small variation with depth is a result of a high permeability skin that formed during well installation. In the future, we will attempt to decrease the vertical permeability of this well skin using thin layers of bentonite pellets as described in subsection II.B.

The dependence of slug-test responses on H_0 was not the only anomalous behavior observed during the multilevel slug testing at GEMS. Figures III.B.1 - III.B.3 are plots of slug-test responses presented in the format of the Hvorslev method (log head versus arithmetic time). Note the concave downward form of the curves. Conventional theory dictates that these plots should be concave upward or straight lines (Chirlin, 1989; McElwee et al., 1990). Nothing in the conventional theory would allow for concave downward plots. Additional indications that the multilevel slug tests at GEMS are being affected by processes not considered in the standard theory are seen in Figures III.B.4 and III.B.5, where the slug-test data are fitted using conventional approaches (CBP and Hvorslev techniques). The systematic deviation displayed on these plots between the fitted model and the data are characteristic of the behavior observed in every multilevel slug test performed in GEMS well 2-5.

Clearly, the processes that are producing these anomalous responses need to be explained before much useful information can be obtained from multilevel slug tests at GEMS. The decision was made to suspend multilevel slug testing and to concentrate on trying to explain the observed behavior. The objective of the work in the first year of this project thus shifted to the definition of the underlying mechanisms causing the anomalous behavior and the incorporation of these mechanisms into a general theory that can be the basis of new techniques for slug-test analysis. In the following pages, a series of field experiments, which were performed in an attempt to define the relevant processes, are described. These experiments led to the development of nonlinear flow models that are described in a later subsection.

Field Experiments to Explain Anomalous Behavior

A series of field experiments was designed to assess the role of several possible factors in explaining the observed behavior. Factors that could be causing the observed behavior include the following: 1) Frictional flow losses - these could occur in the cased region of the well above the top packer, within the PVC pipe connecting the straddle packer to the top packer, within the packer flow-through pipes, and within the well screen; 2) Non-Darcian flow within the aquifer in the vicinity of the well screen; 3) Aquifer heterogeneities; and 4) Measured pressure not reflective of water level position - the transducers used in the field tests are measuring pressure, which may not always equate to the position of the water level.

An extensive series of field experiments was designed to test the possibility of frictional flow losses in each of the components of the system listed above. In order to simplify the testing procedure, the multilevel slug-test system was not used for these experiments. Instead, all experiments were carried out using a single packer inflated in the cased region of a well with a short screened interval. This configuration allows for a long length of well casing between the top of the packer and the static water level.

GEMS well 10-1 (depth = 17.25 m, screen length = .76 m) was selected for the initial series of tests. The packer was placed just above the screened region and two transducers were placed in the well above the packer. One transducer was placed immediately above the packer (7.59 m below static water level) and one was placed slightly below the static water level (.58 m below static water level). Thus, there was 7.01 m of casing separating the two transducers. If there are significant flow losses within the casing, normalized plots of the data from the two transducers should differ. Figure III.B.6 displays data from two tests of this series: Test 1, which employed an H_0 of 1.07 m, and Test 6, which employed an H_0 of 6.83 m. Note that on both plots the early-time data display pressure oscillations that are attributed to the water hammer effects accompanying the opening of the flow-through pipe in the packer. In both plots, the transducer closest to the packer displays the largest early-time pressure oscillation, consistent with a water hammer explanation (Parmakian, 1963). After the early-time pressure transients have passed, there is little to no difference between the normalized pressure measurements from the transducers. Thus, frictional flow losses within the cased region of the well do not appear to be an important mechanism for these tests. Note that Figure III.B.6 clearly indicates that the dependence of slug-test responses on H_0 is seen with the single packer setup.

Note also that a Hvorslev plot of the tests of Figure III.B.6 will display a marked concave downward curvature. Thus, the same behavior was observed in the single packer tests as in the multilevel packer tests. This would imply that the PVC pipe employed in the multilevel system is not primarily responsible for the observed behavior.

The next series of field tests was designed to assess whether frictional losses within the flow-through pipe of the packer could be an explanation for the observed behavior. In order to test the importance of this mechanism, a transducer must be placed below the packer and isolated from the region above the packer. Unfortunately, there is not enough room in a .05 m ID well to place such a transducer-packer arrangement. Therefore, work was shifted to GEMS well 0-6 (depth = 24.69 m, screen length = 1.52 m, radius = .127 m), which is currently the only large-diameter observation well at the site. Unfortunately, GEMS 0-6 is screened in the bedrock underlying the alluvial deposits, so the velocity of the slug-test induced flows is considerably lower than in the wells sited in the sand and gravel section of the alluvium. Preliminary testing, however, did reveal that the slug-test responses at this well displayed a similar dependence on H_0. In addition, a slight downward curvature was seen on Hvorslev plots of tests when a very large H_0 (7.39 m) was employed. Thus, even a well sited in material of lower permeability displayed much of the same anomalous behavior.

A simple transducer-packer arrangement was constructed at the KGS for this set of experiments. The transducer cable was run through the central flow-through pipe of the packer until the bottom of the packer, a short distance above the location of the plug used to initiate the slug tests, at which point it was passed out of the flow-through pipe at a T connection. A compression fitting was placed on the cable at the T connection to ensure that no water leaked into the flow-through pipe along the transducer cable. This setup enabled the transducer sensor to be placed below the packer, isolated from the region above the packer. A series of experiments was performed in the field and laboratory to ensure a watertight seal was obtained with the compression fitting and that the transducer was truly isolated from the cased region above the packer. Neither in these experiments nor in any of the following tests was there any indication of leakage in this system.

Figure III.B.7 displays the head data from a test (H_0 = 6.88 m) using the transducer-packer arrangement. The upper transducer is located above the packer, .46 m below the static water level. The lower transducer is located below the packer, 11.88 m below the static water level (total distance between the two transducers is

11.42 m). The plotted data show that there are differences between the two transducers in the early portions of the test. These differences, however, become negligible later in the test. Some flow losses do seem to occur within the packer flow-through pipe, but, since the differences do not extend through the entire test, they are probably not the primary reason for the observed anomalous behavior. A comparison of Figures III.B.6 and III.B.7 shows that recovery to the static water level in the bedrock well takes much longer than in the wells sited in the sand and gravel section. The velocities in the flow-through pipe in the wells in the sand and gravel section are clearly much greater than in the bedrock well and thus the effect of frictional losses in the flow-through pipe should be larger. However, given that a similar dependence on H_0 is observed in the bedrock and alluvial wells, frictional losses in the flow-through pipe are probably still not the primary mechanism producing the anomalous responses.

In order to further assess the possible role of the packer in the production of the observed behavior, an additional series of experiments was run in which the packer arrangement was not employed. Instead, PVC pipes (.06 m OD) of differing lengths (1.60 and 3.10 m), which had been filled with sand and sealed at both ends, were used to perform the slug tests. A slug test was initiated by rapidly lowering a PVC pipe below the static water level, causing a rise in water levels. Pipes of different lengths cause the H_0's to be different (H_0 = .36 m for short pipe and = .69 m for large pipe). Figure III.B.8 displays the results from two tests of this series. As with tests using the packer, a dependence on H_0 is observed. Thus, flow losses in the central flow-through pipe in the packer do not appear to be the primary mechanism producing the observed dependence on H_0.

Frictional losses in the well screen appear to be a likely source of the observed behavior. Unfortunately, there is not an easy way of testing the importance of this mechanism in the field. An initial attempt at assessing the importance of frictional losses in the well screen was made using the transducer-packer arrangement discussed earlier. In this case, a piece of well screen (1.52 m in length) was screwed on to the bottom end of the flow-through pipe. The transducer situated below the packer was located outside this section of screen. The idea was to mount a piece of screen whose slot size was smaller than that used in the well screen at GEMS 0-6. The screen with the smallest slot size should be the feature with the most resistance to flow in the system. If frictional losses in this screen are important, measurements from the transducer located below the packer outside the mounted screen should differ from the measurements from transducers above the packer. A series of

experiments with screens of two different slot sizes were performed. In all cases, the responses were similar to those of Figure III.B.7. There were no additional losses of any significance. We suspect, however, that this result may be more of a function of experimental design (i.e. slot sizes of mounted screen are too large, slots of screen in well are encrusted with mud, etc.), so further tests are planned both in the laboratory and field in an attempt to better assess the importance of this mechanism.

Non-Darcian flow within the aquifer in the vicinity of the well screen is also a likely source of the observed behavior. During the first year of this project, no field experiments were performed to assess the importance of this mechanism. An approximate analytical model described in the succeeding subsection of this report, however, demonstrates that non-Darcian flow can produce the behavior observed at GEMS. A series of laboratory experiments will be performed in the second year of this project to examine this behavior in more detail.

Aquifer heterogeneities could perhaps be invoked as an explanation of the observed phenomenon. However, simulations that were performed as part of the theoretical work described in subsection II.B (scenario 4D of Table II.B.1) demonstrated that aquifer heterogeneities are not going to produce a dependence on H_0 in perfectly stratified systems. This result will apply to a system of discontinuous layers as well.

Most slug tests in moderate to highly permeable media are performed using submersible pressure transducers to record changes in water levels. These transducers are assumed to be measuring the static pressure exerted on the sensor by the overlying column of water. Actually, however, these sensors are measuring both static and dynamic components of pressure. If the dynamic component of pressure is significant, the measured pressures will not be reflective of actual water levels. Potentially, this effect could be contributing to the observed behavior at GEMS.

A series of experiments was performed in order to assess the difference between the pressure measured by the transducers and the actual water level in the well. GEMS well 0-6 was employed for this series of experiments because it is the only large-diameter well located at GEMS and the experimental setup required a .01 m ID well or larger. These experiments used a single packer inflated above the well screen. A transducer was placed above the packer, several meters below the static water level. An ultrasonic distance transmitter (LV401 non-contact ultrasonic level/distance transmitter, Omega Engineering, Inc.), placed over the top of a .05 m ID drop pipe held in position by chain vice grips, was used to provide an independent

measurement of the position of the actual water level. This transmitter measures the position of the water level using the travel time of an ultrasonic signal reflecting off the water surface. A comparison of the ultrasound data and the pressure transducer data should reveal any errors arising from use of pressure transducers to record changes in water levels. Note that the ultrasonic transmitter was placed in a drop pipe so that reflections off the pump rods used with the packer could be avoided. Note also that the ultrasonic transmitter had been preset at the factory for measurement in air at a temperature of 20°C. Thus, immediately prior to performing this series of slug tests, the ultrasonic transmitter was calibrated to reflect the air temperature at the onset of the test period. The manufacturer estimates that there is an approximate 1 percent shift in accuracy per 10°C deviation from 20°C.

Figure III.B.9 displays plots of the ultrasound and transducer data (both adjusted so that the static water level is the reference point) and their difference for one of the slug tests performed in this series of experiments. Note that nonnegligible differences are displayed at two intervals on the plot. The first interval encompasses the initial seconds of the slug test. Clearly, there are pressure oscillations during this period that are not due to actual movement of the water level in the well. We feel that these oscillations are due to the earlier-described water hammer effects and do not play a role in the anomalous behavior observed at larger times. The second interval occurs at the end of the plotted record and is due to the water level beginning to fall outside of the range of the ultrasonic distance transmitter that we were employing for this series of experiments. Although we were only able to compare the ultrasound and transducer data over a limited range of distances, it is clear that the assumption that a pressure transducer is measuring the static pressure exerted by the overlying column of water is appropriate for slug tests performed in wells screened in moderately permeable systems such as the bedrock in which GEMS well 0-6 is screened. Note that the results displayed in Figure III.B.9 are reflective of all the tests performed as part of this series of experiments at GEMS well 0-6, regardless of the H_0. A further series of tests will be carried out early in the second year of this project to examine if the assumption is valid in wells sited in the sand and gravel section at GEMS. These tests will be performed in a series of large diameter wells that will be drilled in the sand and gravel interval early in the second year of the project.

Summary

An initial series of multilevel slug tests was performed at a well sited in the

sand and gravel section at GEMS. The data from this series of tests indicated that the slug-test responses at this well were being affected by mechanisms not accounted for in the conventional theory. An inverse relationship between the magnitude of the induced slug (H_0) and the estimated conductivity, a concave downward curvature to data plotted in the Hvorslev format, and systematic deviations between the test data and the best-fit conventional models were the most obvious indications of these mechanisms. Additional experiments indicated that some of these processes also affect slug-test responses in a well in the moderately permeable bedrock underlying the alluvial section at GEMS.

A large number of field experiments were performed in an attempt to identify the relevant mechanisms producing the observed behavior. The results of these experiments indicated that frictional flow losses in the well casing, in the PVC pipe string used in the multilevel slug-test system, and in the flow-through pipe in the packer were not the primary mechanisms producing the observed responses. Experiments to assess the importance of frictional flow losses within the well screen produced ambiguous results. An initial set of experiments to assess the magnitude of dynamic pressure effects on transducer measurements indicated that dynamic pressure effects are probably not a significant contributor to the observed behavior. Further work is needed to assess the role of flow losses within the well screen and possible non-Darcian flow in the aquifer.

Although the work described here is ongoing, an important recommendation can be made about the performance and analysis of slug tests. A series of slug tests at a well should always be performed using at least two different H_0's (preferably differing by at least .5 m). If plots of the response data normalized by the corresponding H_0 all coincide, then one can feel confident that some variant of the conventional approach for analysis of slug-test data can be employed. As shown in the experiments described in this section, the use of only one H_0 in a series of slug tests could lead to considerable error in the estimated parameters. It is important to note that the behavior described here has, to the best knowledge of the authors, never been reported on in the literature. This is not especially surprising due to the fact that H_0 is almost never varied during a program of slug testing and that most slug tests are performed and analyzed in a rather approximate fashion. However, if our ability to predict contaminant movement in the subsurface is to be improved, it is essential that the error being introduced into the modeling analyses by the use of incorrect parameter values be diminished.

Although field experiments directed at defining the relevant mechanisms

producing the anomalous behavior have not yet been completed, work has already begun on the development of a theory to account for some of the observed behavior. In the next subsection of this report, a theory based on the incorporation of a nonlinear flow term into the Hvorslev model is described and examples of application of the theory to data from wells at GEMS are presented.

Interval (m)	K_{HV} (10^{-3} m/s)	K_{CBP} (10^{-3} m/s)	H_0 (m)
20.07 - 20.36	0.2105	0.0682	6.88
20.07 - 20.36	0.2136	0.0693	6.86
20.07 - 20.36	0.3499	0.1124	1.66
20.07 - 20.36	0.2856	0.0921	3.06
20.07 - 20.36	0.2960	0.0956	3.12
19.77 - 20.05	0.3499	0.1135	1.65
19.77 - 20.05	0.2785	0.0904	3.04
19.77 - 20.05	0.2881	0.0938	3.01
19.77 - 20.05	0.2045	0.0664	6.85
19.46 - 19.74	0.3377	0.1098	1.74
19.46 - 19.74	0.2797	0.0911	3.05
19.46 - 19.74	0.2805	0.0913	3.03
19.46 - 19.74	0.2074	0.0676	6.86
19.15 - 19.43	0.3347	0.1085	1.62
19.15 - 19.43	0.2823	0.0917	3.04
19.15 - 19.43	0.2673	0.0864	3.28
19.15 - 19.43	0.2011	0.0652	6.85
18.83 - 19.12	0.3539	0.1177	1.58
18.83 - 19.12	0.2839	0.0922	3.03
18.83 - 19.12	0.2777	0.0900	3.19
18.83 - 19.12	0.2031	0.0660	6.87
18.52 - 18.81	0.3481	0.1124	1.60
18.52 - 18.81	0.2723	0.0882	3.23
18.52 - 18.81	0.2908	0.0943	2.94
18.52 - 18.81	0.2068	0.0672	6.90
18.22 - 18.50	0.3441	0.1111	1.69
18.22 - 18.50	0.2868	0.0929	3.01
18.22 - 18.50	0.2941	0.0955	2.99
18.22 - 18.50	0.2117	0.0688	6.92

Table III.B.1 - Results of Hvorslev (K_{HV}) and CBP (K_{CBP}) analyses for the multilevel slug tests using different initial heads (H_0). Interval nos. increase down table (top is no.2).

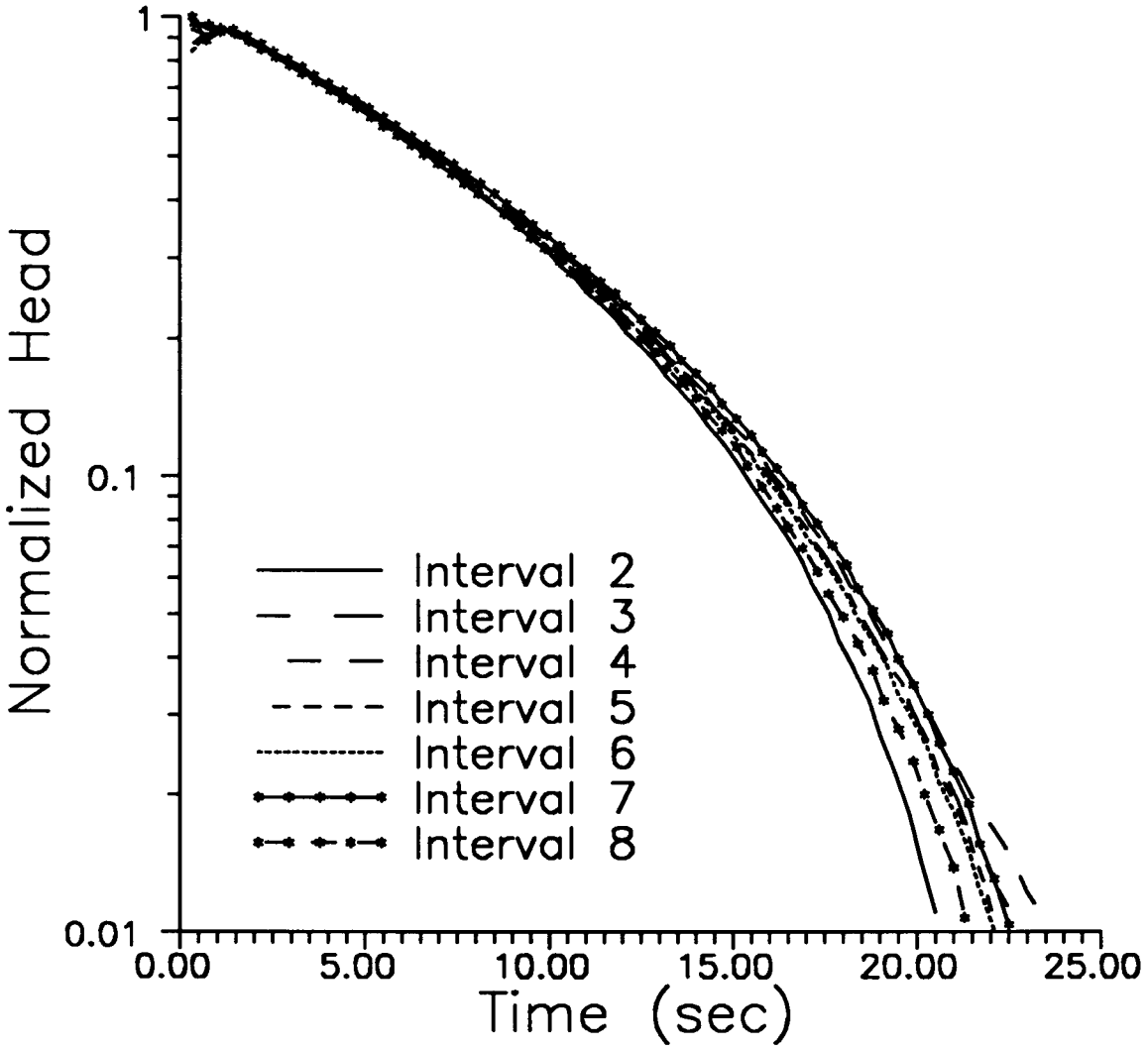

Figure III.B.1 - Normalized head (H/H_0) versus time plots for slug tests in seven intervals of GEMS well 2-5 (H_0 = 3.07 m). See Table III.B.1 for depths corresponding to each interval.

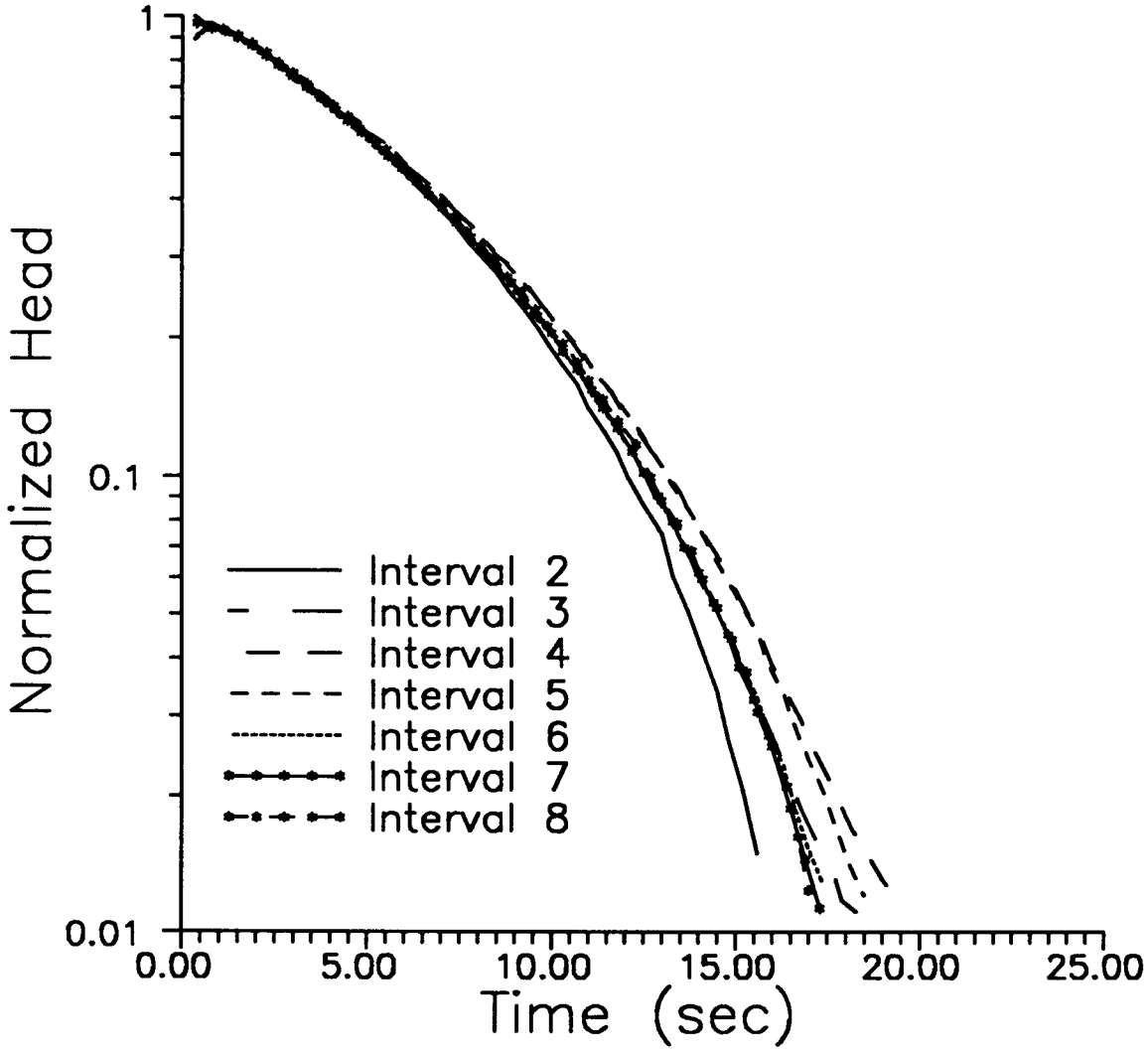

Figure III.B.2 - Normalized head (H/H_0) versus time plots for slug tests in seven intervals of GEMS well 2-5 (H_0 = 1.65 m). See Table III.B.1 for depths corresponding to each interval.

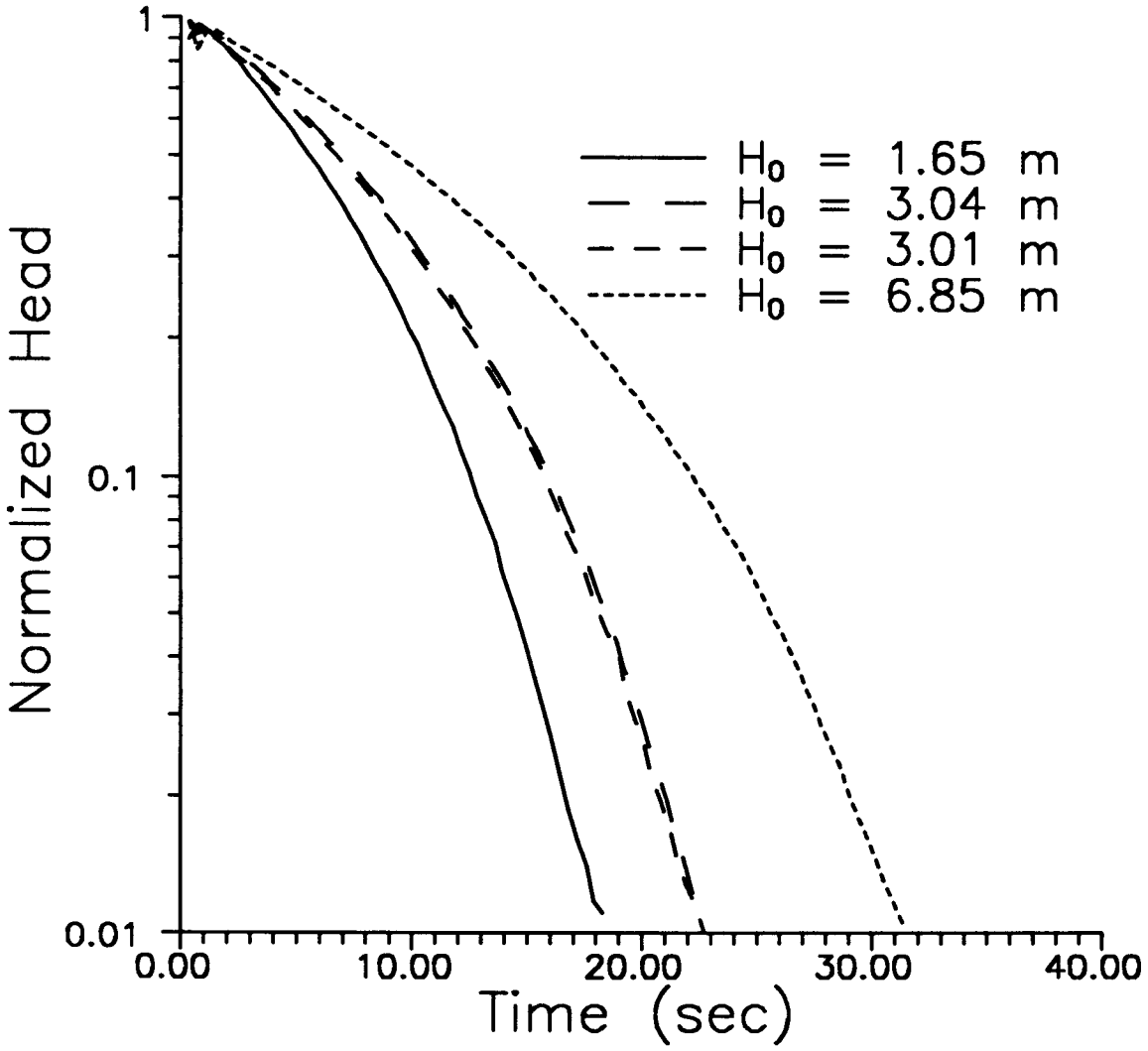

Figure III.B.3 - Normalized head (H/H_0) versus time plots for slug tests in the third interval (19.77-20.05 m) of GEMS well 2-5 using H_0's of different magnitudes.

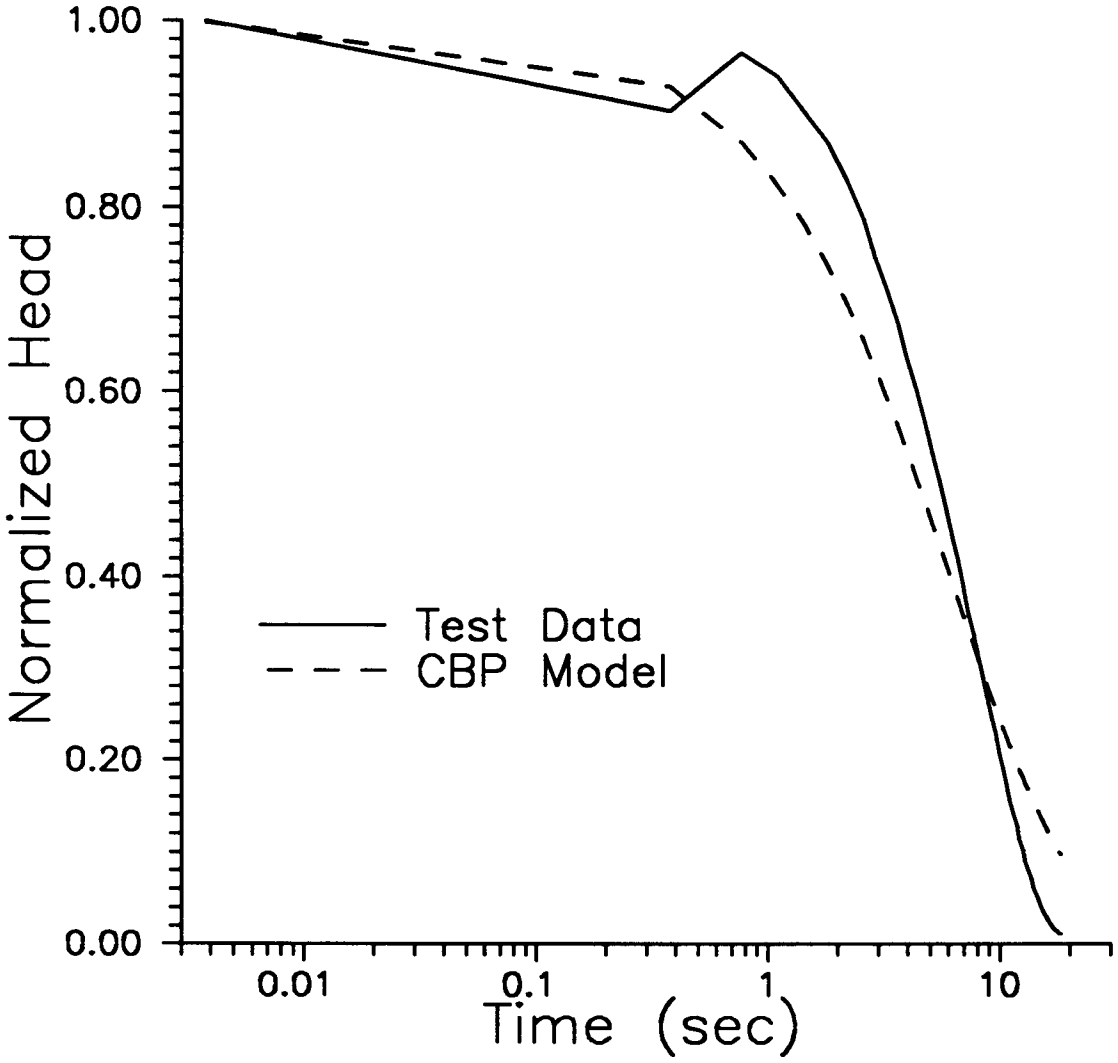

Figure III.B.4 - Normalized head (H/H_0) versus time plots of slug-test data from interval 3 (19.77-20.05 m) of GEMS well 2-5 and the best-fit CBP model.

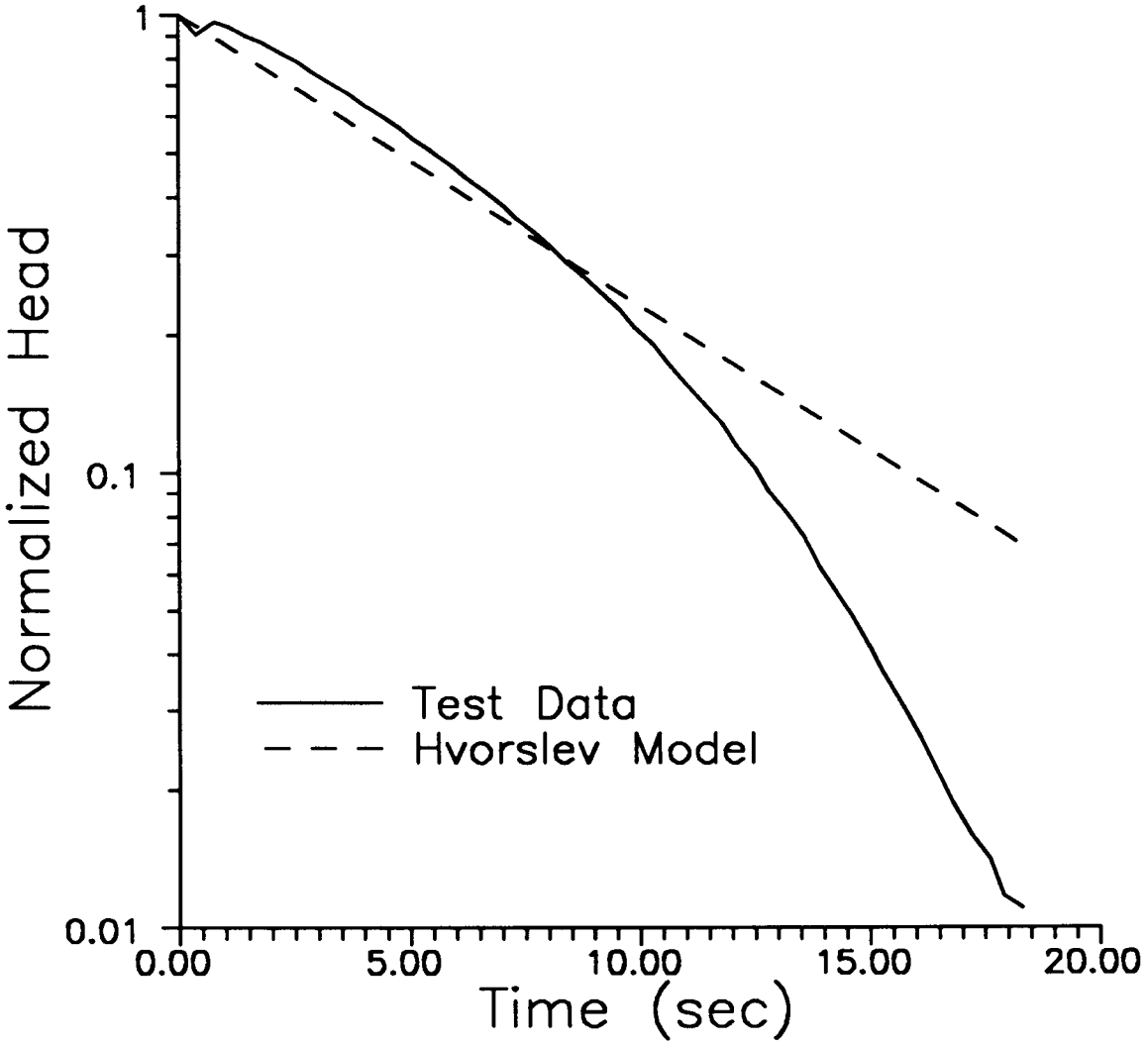

Figure III.B.5 - Normalized head (H/H_0) versus time plots of slug-test data from interval 3 (19.77-20.05 m) of GEMS well 2-5 and the best-fit Hvorslev model.

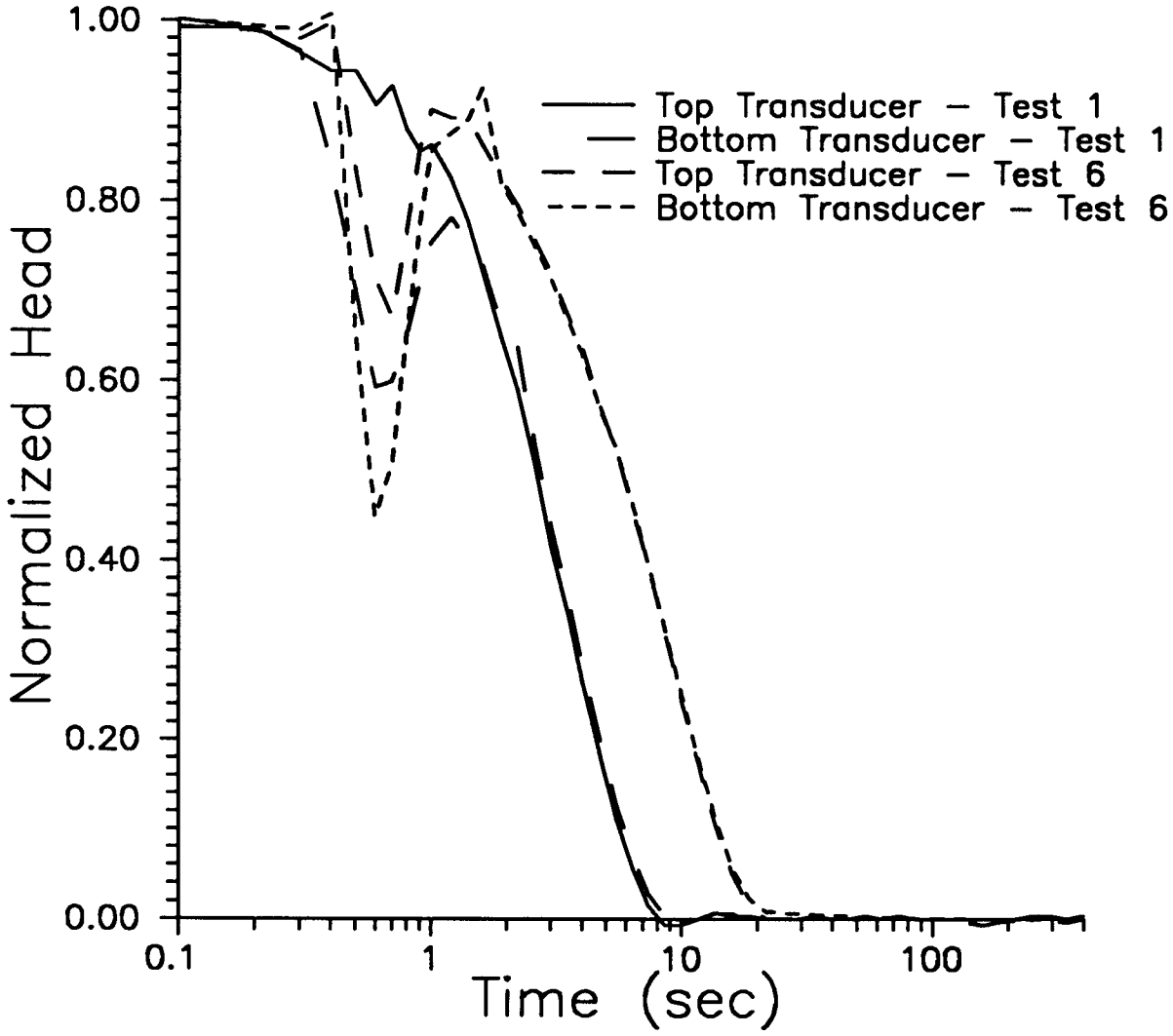

Figure III.B.6 - Normalized head (H/H_0) versus time plots for two slug tests at GEMS well 10-1 (H_{01} = 1.07 m; H_{06} = 6.83 m). Note that two transducers were used in each test.

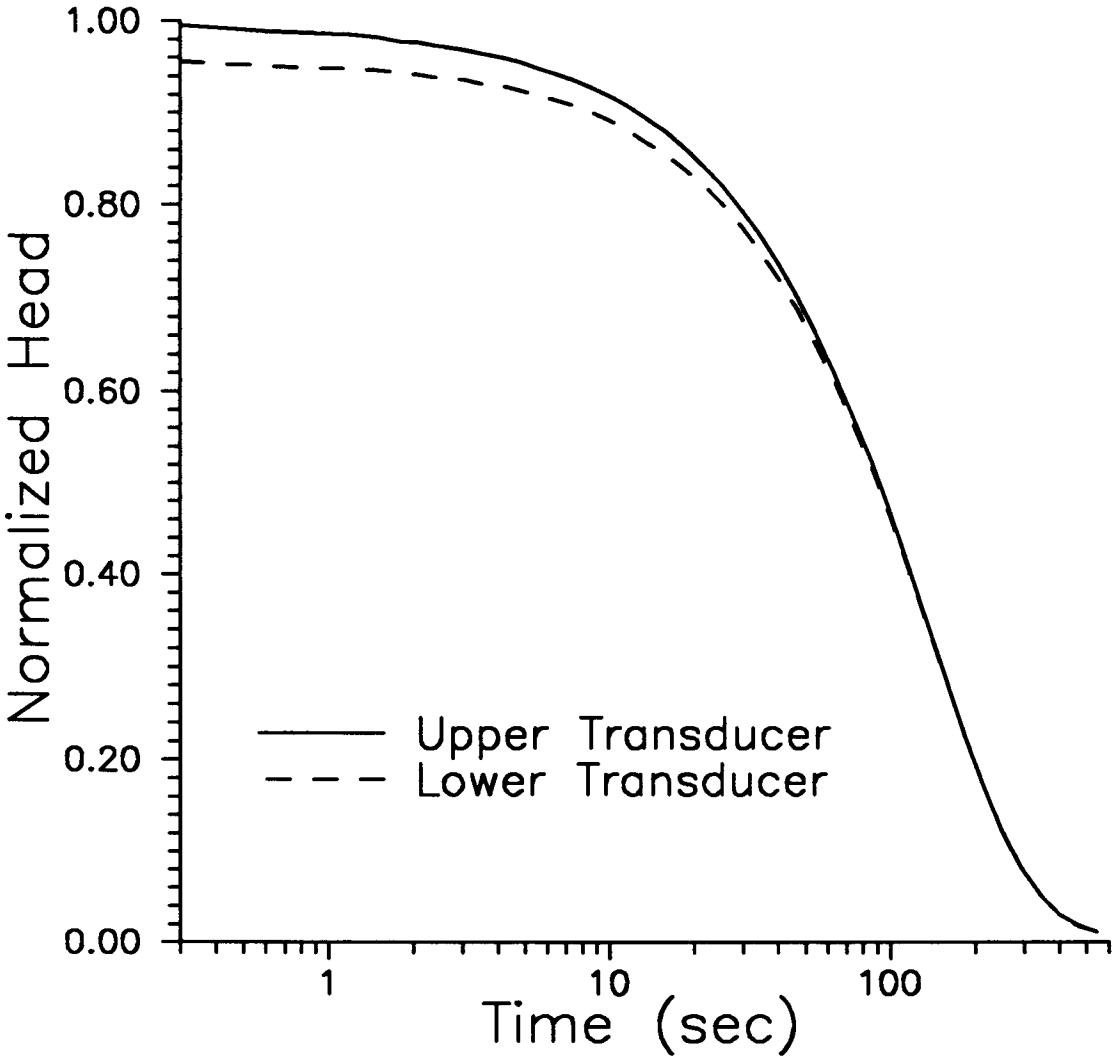

Figure III.B.7 - Normalized head (H/H_0) versus time plots for slug test at GEMS well 0-6 (H_0 = 6.88 m). Note that the transducer-packer arrangement described in the text was used in this test.

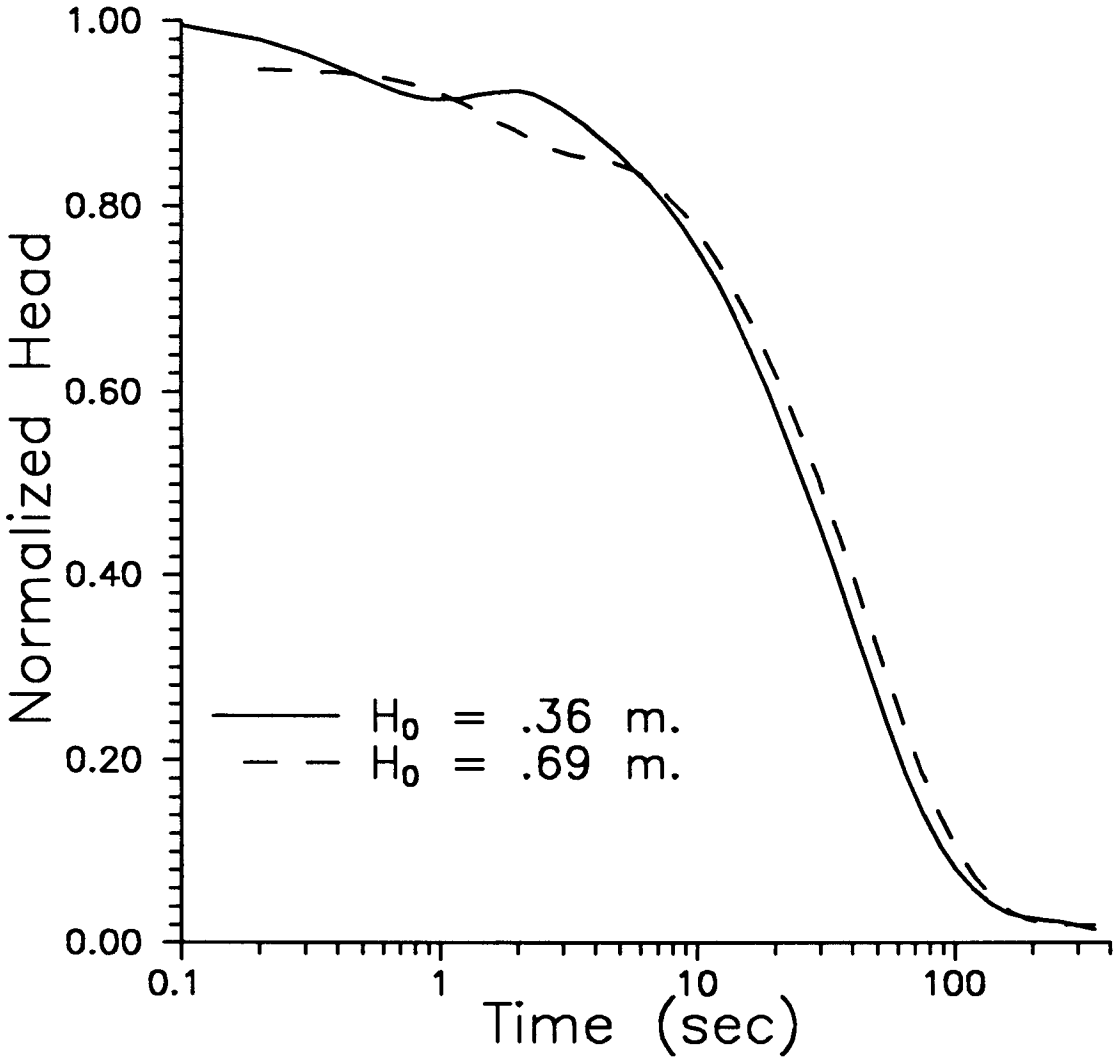

Figure III.B.8 - Normalized head (H/H_0) versus time plots for two slug tests at GEMS well 0-6 (H_{01} = 0.36 m; H_{02} = 0.69 m). Note that these slug tests were initiated using the PVC pipes described in the text.

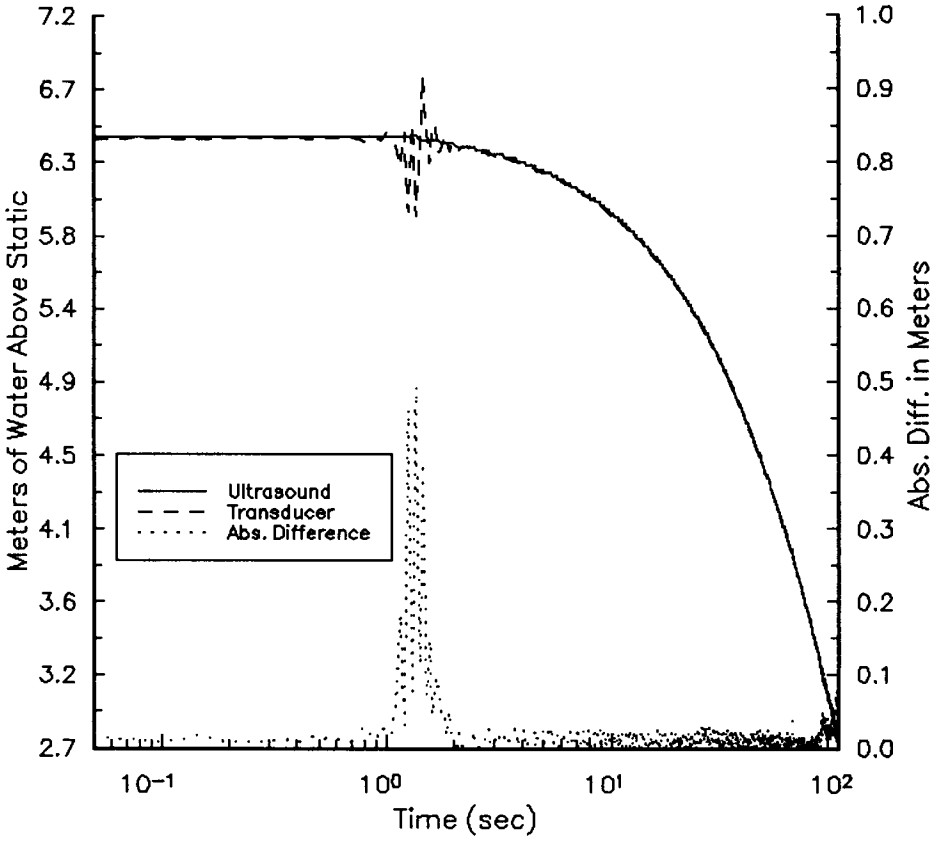

Figure III.B.9 - Meters of water above static versus time plot for a slug test at GEMS well 0-6 (H_0 = 6.46 m). Note that the height of the water column above static is being measured using both a pressure transducer and an ultrasonic distance transmitter. The absolute difference between these two measurements is also plotted.

C. DEVELOPMENT OF NONLINEAR MODELS FOR ANALYSIS OF SLUG-TEST DATA

Introduction

As described in the previous subsection, slug-test response data from wells in the sand and gravel aquifer at GEMS are being affected by mechanisms not accounted for in the conventional theory on which the standard methods for data analysis are based. Two possible mechanism that could be producing the anomalous observed behavior are friction between the water and the casing walls or screen slots, and non-Darcian flow within the aquifer. In this subsection, additional terms to account for the nonlinearities introduced by these mechanisms are added into the standard Hvorslev model. Following the development of the model accounting for frictional losses within the casing and screen, several example applications of this model to data from slug tests at GEMS are given.

Incorporation of Frictional Flow Losses into the Hvorslev Model

In the following derivation, an additional term is incorporated into the Hvorslev model to account for frictional losses within the well screen. The initial model that is developed will assume that frictional losses in the well screen are independent of water velocity. However, since frictional effects are generally proportional to some power of the velocity, the final model developed here will assume a dependence of frictional losses on velocity. This velocity dependence will lead to a model of a nonlinear form.

Constant Resistance

The conventional Hvorslev equation is

$$Q(t) = \pi r_c^2 \frac{dH(t)}{dt} = -FK \cdot h(t) \qquad \text{(III.C.1)}$$

where

Q(t) = flow into/out of the well in response to induced slug;

H(t) = height of water in well at time t;

h(t) = head of water in the aquifer just outside the screen;

K = hydraulic conductivity;

F = Hvorslev geometric factor;

r_c = casing radius.

If there is a loss in head across the screen due to wall or slot friction, H(t) and h(t) will not be the same. This results in

$$Q(t) = -\left(\frac{H(t) - h(t)}{R}\right) \tag{III.C.2}$$

where R is the resistance factor. In this first case, we consider R a constant and see what are the consequences. Replacing h(t) in equation (III.C.1) with equation (III.C.2) and eliminating Q(t) gives

$$\pi r_c^2 \frac{dH(t)}{dt} = -FK \cdot (Q(t)R + H(t)) \tag{III.C.3a}$$

$$\frac{dH(t)}{dt} = \frac{-FK}{\pi r_c^2 (1 + FKR)} \cdot H(t) \tag{III.C.3b}$$

Equation (III.C.3b) is easily solved to give the solution

$$Ln(H(t)) = \frac{-FK}{\pi r_c^2 (1 + FKR)} t + const. \tag{III.C.4}$$

Clearly, this equation will plot as a straight line on a log-linear plot just as the traditional Hvorslev method, the only difference being that the slope is modified by the resistance factor (R). Equation (III.C.4) shows that a constant resistance can not give the concave downward behavior or the dependence on initial head that we observe in the slug-test data from GEMS.

Resistance Proportional to a Power of the Velocity

The more realistic assumption is that the resistance is proportional to some power of the velocity. For simplicity, usually only the first or second power of velocity is considered. If we assume R is proportional to the first power of the water velocity in the well casing, we obtain

$$R = A \cdot |V| = A\left|\frac{dH(t)}{dt}\right| \qquad \text{(III.C.5)}$$

where A is an assumed constant of proportionality. Using equation (III.C.5) for R and substituting into equation (III.C.3a) gives

$$\pi r_c^2 \frac{dH(t)}{dt} = -FK\left[H(t) + Q(t)A\left|\frac{dH(t)}{dt}\right|\right]. \qquad \text{(III.C.6a)}$$

Using equation (III.C.1) to eliminate Q(t) gives the result

$$\frac{dH(t)}{dt}\left[1 + FKA\left|\frac{dH(t)}{dt}\right|\right] = -\frac{FK}{\pi r_c^2}H(t) \qquad \text{(III.C.6b)}$$

The generalization of equation (III.C.5) for any power (N) of the velocity is

$$R = A \cdot |V|^N = A\left|\frac{dH(t)}{dt}\right|^N. \qquad \text{(III.C.7)}$$

Similarly, the generalization of equation (III.C.6) is

$$\frac{dH(t)}{dt}\left[1 + FKA\left|\frac{dH(t)}{dt}\right|^N\right] = -\frac{FK}{\pi r_c^2}H(t). \qquad \text{(III.C.8)}$$

Numerical Solution

Equation (III.C.8) is nonlinear in the variable H(t) and in general can not be solved in closed form. However, it does yield to standard numerical solution techniques. We have tried several possibilities. One form that has worked well is explored here. Solving equation (III.C.8) for the time derivative of H(t) results in the following

$$\frac{dH(t)}{dt} = \frac{-\frac{FK}{\pi r_c^2} H(t)}{\left[1 + FKA\left|\frac{dH(t)}{dt}\right|^N\right]} \qquad \text{(III.C.9)}$$

The time derivatives in equation (III.C.9) can be evaluated numerically by the central difference rule.

$$\left[\frac{dH(t)}{dt}\right]^{n+1/2} = \frac{H^{n+1} - H^n}{\Delta t} \qquad \text{(III.C.10)}$$

where H^n is the value of H(t) at time n and Δt is the time step between times n+1 and n. Evaluating equation (III.C.9) at time n+1/2 and using equation (III.C.10) along with the Crank-Nicolson approximation

$$H^{n+1/2} = \left(H^{n+1} + H^n\right)/2$$

gives the following numerical approximation

$$H^{n+1} = H^n - \frac{\frac{\Delta t \cdot FK}{2\pi r_c^2}\left(H^{n+1} + H^n\right)}{\left[1 + FKA\left|\frac{H^{n+1} - H^n}{\Delta t}\right|^N\right]}. \qquad \text{(III.C.11)}$$

However, equation (III.C.11) still can not be solved directly since H^{n+1} appears on both sides of the equation. Therefore, we must resort to an iterative scheme by adding another superscript to be the interactive index. $H^{n(m)}$ is the m th iteration value at the n^{th} time level. Rewriting equation (III.C.11) with iteration indices results in the following form

$$H^{n+1(m+1)} = H^n - \frac{\frac{\Delta t}{2t_0}\left(H^{n+1(m)} + H^n\right)}{\left[1 + FKA\left|\frac{H^{n+1(m)} - H^n}{\Delta t}\right|^N\right]} \qquad \text{(III.C.12)}$$

where we have also used the standard definition of the Hvorslev time lag

$$t_0 = \frac{\pi r_c^2}{FK} \qquad \text{(III.C.13)}$$

Equation (III.C.12) must be iterated until there is relatively little difference in the H(t) for consecutive iterations. At that point one can move on to another time step and repeat the iteration procedure. In this way the complete time dependence of H(t) can be generated numerically. We have implemented this scheme with N=2 in the automated well-test analysis program SUPRPUMP (Bohling and McElwee, 1992). Note that when N=2 is employed, the simulated data does display a pronounced downward curvature on the standard log-linear Hvorslev plot. Also, examination of (III.C.12) shows that this model will produce a dependence on initial head. Thus, the two major anomalous features seen in the GEMS data can be reproduced by this model.

Application of the Nonlinear Model to GEMS Data

This nonlinear model was applied to data from a series of slug tests at GEMS. Figures III.C.1-III.C.3 are representative of the model fits that were obtained. In all cases, when slug-test data from a well sited in the sand and gravel section of GEMS were analyzed with this model, very good fits were obtained.

Although the fits were dramatically improved by use of this approach (compare Fig. III.C.3 with Figs. III.B.4-III.B.5), the conductivity estimates indicate that we still have not incorporated all the relevant mechanisms into the model. This is clearly shown by Figures III.C.1-III.C.2, which display slug-test response data from two tests done at the same well using different initial heads. The conductivities estimated from these data using the nonlinear Hvorslev model are .000984 m/s and .000641 m/s for the low and high initial head cases, respectively. Thus, there still seems to be an inverse dependence of estimated conductivity on the magnitude of the initial head. Further work is being carried out in an attempt to explain this continued dependence on initial head.

Incorporation of Non-Darcian Flow into the Hvorslev Model

In the previous derivation, we assumed that nonlinearities were introduced into the Hvorslev model via frictional losses in the well screen. In the following development, we will instead assume that the nonlinearities are introduced by non-Darcian flow within the aquifer itself. Non-Darcian flow arises when velocities within the porous media are large enough that the hydraulic gradient is no longer a linear function of the specific discharge. For this development, we will assume that the relationship between the hydraulic gradient and specific discharge under non-Darcian flow conditions can be expressed as

$$\frac{\partial h}{\partial r} = wv + bv^2 \qquad \textbf{(III.C.14)}$$

where

v = specific discharge;

w, b = constants of proportionality.

Note that although in equation (III.C.14) the second power of the velocity is employed, any arbitrary power could be incorporated into the derivation. The second power was employed here to be consistent with most past work on non-Darcian flow in porous media (Bear, 1972; Guppy et al., 1982).

Equation (III.C.14) can be rearranged and expressed in terms of the specific discharge using the quadratic formula:

$$v = -\frac{w}{2b} \pm \sqrt{\frac{w^2}{4b^2} + \frac{1}{b}\frac{\partial h}{\partial r}} = -\frac{w}{2b} \pm y \qquad \textbf{(III.C.15)}$$

Since the Hvorslev model is based on the assumption of incompressible matrix and pore fluids, the continuity equation can be written in its steady-state form as

$$\frac{1}{r}\frac{\partial}{\partial r}(rv) = \frac{\partial v}{\partial r} + \frac{v}{r} = 0 \qquad \textbf{(III.C.16)}$$

Substitution of equation (III.C.15) into equation (III.C.16) yields

$$\frac{\pm y \partial y}{wy \mp 2by} = \frac{\partial r}{2br} \qquad \text{(III.C.17)}$$

A straight-forward integration of equation (III.C.17) results in

$$-\ln(w \mp 2by) = \ln(r) + \ln(C') \qquad \text{(III.C.18)}$$

where

C' = integration constant.

Use of the additive properties of logarithms enables equation (III.C.18) to be rewritten as

$$\ln[rC'(w \mp 2by)] = 0 \qquad \text{(III.C.19)}$$

Equation (III.C.19) can be readily solved for y producing the following expression:

$$y = \pm\frac{w}{2b} \mp \frac{1}{2bC'r} \qquad \text{(III.C.20)}$$

Substitution of equation (III.C.20) back into equation (III.C.15) yields an expression for the specific discharge:

$$v = -\frac{1}{2bC'r} \qquad \text{(III.C.21)}$$

An expression for specific discharge can also be obtained by employing the

boundary condition at the slugged well. Using the same notation as in the previous derivation, an expression for the flow into/out of the well in response to the induced slug can be written as

$$Q(t) = \pi r_c^2 \frac{dH(t)}{dt} = [vA_{sc}]_{r=r_w} = -\frac{1}{2bC'r_w} 2\pi r_w L \qquad \text{(III.C.22)}$$

where

A_{sc} = surface area of the well screen;
r_w = radius of the well screen;
L = screen length.

Rearrangement of equation (III.C.22) leads to an expression for specific discharge in terms of the head in the slugged well:

$$v = \frac{r_c^2}{2L} \frac{dH(t)}{dt} \frac{1}{r} \qquad \text{(III.C.23)}$$

Substitution of equation (III.C.23) back into equation (III.C.14) and integration in the radial direction yields

$$h = \frac{wr_c^2}{2L} \frac{dH(t)}{dt} \ln(r) - b\left[\frac{r_c^2}{2L} \frac{dH(t)}{dt}\right]^2 \frac{1}{r} + C'' \qquad \text{(III.C.24)}$$

where

C'' = integration constant.

If we assume that the head is unchanged from static conditions (= 0) at some distance r_e (effective radius) from the slugged well, then the integration constant can be written as

$$C'' = b\left[\frac{r_c^2}{2L} \frac{dH(t)}{dt}\right]^2 \frac{1}{r_e} - w\frac{r_c^2}{2L} \frac{dH(t)}{dt} \ln(r_e) \qquad \text{(III.C.25)}$$

Substitution of equation (III.C.25) back into equation (III.C.24) yields an expression for the head within the aquifer

$$h = w\frac{r_c^2}{2L}\frac{dH(t)}{dt}\ln\left(\frac{r}{r_e}\right) + b\left[\frac{r_c^2}{2L}\frac{dH(t)}{dt}\right]^2\left[\frac{1}{r_e} - \frac{1}{r}\right] \qquad \textbf{(III.C.26)}$$

An expression for head in the slugged well can be obtained by setting $r=r_w$ and $h=H(t)$ in equation (III.C.26)

$$H(t) = \left(w\frac{r_c^2}{2L}\ln\left(\frac{r_w}{r_e}\right) + b\left[\frac{r_c^2}{2L}\right]^2\left[\frac{r_w - r_e}{r_e r_w}\right]\left[\frac{dH(t)}{dt}\right]\right)\frac{dH(t)}{dt} \qquad \textbf{(III.C.27)}$$

Equation (III.C.27) can be rewritten into a form similar to equation (III.C.6b)

$$\left(\frac{2L}{wr_c^2\ln\left(\frac{r_w}{r_e}\right)}\right)H(t) = \left[1+\frac{r_c^2 b}{2Lw\ln\left(\frac{r_w}{r_e}\right)}\left(\frac{r_w-r_e}{r_e r_w}\right)\frac{dH(t)}{dt}\right]\frac{dH(t)}{dt} \qquad \textbf{(III.C.28)}$$

Equating the constant terms on the lefthand sides of equations (III.C.28) and (III.C.6b) yields

$$\frac{2L}{wr_c^2\ln(r_w/r_e)} = -\frac{FK}{\pi r_c^2} \qquad \textbf{(III.C.29)}$$

If K = -1/w, then the Hvorslev formation factor (F) can be defined as

$$F = \frac{2\pi L}{\ln(r_w/r_e)} \qquad \textbf{(III.C.30)}$$

Substitution of equation (III.C.30) into equation (III.C.28) yields

$$-\frac{FK}{\pi r_c^2}H(t) = [1-\frac{Fr_c^2bK}{4L^2\pi}(\frac{r_w-r_e}{r_e r_w})\frac{dH(t)}{dt}]\frac{dH(t)}{dt} \qquad \textbf{(III.C.31)}$$

If $r_e >> r_w$

$$(\frac{r_w - r_e}{r_e r_w}) \approx -\frac{1}{r_w} \qquad \textbf{(III.C.32)}$$

and equation (III.C.31) can be simplified to

$$-\frac{FK}{\pi r_c^2}H(t) = [1 + \frac{FKb}{4\pi L^2}\frac{r_c^2}{r_w}\frac{dH(t)}{dt}]\frac{dH(t)}{dt} \qquad \textbf{(III.C.33)}$$

Note that if b=0 ($\frac{\partial h}{\partial r} = wv$), then equation (III.C.33) will reduce to the conventional form of the Hvorslev equation. Also note that by employing the equivalence of equations (III.C.33) and (III.C.6b), an expression for the constant A can be written as

$$A = \frac{br_c^2}{4\pi L^2 r_w} \qquad \textbf{(III.C.34)}$$

Substitution of (III.C.34) into (III.C.33) yields

$$-\frac{FK}{\pi r_c^2}H(t) = [1 + FKA\frac{dH(t)}{dt}]\frac{dH(t)}{dt} \qquad \textbf{(III.C.35)}$$

Normalizing the heads on both sides of equation (III.C.35) by the height of the initial slug produces an expression for the normalized head within the well

$$H'(t) = -\frac{\pi r_c^2}{FK}\frac{dH'(t)}{dt} - H_0\pi r_c^2 A\left(\frac{dH'(t)}{dt}\right)^2 \qquad \textbf{(III.C.36)}$$

where

H'(t) = normalized head = $H(t)/H_0$.

Note that the response to the induced slug is now a function of the height of the initial slug in agreement with the behavior we observed in the slug tests at GEMS.

At large times, the second term on the righthand side of (III.C.36) becomes negligible and equation (III.C.36) can be simplified to

$$\left(\frac{FK}{\pi r_c^2}\right)dt = -\frac{dH'(t)}{H'(t)} \qquad \textbf{(III.C.37)}$$

Integration of equation (III.C.37) leads to the conventional Hvorslev equation

$$\left(\frac{FK}{\pi r_c^2}\right)t = -\ln(H'(t)) \qquad \textbf{(III.C.38)}$$

Thus, use of equation (III.C.38) with large-time data could be a means to avoid additional complexities introduced by the nonlinear component of the non-Darcian flow Hvorslev model.

A striking feature of this development is the equivalence between equation (III.C.35), the non-Darcian flow form of the Hvorslev model, and equation (III.C.6b), the form of the Hvorslev model derived assuming nonlinear frictional losses within the well screen. These two forms will be equivalent when the power of the velocity to which resistance in the well screen is proportional is one less than the power of the velocity in the second term of equation (III.C.14). This equivalence appears to arise from the quasi steady-state assumption that is the basis of the Hvorslev model.

Note that (III.C.36) must be solved iteratively in a manner similar to that employed for the previously described model. Although an implementation of this model was incorporated into SUPRPUMP (Bohling and McElwee, 1992) during the

first year of this research, the model has not yet been used to analyze field data from GEMS. Analysis of field data with the non-Darcian flow variant of the Hvorslev model will be performed early in the second year of this research.

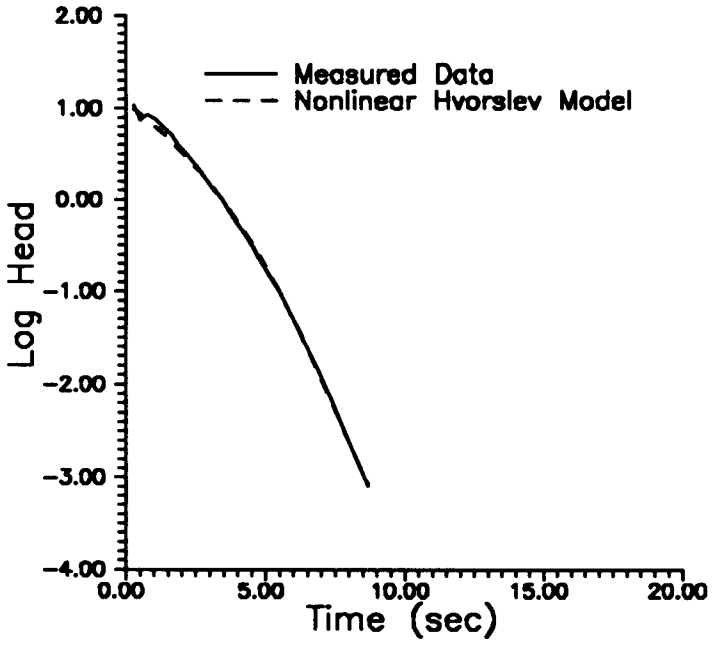

Figure III.C.1 - Natural logarithm of head versus time plots of slug-test data from GEMS well 0-2 (H_0=.88 m) and the best-fit nonlinear Hvorslev model

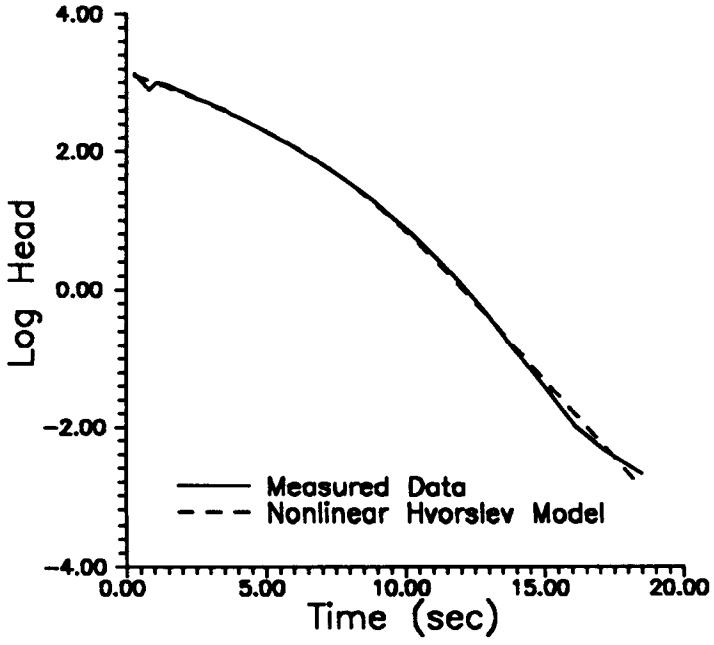

Figure III.C.2 - Natural logarithm of head versus time plots of slug-test data from GEMS well 0-2 (H_0=7.05 m) and the best-fit nonlinear Hvorslev model

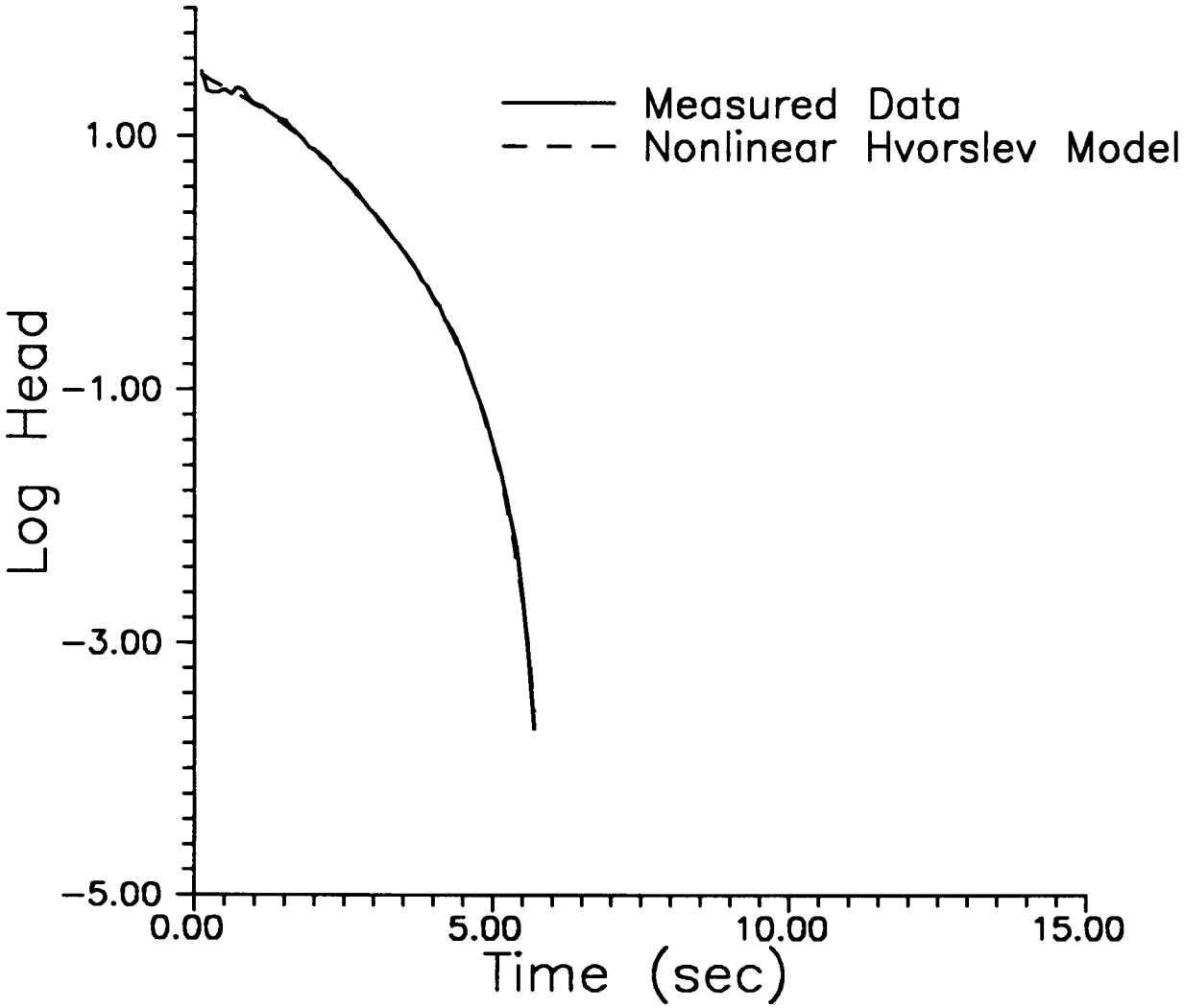

Figure III.C.3 - Natural logarithm of head versus time plots of slug-test data from a fully penetrating slug test at GEMS well 2-5 (H_0=.79 m) and the best fit nonlinear Hvorslev model.

IV. SITE CHARACTERIZATION ACTIVITIES

A. DRILLING AND SAMPLING ACTIVITIES

Introduction

Prior to 1991, twenty five wells had been installed at GEMS. Samples from the sand and gravel interval (10.7-21.3 meters below land surface) were taken at six of these wells using various techniques (McElwee et al., 1991). A modified Waterloo sampler (Zapico, 1987; Zapico et al., 1987) was employed with good success when drilling mud was used in the auger flights to control heaving sands and to help prevent the sediment from falling out the bottom of the sampler. The use of drilling muds, however, has disadvantages (potential to contaminate the formation and the cores) and recovery without sample loss is difficult since the recovery procedure is very sensitive to vibration and other mechanical forces. Without the use of drilling muds, the modified Waterloo sampler performed unsatisfactorily due to a large percentage of the sediment falling out the bottom of the sampler. In order to address this limitation, new sampler designs were developed and field tested. The most promising design did not require drilling mud, achieved a very high recovery percentage, and was not very sensitive to vibration and other mechanical forces during recovery. In addition to the piston used in the Waterloo sampler, the new design incorporates an inflatable bladder, located in the drive shoe, which closes off the end of the sampler (McElwee et al., 1991). In the initial phase of the sampling, the rubber bladder lies deflated behind a plastic sample liner as the core enters the sampler. Near the end of the 1.52 meter sample drive, an extension at the upper end of the piston triggers a release mechanism and allows a .102 meter retraction of the plastic liner, resulting in the bladder being in direct contact with the sediment. The bladder is then inflated from the surface with nitrogen gas, closing off the bottom of the sampler and allowing recovery with minimal opportunity for sediment to fall out. We consistently have been able to achieve about 85% recovery out of a possible 90% (drive shoe loss is .152 m out of 1.52 m due to bladder length and placement) with this bladder sampler. The remaining 5% loss is due to compaction, premature piston movement, or wall friction preventing movement of material into the sampler. After recovery, the cores are taken to the laboratory for storage until measurement of hydraulic conductivity, porosity, density, and particle-size fraction, which is described in subsection IV.B, can be done.

Drilling and Sampling Procedures

All except one of the monitoring wells at GEMS have been installed with hollow-stem auger techniques (Hackett, 1987). Auger flights with an inside diameter of .083 meters and an outside diameter of .168 meters were used in all cases. As noted earlier, the near-surface stratigraphy at GEMS consists of approximately 10.6 meters of clay and silt overlying approximately 10.6 meters of sand and gravel. If samples from the clay and silt interval are desired, a split-spoon sampler with an overshoot mechanism for attachment inside the auger flights is used. The split-spoon samplers are .61 meters in length and must be retrieved after every .61 meters of drilling. Retrieval is done using a wire line on the drill rig.

Although we have taken continuous samples through the clay and silt interval at four well locations scattered over the site, our primary interest at GEMS is in the sand and gravel interval. One of the biggest problems faced in obtaining samples from the sand and gravel interval is heaving sands or sandblows (Minning, 1982; Perry and Hart, 1985; Keely and Boateng, 1987; and Hackett, 1987). It is absolutely essential to maintain greater hydrostatic pressure inside the auger flights than in the formation when working in heaving sands. The water level inside the auger flights is maintained higher than the ambient water level by adding water at critical times (i.e. any time when tools are moved within the open flights or the open flights themselves are moved). If a greater hydrostatic head is not maintained within the auger flights at these critical times, up to one or more meters of sediment may quickly enter the flights, making it impossible to obtain an undisturbed sample at that depth. Adding water to maintain a higher head in the flights may affect the chemistry and biota of an aquifer, so one must balance this concern with the need to control heaving sands. At GEMS, we simply pump water from a nearby well in the sand and gravel interval into the flights. There is no known contamination at GEMS, so we are adding water of a similar composition to the flights. This procedure seems appropriate for our purposes.

Samples are obtained from the sand and gravel interval using the sampler described earlier (McElwee et al., 1991). If samples are not taken in the overlying clay and silt interval, we first drill down to approximately 10.7 meters. The pilot bit is withdrawn via a wireline and the sampler emplaced at the bottom of the flights. The sampler is then driven 1.52 meters in advance of the flights. The sampler is retrieved using drill rods or a wireline, after which the pilot bit is reinserted and the augers advanced to the depth for the next sample. Figure IV.A.1 summarizes the steps involved in obtaining a sample. Note that due to the close fit of the pilot bit

and the sampler in the interior of the flights, there is great potential to induce heaving sands during removal of the pilot bit and retrieval of the sampler. Special care must be taken to add water to the flights during these procedures.

If no samples are to be obtained during drilling, a knock-out plate is installed in the auger head in place of a pilot bit (Perry and Hart, 1985; Hackett, 1987). The plate is left in place until the completion depth is achieved. At that point, the plate is knocked out of the bottom of the flights using the casing string. The plate is then left in the formation below the well. Stainless steel, PVC, and aluminum knock-out plates have been used at GEMS. Note that water must be added to the flights when the plate is knocked out in order to prevent movement of sediment into the interior of the flights and possible binding of the casing string in the flights.

Drilling and Sampling - Year One

During the first year of this project, ten additional wells were drilled and completed. Four of these wells were cored from the surface to the bedrock using the techniques outlined above. The split-spoon sampler was used for approximately the first 10.7 meters and then the bladder sampler was used until bedrock was reached at approximately 21.3 meters below land surface.

These ten additional wells bring the total number of wells at GEMS to thirty five. Table IV.A.1 is a summary of pertinent information about the GEMS wells. The elevation data given in Table IV.A.1 were obtained through a cooperative surveying exercise with the 1st Battalion of the 127th Field Artillery of the Kansas National Guard performed in March of 1992. Note that a reference point was established at a central location on the site during this exercise. This reference point will be used in all future surveys at the site. The elevation as well as the longitude and latitude of the reference point are given in Table IV.A.1. The samples of silt and clay from the first 10.7 meters were examined visually and detailed written logs of the visible features were prepared. Although no additional work was done with these samples, in future years we plan to measure the hydraulic conductivity of cores from this interval while they are still saturated. We have just recently purchased a permeameter for use with low-conductivity samples (S-480 Permeability Cell and Pressure Control Panel, Brainard-Kilman Co.) and are preparing to use it in the next year of this project.

The bladder sampler was used to collect samples of the sand and gravel interval beginning at approximately 10.7 meters below land surface. Table IV.A.2 summarizes the sample recovery for all holes drilled in the reporting period (00-1,

1-7, 8-1, and 10-1). Other data about these wells can be found in Table IV.A.1. The overall recovery was approximately 75%, which was about 10% lower than expected. As described earlier, 85% has been an average recovery for previously sampled wells at GEMS. The lower than expected recovery obtained at these wells was due to a number of factors. In several instances, we had problems with large rock fragments blocking the sampler throat. In one extreme case, a .05 meter pebble (the sampler has an inner diameter of only .038 meters), blocking the entrance of the sampler, was recovered with the sampler. Another factor affecting recovery was the testing of different sampler driving mechanisms. At two holes, the sampler was driven in advance of the auger flights with a hydraulic hammer on the drill rig (00-1 and 1-7), while in one hole the sampler was driven with an electric jackhammer (8-1), and in the other the sampler was driven with an air jackhammer (10-1). The hole at which the air jackhammer was employed (10-1) had the highest recovery. Based on this series of tests and earlier experience (previously we had driven the sampler using either an air jackhammer or a hammer operated with the rig cathead), we feel that the air jackhammer is the most suitable tool for driving the sampler. Therefore, we intend to use a recently purchased air jackhammer in all future sampling. We believe that the better recovery and ease of driving found with the air jackhammer is due to the increased weight, power, and blow frequency of the tool. Note that in June of 1991, shortly before the start of the research described in this report, the co-PI of this research, Carl McElwee, travelled to Otis Air Force Base on Cape Cod, Mass. where he demonstrated the use of the bladder sampler to USGS researchers. Kathryn Hess of the Marlborough, Mass. office of the USGS can be contacted for further details of that demonstration.

Table IV.A.1

Well Data

Well Number	Elevation (m)	Depth (m)	Screen Length (m)
00-1	252.724	17.04	0.76
00-2	252.780	14.41	0.76
00-3	252.670	21.37	NA
00-4	252.667	11.18	NA
00-5	252.021	9.74	NA
00-6	252.746	12.91	NA
00-7	252.734	20.34	NA
0-1	252.796	21.74	9.14
0-2	252.756	14.08	0.70
0-3	252.787	11.00	0.74
0-4	252.707	7.94	0.76
0-5	252.793	19.84	0.70
*0-6	252.945	24.66	1.52
0-7	252.743	16.57	0.70
1-1	252.799	14.26	0.76
1-2	252.714	11.22	0.61
1-3	252.814	8.55	0.65
1-4	252.796	6.15	1.45
1-5	252.791	20.33	9.14
1-6	252.899	17.06	0.73
1-7	252.735	21.42	9.14

2-1	252.791	11.92	0.57
2-2	252.785	14.72	0.56
2-3	252.784	8.53	0.63
2-4	252.779	6.04	1.41
2-5	252.791	21.42	9.14
2-6	252.735	20.24	9.14
2-7	252.728	17.17	0.79
4-1	252.724	21.58	9.14
5-1	252.949	21.54	9.14
6-1	252.753	20.34	0.77
6-2	252.754	21.55	11.55
8-1	252.703	17.44	NA
9-1	252.639	20.93	13.26
10-1	252.566	17.32	NA
A1	252.511	9.91	0.76
A2	252.931	7.86	0.61
+PW	NA	21.84	6.10

KGS Reference Mark: Latitude-North 39°00' 55.628"
Longitude-West 95°12' 21.272" Elevation 252.242 m

* Well diameter is .127 m; all other wells except PW are .051 m diameter.
+ High capacity pumping well, screen and casing is .254 m in diameter, drop pipe is .102 m in diameter.
NA - information not currently available.

Table IV.A.2

Sample Recovery Analysis

Well Number	Segment Number	Segment Length (m)	Head Space (m)	% of Segment Length
Procedure: Hydraulic Hammer				
00-1	19	1.524	0.062	4.06
00-1	20	1.524	0.087	5.73
00-1	21	1.524	0.108	7.08
00-1	22	1.423	0.876	61.56
00-1	23	1.524	0.403	26.46
00-1	24	1.524	0.064	4.14
00-1	25	1.219	0.206	16.93
00-1 Totals		10.262	1.807	17.60
		Theoretical Recovery		82.40
		Bladder Loss		10.00
		Actual Recovery		72.40
Procedure: Hydraulic Hammer				
1-7	20	1.486	0.098	6.62
1-7	21	1.473	0.118	7.97
1-7	22	1.524	0.098	6.46
1-7	23	1.524	0.102	6.67
1-7	24	1.524	0.121	7.92
1-7	25	1.524	1.321	86.67
1-7	26	1.524	0.152	10.00
1-7	27	1.524	0.410	26.88
1-7 Totals		12.102	2.419	19.99
		Theoretical Recovery		80.01
		Bladder Loss		10.00
		Actual Recovery		70.01
Procedure: Electric Jackhammer				

8-1	20	1.311	0.140	10.66
8-1	21	1.524	0.184	12.08
8-1	22	1.539	0.162	10.52
8-1	23	1.524	0.111	7.29
8-1	24	1.539	0.248	16.09
8-1	25	1.524	0.159	10.04
8-1	26	1.524	0.298	19.58
8-1 Totals		10.485	1.300	12.40
		Theoretical Recovery		87.60
		Bladder Loss		10.00
		Actual Recovery		77.60
Procedure: Air Jackhammer				
10-1	19	1.524	0.064	4.17
10-1	20	1.539	0.051	3.33
10-1	21	Numbering Omission		
10-1	22	1.554	0.073	4.79
10-1	23	1.524	0.140	9.17
10-1	24	1.509	0.070	4.53
10-1	25	1.509	0.140	9.23
10-1	26	1.509	0.241	15.94
10-1 Totals		10.668	0.778	7.29
		Theoretical Recovery		92.71
		Bladder Loss		10.00
		Actual Recovery		82.71
Well Totals		43.517	6.304	14.48
		Theoretical Recovery		85.52
		*Bladder Loss		10.00
		Actual Recovery		75.52
* 10% of the total length, 4.352 m, is lost due to the bladder mounting dimensions.				

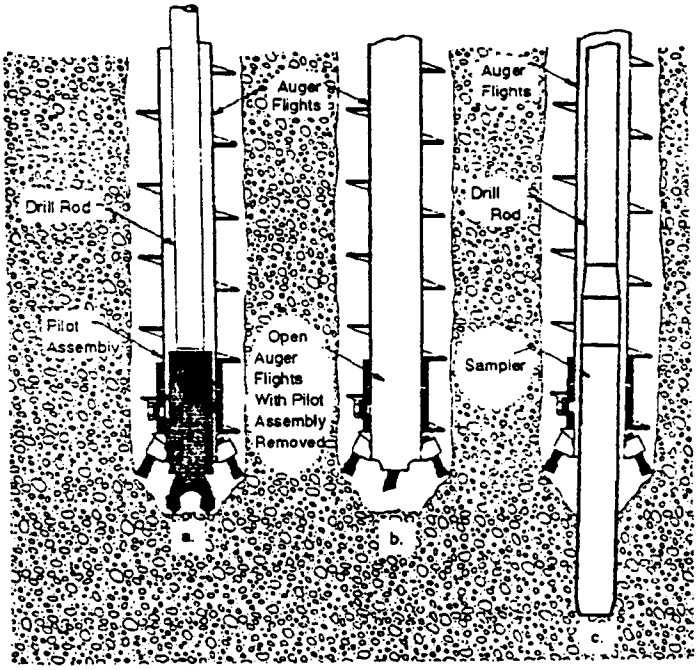

Figure IV.A.1. Sequential steps showing borehole advancement with pilot assembly and collection of a formation sample (after Riggs 1983).

B. LABORATORY ACTIVITIES

Laboratory Procedures and Methods

The cores recovered from the drilling and sampling summarized in the previous subsection of this report were taken to the laboratory for measurement of hydraulic conductivity in a constant-head permeameter. Prior to measurement, cores are stored under refrigeration to keep bacterial growth and evaporation to a minimum. With the exception of the changes noted below, the procedures and methods used in analyzing the core samples are essentially the same as those described in Butler et al. (1991) and Jiang (1991).

A new apparatus was developed to more accurately and efficiently calibrate the pressure transducers used in the permeameter. The calibration apparatus consists of metal pipe into which pressure transducers can be inserted with an air-tight seal, a rubber bladder to increase the volume of gas within the system, and a high-accuracy pressure transducer (Druck PTX 620 pressure transmitter) to serve as a pressure standard. Nitrogen gas can be introduced into or released from the system in small amounts, simultaneously changing the pressure on both the pressure transducers and the pressure standard, while readings are recorded by a datalogger. The pressure transducers are then calibrated against the pressure standard. This new system can be used to calibrate both the pressure transducers used in the permeameter (0-5 psig) and the pressure transducers used in the field for hydraulic testing (0-15 and 0-25 psig). Up to four pressure transducers can be calibrated at one time.

The constant-head permeameter used in this work was originally designed to process four cores at one time. The permeameter has now been expanded to increase the number of cores that can be processed at one time to eight.

A temperature transmitter (Dwyer Series 650-2) has been installed next to the mercury thermometer in the permeameter. Water temperature is recorded by the datalogger at the same interval as water pressure in the outflow tubes of the permeameter. This enables a more accurate representation of the temporal variation in viscosity to be incorporated into the hydraulic conductivity calculations.

In order to more accurately determine the head drop over the cores, an instrument incorporating a dial caliper has been constructed and mounted on the permeameter. Water levels in glass-topped manometer tubes, which measure head at the top of each core and at the constant head boundary, can be read to the nearest .025 mm (readings are generally reproducible to better than .13 mm). This device allows us to use smaller head drops over the cores without increasing the

percent error in our calculations.

Occasionally, a decrease in head at the constant head boundary is experienced due to lack of flow from the upper reservoir. To reduce the frequency of this occurrence, a new reservoir was installed that drains from the bottom rather than relying on a siphon tube exiting from the reservoir top.

X-rays are taken of each core sample to aid in the determination of changes in grain size and the identification of sedimentary structures. An aluminum filter is used to improve resolution at the edges of the core (Baker and Friedman, 1969). Using the X-rays as a guide, the core is cut into segments that are as homogeneous as possible within the .1-.2 meter limit on segment size imposed by the permeameter setup. To inhibit organic growth, the core segments are wrapped in plastic and aluminum foil and refrigerated until they are placed in the permeameter.

The amount of Thymol added to the water used in the permeameter has been increased to .1 g/l to further inhibit the growth of organic matter.

In order to keep the Reynolds number below one and reduce the possibility of non-Darcian flow, the head drop over the cores is kept as small as possible. This also decreases the entrainment of fine material as water moves through the core. Typically, the head drop is initially set at approximately .013 meters and increased only if no flow occurs after 12 to 24 hours. With this small head drop, it takes a minimum of 36 hours to process a core segment, with some segments requiring four to five days.

During the drying process, which precedes particle density analysis and dry sieving, clay-sized particles tend to coat larger grains and form sand-sized aggregates. This will cause the weight percentages of the larger grain sizes to be overestimated at the expense of the fines. To more accurately determine the weight percent of fine material in the core, the samples are wet-sieved with a 53 micron sieve after the particle density analysis. The weight percent of fine material is determined by comparing the dry weight of the sample before and after wet sieving. The coarse fraction is then dry-sieved to complete the grain size analysis. Even though some material is lost during the permeameter tests and the repacking process, this method of determining the amount of fine material should still be reasonably accurate, since most of the material that is lost is clay and silt sized.

No photographs are taken of the sediment before sieving.

Results and Discussion

Hydraulic conductivity values have been obtained for 49 of 50 segments from

GEMS well 00-1, both in the undisturbed state (Figure IV.B.1) and after being dried and repacked (Figure IV.B.2). A comparison of the original and repacked hydraulic conductivity values is presented in Figure IV.B.3. The segment from depth 14.27-14.41 m below datum is composed of material that appears to be wood, so no permeameter tests were run on that segment. Note that the datum on all plots is the elevation of the KGS reference mark (252.242 m) described in the previous section.

The undisturbed cores have an arithmetic mean conductivity of 20.16 m/day, with a sample standard deviation of 24.26 m/day. Values range from a minimum of .06 m/day to a maximum of 94.28 m/day. There is no apparent trend in hydraulic conductivity with depth.

The repacked cores exhibit a higher mean conductivity and greater variability than the undisturbed cores. Values range from .04 m/day to 185.43 m/day with a mean of 44.82 m/day and standard deviation of 44.65 m/day.

For 44 of the 49 segments, the repacked hydraulic conductivity is greater than the original measurement. This is most likely due to the elimination during the repacking process of thin layers of fine material that may be exerting a strong influence on the hydraulic conductivity calculations. The redistribution of this fine material during the repacking process results in the repacked cores generally being more homogeneous than the undisturbed cores. In some cases, it is possible that the repacked cores could be less homogeneous than the undisturbed cores. Layers can be created within the core if a poorly sorted sediment is not sufficiently mixed while being repacked into the sample tube. For example, a one centimeter layer of fine material was noted at the top of the repacked sample 001-24-7 (depth 20.37- 20.56 m). For future repacks, we plan to use a sediment sample splitter to produce numerous small, homogeneous amounts of material to introduce into the sample tube to help eliminate this problem.

Porosity values were calculated for both the original and repacked cores from the particle density, bulk density and core volume measurements (Figures IV.B.4 and IV.B.5). The original cores have porosities ranging from 23.2% to 37.4% with an arithmetic mean of 28.4% and standard deviation of 3.1%. The porosity of the repacked cores ranges from 23.8% to 35.8% with an arithmetic mean of 28.8% and standard deviation of 2.7%.

The difference between the original and repacked porosities ranged from 0.03% to 3.22% with an arithmetic mean of 1.23%. For 35 of the 49 cores, the repacked porosity is greater than the original porosity; 14 of the repacked cores have lower porosities than the original cores. The primary reasons for differences between

the original and repacked porosities are 1) inability to repack the cores to exactly the same volume as the original cores, and 2) loss of sediment during the repacking process.

The mean phi size was calculated for each core using the method of moments (Figure IV.B.6). The phi sizes range from -1.02 to 2.55 with an arithmetic mean of -0.02 and standard deviation of .65. The profile shows a general fining upward sequence. The percent fines (<53 microns) was also calculated for each core (Figure IV.B.7). The percent fines exhibits a range from .2% to 40.6% with an arithmetic mean of 2.9% and standard deviation of 6.1%. There is no apparent trend in percent fines with depth.

Decreases in Hydraulic Conductivity with Time

We have found that for many cores hydraulic conductivity increases (as the core completely saturates), reaches a maximum, and then decreases as the test continues. An example of this phenomenon for one core segment is illustrated in Figure IV.B.8. Possible explanations for this decrease in conductivity at large times include biological growth, movement of fines, and mineral deposition. Maintaining the concentration of the biocide Thymol and employing as low a flow rate through the core as practical should reduce the influence of the first two factors. Calcite deposits have been observed on the plastic tubing, thermometer, and temperature transmitter of the permeameter, so a simulation using PHREEQE (Parkhurst et al., 1980) was run to determine the nature and amount of mineral material that might be deposited during the hydraulic conductivity tests.

The water in use in the permeameter is taken from the same site and depth from which the cores are taken to ensure as much as possible that the water will be in chemical equilibrium with the cores during the permeameter experiments. The water does experience some changes, however, before it is used in the permeameter: increased temperature, decreased partial pressure of PCO2, and addition of Thymol. These changes may cause the water to precipitate mineral material in order to regain equilibrium. Chemical analyses of water samples from GEMS are available from the fall of 1990 and the summer of 1991. Two of these samples are from the same depth from which water for the permeameter is collected. Both samples have similar chemical characteristics.

The PHREEQE simulation was performed by first creating a solution matching the temperature, pH and chemical composition of the two well water samples. Alkalinity was input as HCO3-, aqueous nitrogen gas was removed from

the data base, and the pe was set at 9.0. The pe and pH were allowed to be determined by the reaction. The most abundant constituents of the coarse fraction in the cores are quartz and K-feldspar, so the saturation indices of quartz and microcline were adjusted to match the silica and potassium contents of the water samples. This resulted in the solution being slightly oversaturated with respect to quartz and undersaturated with respect to microcline. The solution was then equilibrated with laboratory temperatures (22 degrees C) and surface partial pressure of PCO2 (log PCO2 = -3.5). Thymol was added as a reaction to the computer simulated solution, and the solution was equilibrated with calcite to determine the amount of calcium carbonate that might be deposited.

The changes in alkalinity, pH, and pe that take place in the water according to the PHREEQE simulation are shown in Figure IV.B.9. The changes in the saturation index (log IAP/KT) of calcite are shown in Figure IV.B.10. The simulation shows that when well water is equilibrated with surface temperatures and pressures, calcite should precipitate. Calculations indicate that 38 liters of GEMS well water (approximately the amount used in the permeameter at one time) precipitate 3.56 cm^3 of calcite. What is not presently know is the kinetics of the situation. PHREEQE assumes all reactions reach equilibrium instantaneously. It is unclear how much of the calcite precipitates during the time the water is left to equilibrate with laboratory conditions (two weeks minimum) and how much is deposited in the cores and on the permeameter. Observation of the gradual buildup of a calcite film on permeameter tubing indicates that some deposition is occurring throughout the period during which a single 38-liter supply of water is being used in the permeameter. It is probable that a similar film is being deposited in the cores themselves.

Insight into the impact of the deposition of 3.56 cm^3 of calcite on the core measurements can be obtained by calculating the volume of the pore space of the cores used in the permeameter. Using values representative of the cores at GEMS (core volume = 47.5 cm^3, porosity = 30%), the pore volume of a typical core at GEMS is calculated to be 14.25 cm^3. Assuming that approximately 32 cores are processed per each 38 liters of water employed in the permeameter, the total pore volume of the processed cores is 456 cm^3. If the deposited calcite can be considered to be equally distributed over the 32 cores, the total amount of deposition amounts to 0.8% of the pore volume. Given that a very small amount of deposition in the pore throats can have a considerable impact on the permeability of the core, it appears that calcite deposition could be responsible for the observed decreases with

time. However, further work needs to be done on the kinetics of this reaction before the role of the calcite deposition can be clarified. Note that the observed deposition of calcite in the permeameter tubing is ignored in the above calculations because of the much greater surface area of the cores.

In the second year of this project, chemical analyses will be performed to compare the calcium carbonate content of the water before and after the equilibration period in the lab, and before and after running a permeameter experiment. These analyses will allow us to better determine if deposition of calcite in the cores is contributing to the observed decrease in hydraulic conductivity with time and, if so, how might its impact be lessened.

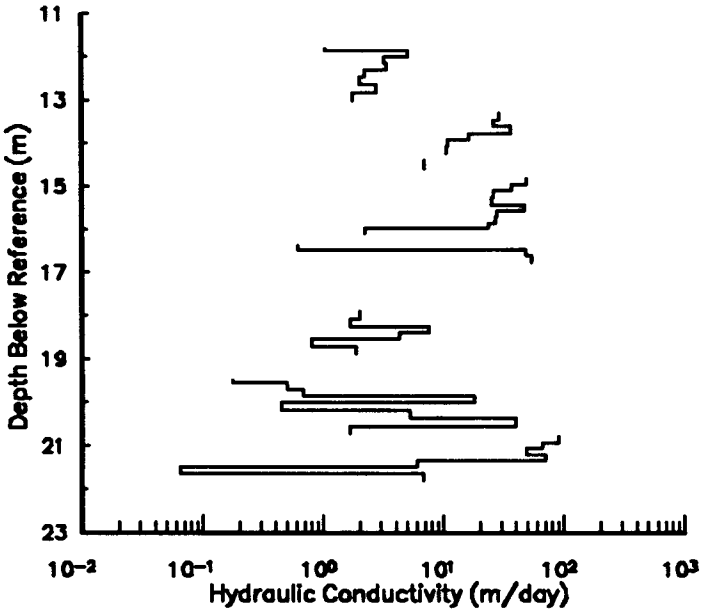

Figure IV.B.1 - Original conductivity versus depth plot for GEMS well 001.

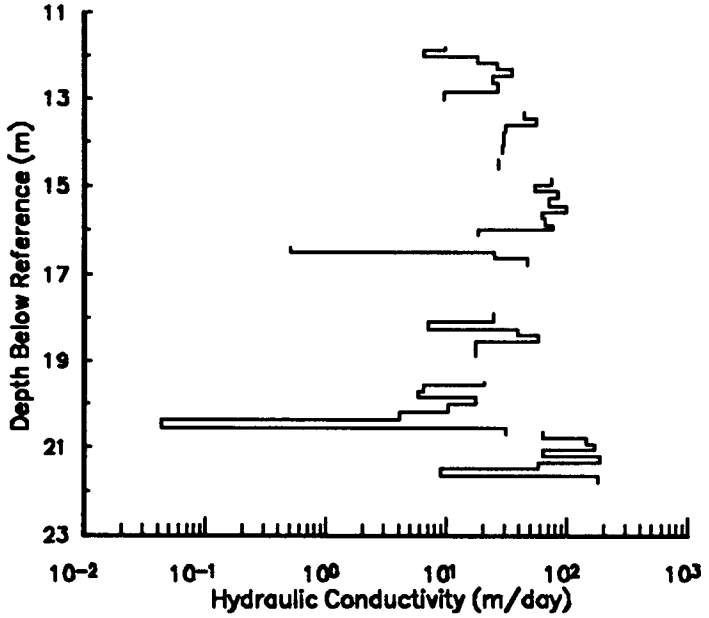

Figure IV.B.2 - Repacked conductivity versus depth plot for GEMS well 001.

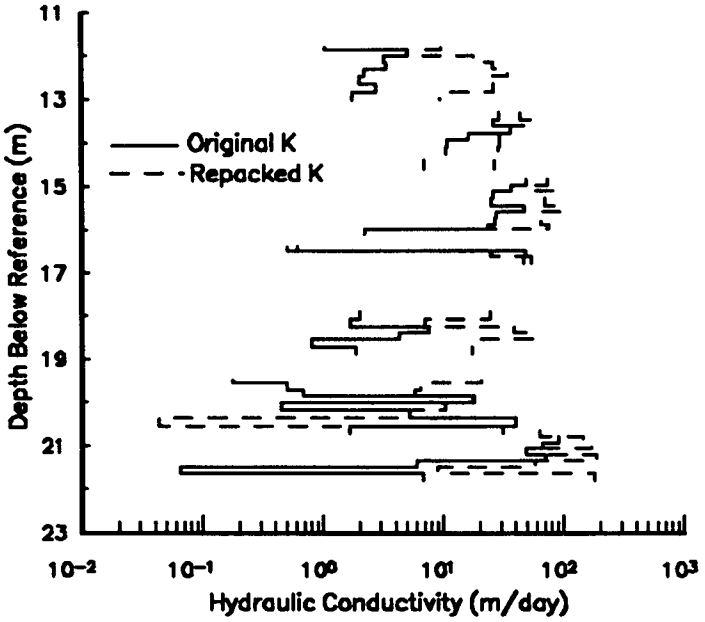

Figure IV.B.3 - Combined original and repacked conductivity versus depth plot for GEMS well 001.

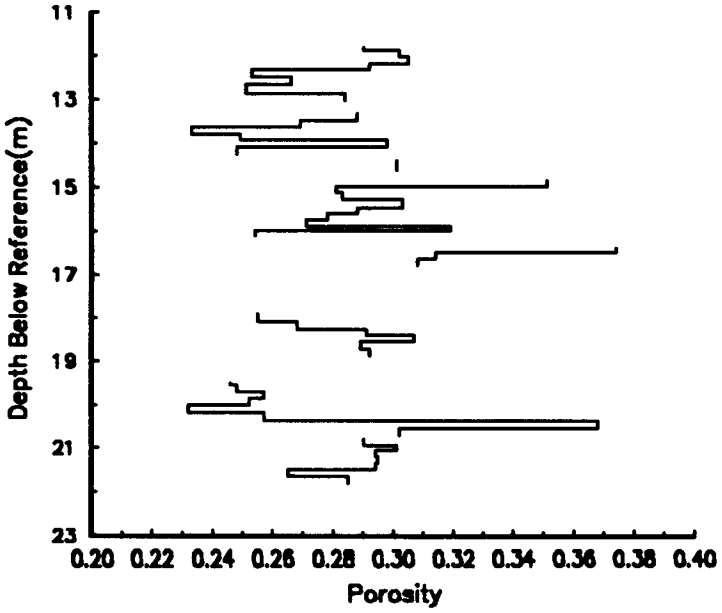

Figure IV.B.4 - Original porosity versus depth plot for GEMS well 001.

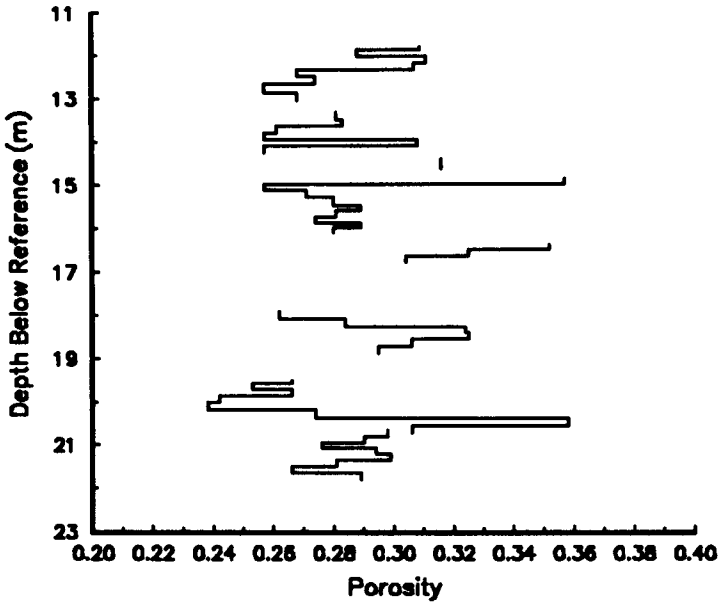

Figure IV.B.5 - Repacked porosity versus depth plot for GEMS well 001.

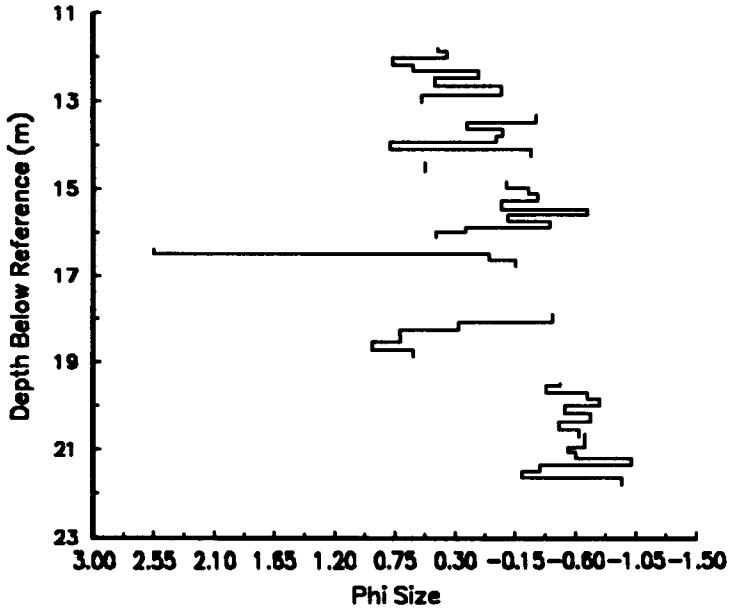

Figure IV.B.6 - Mean grain size (measured in phi units) versus depth plot for GEMS well 001.

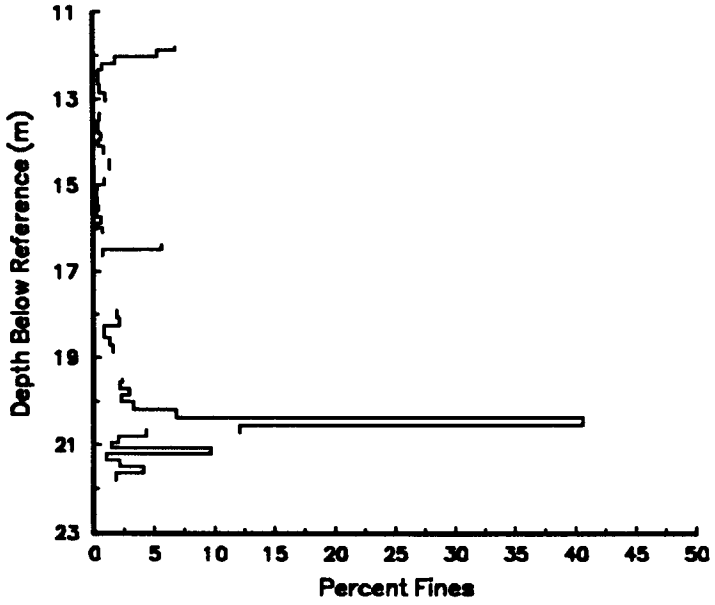

Figure IV.B.7 - Percent fines (<.053 mm) versus depth plot for GEMS well 001.

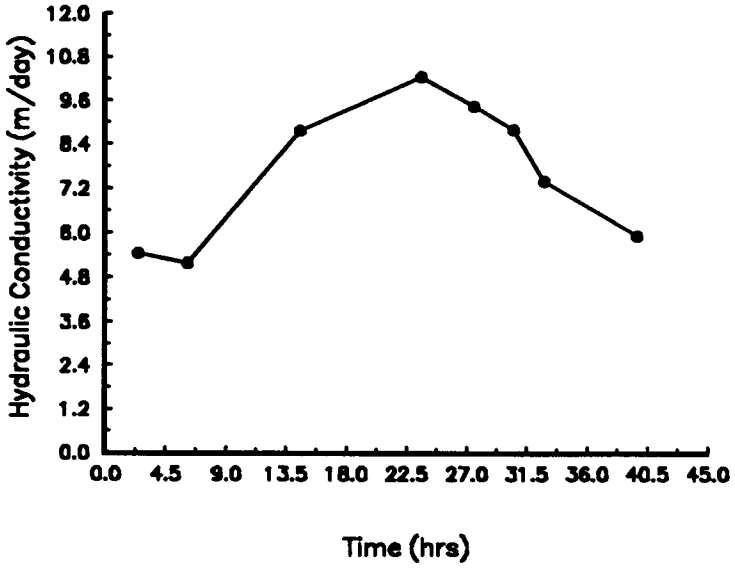

Figure IV.B.8 - Hydraulic conductivity versus time plot for sample 24 of core segment 5 of GEMS well 001.

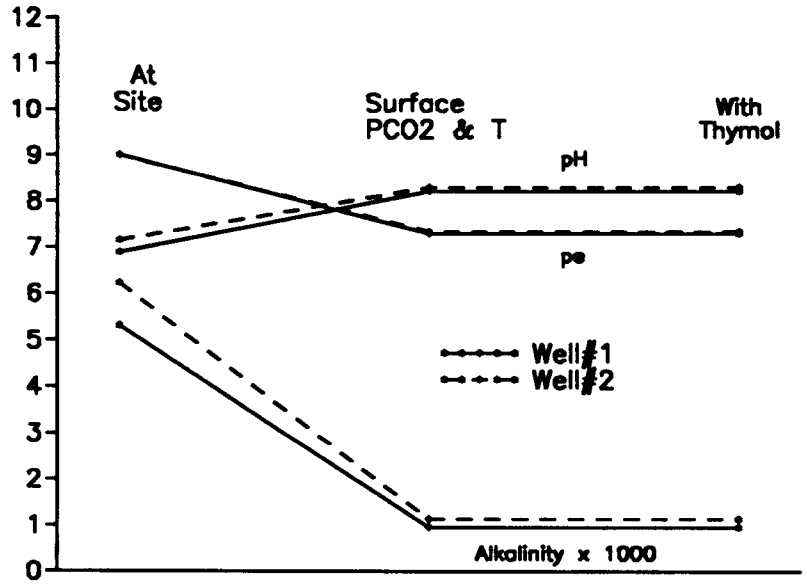

Figure IV.B.9 - Changes in alkalinity, pH, and pe.

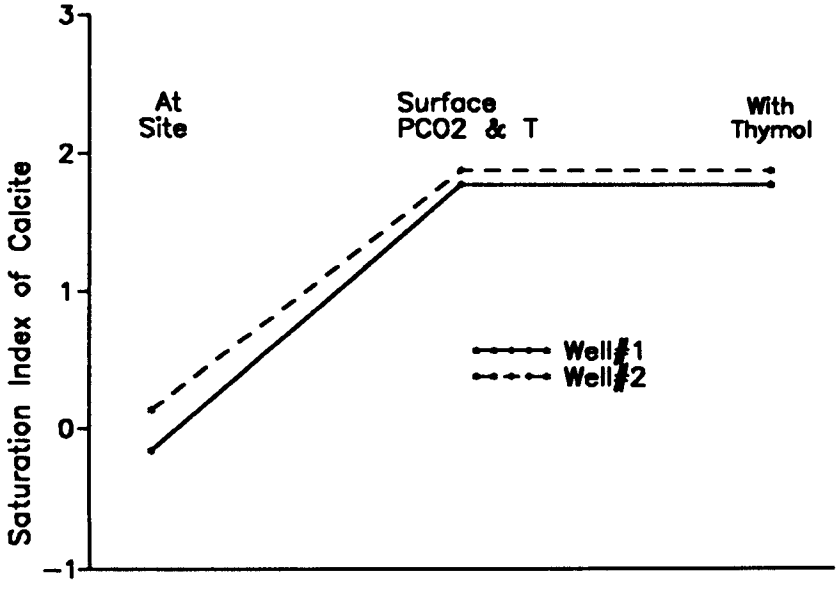

Figure IV.B.10 - Changes in the saturation index (SI) of calcite (SI = log ion activity product/equilibrium constant).

V. SUMMARY OF YEAR ONE RESEARCH AND OUTLOOK FOR YEAR TWO

A. SUMMARY OF RESEARCH IN YEAR ONE

The major focus of the first year of this project was on the use of slug tests to describe spatial variations in hydraulic conductivity. This research on slug tests in heterogeneous formations had both theoretical and field components.

The theoretical work was directed at developing a better understanding of the type of information that can be obtained from slug tests in heterogeneous units. Since traditional modeling techniques are of limited effectiveness for the analysis of slug-test data from wells in heterogeneous formations, a new numerical model, which is continuous in time and employs an approximate representation of flow in the well bore, was developed. This model was then used in a detailed study of slug tests in layered aquifers. The results of this study helped to 1) define the manner in which layer properties are vertically averaged during a slug test, 2) demonstrate that observation wells can potentially provide useful information about vertical variations in formation properties, and 3) delineate conditions under which multilevel slug tests can provide valuable information about vertical variations in hydraulic conductivity within a unit. The best conditions for use of multilevel slug tests were shown to be cases of low frequency vertical variations in hydraulic conductivity using test intervals considerably shorter than the thickness of the average layer. Even in these conditions, however, well skins of both lower and higher permeability than the undamaged formation can dramatically decrease the effectiveness of the approach. Careful well construction and development procedures were stressed as ways of decreasing the impact of such skins. Since observation wells were shown to be of potential use in the analysis of slug tests in layered aquifers, the next component of the theoretical analysis was a detailed examination of slug tests with observation wells. This analysis showed that the use of observation wells in slug tests can significantly improve the reliability of the estimated parameters as a result of a significant decrease in parameter correlation when observation wells are employed. When slug tests are performed in wells surrounded by a finite-radius zone (well skin) of permeability differing from that of the formation, the estimated parameters are a function of both the skin and formation properties. In the final component of the theoretical analysis, the form of these effective parameters is explored. As would be expected, the parameter values are heavily dependent on the properties of the well

skin. The nature of this dependence is a function of the particular technique used to analyze the slug-test data. In general, it will be rather difficult to estimate the conductivity of the formation in the presence of a low-permeability well skin.

The field component of this study of slug tests in heterogeneous formations mainly concentrated on an assessment of multilevel slug tests in highly permeable alluvium. A prototype multilevel slug-test system, built at the KGS, was tested at GEMS. The results of the multilevel tests indicated that slug tests in the sand and gravel section at GEMS are being affected by mechanisms not accounted for in the conventional theory on which the standard methods for slug-test data analysis are based. The existence of these mechanisms were reflected by a concave downward curvature on log head versus arithmetic time plots, a dependence of slug-test responses on the magnitude of the induced slug (H_0), and systematic deviations between plots of the test data and the best-fit conventional models. A series of experiments were carried out at GEMS in order to clarify the mechanisms producing the observed behavior. Although these experiments have not yet been completed, friction within the well screen and non-Darcian flow within the formation are considered the most likely mechanisms producing the observed behavior. Nonlinear terms have been added to the model of Hvorslev (1951) in order to account for these mechanisms. The two nonlinear forms of the Hvorslev model presented here appear to be superior to the conventional approaches for the analysis of slug-test data from the sand and gravel section at GEMS. Further work, however, is still needed to identify all the relevant mechanisms affecting slug-test responses at GEMS and to incorporate these mechanisms into a general model that can be used for the analysis of slug-test data.

In addition to the research on slug tests in heterogeneous formations, a significant amount of the work in the first year of this project was directed at increasing our knowledge of the subsurface at GEMS. This work included continued drilling and sampling activities, further modifications of the bladder sampler developed at the KGS, and continued laboratory analyses of the cores obtained with the bladder sampler. These characterization efforts, which will continue throughout this project, are directed towards the development of a detailed picture of the subsurface at GEMS, so that we can better assess the results of the hydraulic tests that are being performed as part of this research.

B. OUTLOOK FOR RESEARCH IN YEAR TWO

The second year of this project will build upon the progress made in year one. The major task of the early part of year two will be to complete the study of the mechanisms that are producing the anomalous behavior in slug tests at GEMS and to incorporate the relevant mechanisms into a new model for the analysis of slug-test data. Following the completion of the slug-test work, the focus of the research will shift to pulse tests. The primary emphasis of the remainder of year two will be an evaluation of two-dimensional and local three-dimensional pulse tests for providing information concerning the lateral and vertical variations in hydraulic conductivity between wells. A better assessment of this interwell variation should shed light on how these properties might be averaged to form equivalent parameters for mathematical modeling, and thus should lead to more accurate predictions of contaminant movement in the subsurface. As with year one of this project, a significant component of the work in year two will be efforts directed at continued characterization of the subsurface at GEMS. The detailed information collected in this characterization effort will be of vital importance in the third year of this work when high-resolution three-dimensional pulse tests will be performed at GEMS.

VI. REFERENCES

Baker, S.R. and Friedman, G.M., 1969, A non-destructive core analysis technique using x-rays: Jour. Sed. Petrology, v. 39, no. 4, pp. 1371-1383.

Barker, J.A., 1982, Laplace transform solutions for solute transport in fissured aquifers: Adv. Water Resources, v. 5, pp. 98-104.

Bear, J., 1972, Dynamics of Fluids in Porous Media: American Elsevier, New York, 764 pp.

Bohling, G.C. and McElwee, C.D., 1992, SUPRPUMP: An interactive program for well test analysis and design: Ground Water, v. 30, no. 2, pp. 262-268.

Braester, C., and Thunvik, R., 1984, Determination of formation permeability by double-packer tests: J. of Hydrology, v. 72, pp. 375-389.

Butler, J.J., Jr., 1986, Pumping Tests in Nonuniform Aquifers: A Deterministic and Stochastic Analysis (Ph.D. dissertation): Stanford Univ., Stanford, CA. 220 pp.

Butler, J.J., Jr., and Liu, W.Z., 1991, Pumping tests in nonuniform aquifers - the linear strip case: J. of Hydrology, v. 128, pp. 69-99.

Butler, J.J., Jr., and Liu, W.Z., 1993, Pumping tests in nonuniform aquifers: The radially asymmetric case: Water Resour. Res., in press.

Butler, J.J., Jr., and C.D. McElwee, 1990, Variable-rate pumping tests for nonuniform aquifers: Water Resour. Res., v. 26, no. 2, 291-306.

Butler, J.J., Jr., McElwee, C.D., Bohling, G.C., and Healey, J.M., 1990, Hydrogeologic characterization of hazardous waste sites: Kansas Water Resources Research Inst. Contribution No. 283, 114 pp.

Butler, J. J., Jr., McElwee, C. D., Bohling, G. C., and Healey, J. M., 1991, Hydrogeologic characterization of hazardous waste sites: Kansas Water

Resources Research Inst. Contribution No. 289, 129 pp.

Chen, C., 1985, Analytical and approximate solutions to radial dispersion from an injection well to a geological unit with simultaneous diffusion into adjacent strata: Water Resour. Res., v. 22, no. 4, pp. 1069-1076.

Chen, C., 1986, Solutions to radionuclide transport from an injection well into a single fissure in a porous formation: Water Resour. Res., v. 22, no. 4, pp. 508-518.

Chen, H.T., and Chen, C.K., 1988, Hybrid Laplace transform/finite element method for two-dimensional heat conduction: J. Thermophys., v. 2, no. 1, pp. 31-36.

Chirlin, G.R., 1989, A critique of the Hvorslev method for slug test analysis: the fully penetrating well: Ground Water Monitoring Review, v. 9, no. 2, pp. 130-138.

Cooper, H.H., Jr., Bredehoeft, J. D., and Papadopulos, I.S., 1967, Response of a finite-diameter well to an instantaneous charge of water: Water Resour. Res., v. 3, no. 1, pp. 263-269.

Crump, K.S., 1976, Numerical inversion of Laplace transforms using a Fourier series approximation: J. Assoc. Comput. Mach, v. 23, no. 1, pp. 89-96.

Dagan, G., 1978, A note on packer, slug, and recovery tests in unconfined aquifers: Water Resour. Res., v. 14, no. 5, pp. 929-934.

Dagan, G., 1986, Statistical theory of groundwater flow and transport: pore to laboratory, laboratory to formation, and formation to regional scale: Water Resour. Res., v. 22, no. 9, 120S-134S.

De Hoog, F.R., Knight, J.H., and Stokes, A.N., 1982, An improved method for numerical inversion of Laplace transforms: SIAM J. Sci. Stat. Comput., v. 3, no. 3, pp. 357-366.

Desbarats, A.J., 1992, Spatial averaging of transmissivity in heterogeneous fields with flow toward a well: Water Resour. Res., v. 28, no. 3, pp. 757-767.

Dubner, H., and Abate, J., 1968, Numerical inversion of Laplace transforms by relating them to the finite Fourier cosine transform: J. Assoc. Comp. Mach., v. 15, no. 1, pp. 115-123.

Freyberg, D.L., 1986, A natural gradient experiment on solute transport in a sand aquifer, 2, Spatial moments and the advection and dispersion of nonreactive tracers: Water Resour. Res., v. 22, no. 13, 2031-2046.

Gelhar, L.W., 1986, Stochastic subsurface hydrology from theory to applications: Water Resour. Res., v. 22, no. 9, 135S-145S.

Guppy, K.H., Cinco-Ley, H., Ramey, H.J., Jr., and Samaniego, F.V., 1982, Non-Darcy flow in wells with finite-conductivity vertical fractures: Soc. of Pet. Eng. J., v. 22, no. 10, pp. 681-698.

Gurtin, M.E., 1965, Variational principles for initial value problems: Q. App. Math., v. 22, pp. 252-256.

Hackett, G., 1987, Drilling and constructing monitoring wells with hollow-stem augers, Part 1: Drilling considerations: Ground Water Monitoring Review, v. 7, no. 4, pp. 51-62.

Harvey, C.F., 1992, Interpreting Parameter Estimates Obtained From Slug Tests in Heterogeneous Aquifers (M.S. thesis): Stanford Univ., Stanford, Ca, 99 pp.

Hayashi, K., Ito, T., and Abe, H., 1987, A new method for the determination of in situ hydraulic properties by pressure pulse tests and application to the Higashi Hachimantai geothermal field: J. Geophys. Res., v. 92, no. B9, pp. 9168-9174.

Hvorslev, M.J., 1951, Time lag and soil permeability in ground-water observations: Bull. no. 36, Waterways Exp. Sta., Corps of Engrs., U.S. Army, 50 pp.

Javandel, M.S., and Witherspoon, P.A., 1968, Application of the finite element method to transient flow in porous media: Soc. Pet. Eng. J., v. 8, pp. 241-252.

Jiang, X., 1991, A Field and Laboratory Study of Scale Dependence of Hydraulic Conductivity (M.S. thesis), Univ. of Kansas, Lawrence, Ks., 149 pp.

Karasaki, K., 1986, Well Test Analysis in Fractured Media (Ph.D. dissertation): Univ. of Ca., Berkeley, Ca., 239 pp.

Keely, J.F., and Boateng K., 1987, Monitoring well installation, purging and sampling techniques, Part 1: Conceptualizations: Ground Water, v. 25, no. 3, pp. 300-313.

Kipp, K.L., Jr., 1985, Type curve analysis of inertial effects in the response of a well to a slug test: Water Resour. Res., v. 21, no. 9, pp. 1397-1408.

LeBlanc, D.R, 1984, Sewage plume in a sand and gravel aquifer, Cape Cod, Massachusetts: U.S. Geological Survey Water-Supply Paper 2218.

Li, S.G., Ruan, F., and McLaughlin, D., 1992, A space-time accurate method for solving solute transport problems: Water Resour. Res., v. 28, no. 9, pp. 2297-2306.

Liu, W.Z., and Butler, J.J., Jr., 1991, A time-continuous finite difference approach for flow and transport simulations: Kansas Geol. Survey, Open File Report 91-20, 19 pp.

McElwee, C.D., 1982, A one-dimensional study of the groundwater inverse problem using sensitivity analysis: Kansas Geol. Survey, Open File Report 82-12, 68 pp.

McElwee, C.D., 1987, Sensitivity analysis of ground-water models, in: Bear, J., and Corapcioglu, M.Y., ed., Proc. of the 1985 NATO Advanced Study Inst. on Fundamentals of Transport Phenomena in Porous Media: Martinus Nijhoff Publishers, Dordrecht, The Netherlands, pp. 751-817.

McElwee, C.D., Bohling, G.C., and Butler, J.J., Jr., 1989, Sensitivity analysis of slug tests: Kansas Geol. Survey, Open-File Report 89-33, 29 pp.

McElwee, C.D., and Butler, J.J., Jr., 1989, Slug testing in highly permeable aquifers (abstract): GSA 1989 Annual Mtg. Abstract with Program, p. A193.

McElwee, C.D., Butler, J.J., Jr., and Healey, J.M., 1991, A new sampling system for obtaining relatively undisturbed samples of unconsolidated coarse sand and gravel: Ground Water Monitoring Review, v. 11, no. 3, pp. 182-191.

McElwee, C.D., Butler, J.J., Jr., Liu, W.Z., and Bohling, G.C., 1990, Effects of partial penetration, anisotropy, boundaries and well skin on slug tests: Eos, Trans. Amer. Geophys. Union, v. 71, no. 17, p. 505.

Melville, J.G., Molz, F.J., Guven, O., and Widdowson, M.A., 1991, Multilevel slug tests with comparisons to tracer data: Ground Water, v. 29, no. 6, pp. 897-907.

Minning, R.C. , 1982, Monitoring well design and installation: Proceedings of the Second National Symposium on Aquifer Restoration and Ground Water Monitoring, Columbus, Ohio, pp. 194-197.

Moench, A.F., 1984,. Double porosity models for a fissured groundwater reservoir with fracture skin: Water Resour. Res., v. 10, no. 7, pp. 831-846.

Moench, A.F., and Hsieh, P.A., 1985, Analysis of slug test data in a well with finite-thickness skin: in Memoirs of the 17th Intern. Cong. on the Hydrogeology of Rocks of Low Permeability, v. 17, pp. 17-29.

Moench, A.F., and Ogata, A., 1984, Analysis of constant discharge wells by numerical inversion of Laplace transform solutions, in: Rosenshein, J., and Bennett, G.D., ed., Groundwater Hydraulics, AGU Water Resour. Monogr. 9, AGU, Washington, DC., pp. 146-170.

Moltyaner, G.L., and Killey, R.W.D., 1988, Twin Lake tracer tests: Longitudinal

dispersion: Water Resour. Res., v. 24, no. 10, pp. 1613-1627.

Molz, F.J., Guven, O., and Melville, J.G., 1989, Characterization of the hydrogeologic properties of aquifers: The next step: in: Proc. of the Conf. on New Field Techniques for Quantifying the Physical and Chemical Properties of Heterogeneous Aquifers, National Water Well Association, pp. 407-418.

Moridis, G.J., and Reddell, D.L., 1991, The Laplace transform finite difference method for simulation of flow through porous media: Water Resour. Res., v. 27, no. 8, pp. 1873-1884.

Novakowski, K.S., 1989, A composite analytical model for analysis of pumping tests affected by well bore storage and finite thickness skin: Water Resour. Res., v. 25, no. 9, pp. 1937-1946.

Orient, J.P., Nazar, A., and Rice, R.C., 1987, Vacuum and pressure test methods for estimating hydraulic conductivity: Ground Water Monitoring Review, v. 7, no. 1, pp. 49-50.

Papadopulos, I.S., 1966, Nonsteady flow to multiaquifer wells: J. Geophys. Research, v. 71, no. 20, pp. 4791-4797.

Papadopulos, I.S., and Cooper, H.H., Jr., 1967, Drawdown in a well of large diameter: Water Resour. Res., v. 3, no. 1, pp. 241-244.

Parkhurst, D. L., Thorstenson, D. C., and Plummer, L. N., 1980, PHREEQE--A computer program for geochemical calculations: U. S. Geological Survey, Water-Resources Investigations Rept. 80-96, 195 pp.

Parmakian, J., 1963, Waterhammer Analysis: Dover Pub., New York, 161pp.

Perry, C.A. and Hart, R.J., 1985, Installation of observation wells on hazardous waste sites in Kansas using a hollow-stem auger: Ground Water Monitoring Review, v. 5, no. 4, pp. 70-73.

Prijambodo, R., Raghavan, R., and Reynolds, A.C., 1985. Well test analysis for wells producing layered reservoirs with crossflow: Soc. Pet. Eng. J., v. 25, pp. 380-396.

Raghavan, R., 1989, Behavior of wells completed in multiple producing zones: SPE Formation Evaluation, v. 4, no. 2, pp. 219-230.

Rushton, K.R., and Chan, Y.K., 1977, Numerical pumping test analysis in unconfined aquifers: J. Irrigation and Drainage Div., v. 103, no. 1, pp. 1-12.

Russell, D.G., and Prats, M., 1962, Performance of layered reservoirs with crossflow-single-compressible-fluid case: Soc. of Petr. Eng. J., v. 2, no. 12, pp. 53-67.

Settari, A., and Aziz, K., 1974, A computer model for two-phase coning simulation: Society of Petroleum Eng., v. 14, no. 3, pp. 221-236.

Stehfest, H., 1970, Numerical inversion of Laplace transforms: Commun. ACM., v. 13, no. 1, pp. 47-49.

Streltsova, T.D., 1988, Well Testing in Heterogeneous Formations: John Wiley and Sons, Inc., New York, 413 pp.

Sudicky, E.A., 1989, The Laplace transform Galerkin technique: A time-continuous finite element theory and application to mass transport in groundwater: Water Resour. Res., v. 25, no. 8, pp. 1833-1846.

Sudicky, E.A., and McLaren, R.G., 1992, The Laplace transform Galerkin technique for large-scale simulation of mass transport in discretely fractured porous media: Water Resour. Res., v. 28, no. 2, pp. 499-514.

Talbot, A., 1979, The accurate numerical inversion of Laplace transforms: J. Inst. Math. Appl., v. 23, pp. 97-120.

Theis, C.V., 1935, The relation between the lowering of the piezometric surface and the rate and duration of discharge of a well using ground-water

storage: Trans. AGU, 16th Ann. Mtg., pt. 2, 519-524.

Vennard, J.K., and Street, R.L., 1975, Elementary Fluid Mechanics: Wiley and Sons, New York, 740 pp.

Widdowson, M.A., Molz, F.J., and Melville, J.G., 1990, An analysis technique for multilevel and partially penetrating slug test data: Ground Water, v. 28, no. 6, pp. 937-945.

Zapico, M.M., 1987, Aquifer Evaluation Procedures - Core Acquisition and an Assessment of Slug Tests (M.S. thesis): University of Waterloo.

Zapico, M.M., Vales, S. and Cherry, J.A., 1987, A wireline piston core barrel for sampling cohesionless sand and gravel below the water table: Ground Water Monitoring Review, v. 7, no. 3, pp. 74-82.

VII. APPENDIX A - NUMERICAL LAPLACE TRANSFORMS

This appendix begins by briefly discussing three commonly used numerical methods for the back transformation of Laplace-space functions into real space. The Crump (1976) method is the focus of the remainder of the appendix and the algorithm of De Hoog et al. (1982) is introduced as an approach for accelerating the convergence of the summation series employed in the Crump method.

The inversion step, i.e. the back transformation of the Laplace-space function into real space, is probably the most difficult step of a problem involving the Laplace transformation. Many methods for the numerical inversion of Laplace-space solutions have been employed in the groundwater literature. The most commonly used methods are those of Stehfest (1970), Crump (1976), and Talbot (1979). The numerical inversion scheme of Stehfest produces a solution for one specific time. At least 10 or more Laplace solutions (i.e. 10 p_k values) are usually required for the inversion in order to obtain a solution of acceptable accuracy. The maximum number of Laplace solutions (K) that can be used in the Stehfest algorithm is related to the largest number the computer can manipulate. Generally, K should be assigned a value as large as possible for a given machine in order to minimize the error of the inversion. Once the value of K is selected, the accuracy of the inversion is fixed.

The Talbot inversion algorithm also produces a solution for one specific time. In this case, however, there is no limit on the value of K and thus on the accuracy of the inversion. Computations are terminated when a summation series converges to a prespecified criterion by comparing inversion results obtained using two successive p_k values.

The Crump method differs from both of the preceding methods in that a single set of p_k solutions can be employed to perform the inversion for a range of times. The accuracy of the inversion in this case is determined by both the number of terms in the summation and the values of summation-series parameters.

Previous work (e.g., Barker, 1982; Moench and Ogata, 1984; Moench, 1984; Chen, 1985; Kipp, 1985; Chen, 1986) has shown that all three of the above methods can be used in groundwater flow and transport applications with high accuracy. The selection of an inversion method should therefore be based on the specific requirements of the problem being addressed. If solutions are required at only a few

points in time, then the Talbot or Stehfest algorithms are the most appropriate approaches. If, as is often the case in well-test applications, there are a large number of points in time, the method of Crump (1976) is the most efficient approach. Although 3DFDTC enables the user to select either the Stehfest or Crump algorithms, the algorithm of Crump will undoubtedly be the most commonly used approach for well testing applications and thus is the focus of the remainder of this discussion.

Crump (1976) found that a series transformation may be incorporated into equation (II.A.12) to speed up the rate of convergence and, at the same time, reduce the truncation error. This approach, known as the epsilon algorithm, produces, without exception, much faster series convergence than a conventional summation. The number of Laplace-space solutions required in the summation series is reduced from hundreds to tens. The epsilon algorithm involves the approximation of the summation series of (II.A.12) by a sequence of partial sums that are calculated using a recursive equation. De Hoog et al. (1982) present a quotient difference algorithm that dramatically improves on the speed of convergence of the epsilon algorithm. Liu and Butler (1991) provide a detailed description of the De Hoog algorithm, a summary of which is given here.

In the De Hoog algorithm, the summation series inside the brackets of (II.A.12) is rewritten as the real value of the following equation,

$$S_{2N}=\sum_{k=0}^{2N} a_k z^k \qquad \textbf{(1A)}$$

where

$$z = e^{\frac{i\pi t}{Tmax}};$$

$$a_k = \overline{s_j}(p_k)$$

This summation can be approximated by

$$S_{2N} \approx v(z, 2N) = d_0/(1 + d_1 z/(1 + \cdots + d_{2N} z)) \qquad \textbf{(2A)}$$

where $d_j, \cdots, j=1, 2N$ are called the continued fraction coefficients and are defined as $d_0 = a_0$, $d_{2n-1} = -q_n^{(0)}$, $d_{2n} = -e_n^{(0)}$, $n = 1, \cdots\cdots, N$. The initial

$e_r^{(i)}$ and $q_r^{(i)}$ terms are defined as:

$e_0^{(i)}=0$, *for* $i=0, 1, \cdots, 2N$, *and* $q_1^{(i)}=a_{i+1}/a_i$, *for* $i=0, 1, \cdots, 2N-1$.

An array of q and e coefficients can be formed using the following relationships

$$\text{for } r=1,\cdots,2N,\ e_r^{(i)}=q_r^{(i+1)}-q_r^{(i)}+e_{r-1}^{(i+1)},\ i=0,\cdots,2N-2r \quad \text{(3A)}$$

$$\text{and for } r=2,\cdots,N,\ q_r^{(i)}=q_{r-1}^{(i+1)}e_{r-1}^{(i+1)}/e_{r-1}^{(i)},\ i=0,\cdots,2N-2r-1 \quad \text{(4A)}$$

This array can be written out as

$$\begin{array}{ccccc}
 & & q_1^{(0)} & & \\
 & e_0^{(1)} & & e_1^{(0)} & \\
 & & q_1^{(1)} & & q_2^{(0)} \\
e_0^{(2)} & & & e_1^{(1)} & & e_2^{(0)} \\
 & & q_1^{(2)} & & q_2^{(1)} \\
 & e_0^{(3)} & & e_1^{(2)} & \\
 & & q_1^{(3)} & & \\
e_0^{(4)} & & & &
\end{array} \quad \text{(5A)}$$

The following recursive equations can then be used to calculate the terms required in the approximate summation of (2A):

$$\begin{aligned} A_n &= A_{n-1} + d_n z A_{n-2} \\ B_n &= B_{n-1} + d_n z B_{n-2} \end{aligned} \qquad n = 1, 2, \cdots, 2N \quad \text{(6A)}$$

with $A_{-1} = 0$, $B_{-1} = 1$, $A_0 = d_0$ and $B_0 = 1$.

Using these recursive equations, (2A) can now be written as $S_{2n} \approx v(z,2N) = A_{2N}/B_{2N}$. Equation (II.A.12) thus becomes:

$$h_j(t) \approx \frac{1}{Tmax} e^{p_0 t} S_{2N} = \frac{1}{Tmax} e^{p_0 t} RE\left[\frac{A_{2N}}{B_{2N}}\right] \quad \text{(7A)}$$

Liu and Butler (1991) show that use of (7A) instead of the epsilon algorithm approach can reduce the number of terms required in the summation by a factor of two or more. Note that as described by Liu and Butler (1991), careful selection of the Tmax parameter is required in order to realize the maximum computational reductions. Those authors provide recommendations on the selection of Tmax and other summation parameters.

VIII - APPENDIX B - SENSITIVITY ANALYSIS

Introduction

Sensitivity analysis (McElwee, 1987) is a formalism that allows relationships between model responses and model parameters to be examined in considerable detail. In this appendix, a brief summary of the first-order sensitivity approach as applied to the modeling of groundwater flow in response to a stress at a central well is given.

Sensitivity Coefficients

Assuming three parameters of interest, the first-order Taylor expansion for hydraulic head is

$$H^* \approx H^m + U_{P_1}^m \Delta P_1^m + U_{P_2}^m \Delta P_2^m + U_{P_3}^m \Delta P_3^m \qquad \text{(B1)}$$

where

P_i = model parameters such as transmissivity (T), storage (S), initial head (H_0), etc.;

H^* = vector of heads based on the true parameters P_i^* ;

H^m = vector of heads based on current parameter estimates P_i^m ;

$U_{P_i}^m = \dfrac{\partial H^m}{\partial P_i^m}$ = sensitivity coefficient;

ΔP_i^m = unknown perturbation in the parameter estimates;

m = iteration index.

Note that equation (B1) is a linear approximation of a nonlinear process as a result of the neglection of the higher order terms in the expansion.

Normalized Sensitivities

The multiplication of a sensitivity coefficient by the parameter of interest is defined as a normalized sensitivity coefficient (McElwee, 1987) and is denoted by U_{P_i}' . When investigating the head response in a slug test, the normalized sensitivity to relative head (u_{P_i}') is often used. This quantity is defined as

$$u'_{P_i} = P_i \frac{\partial (H/H_0)}{\partial P_i} = P_i \frac{\partial h}{\partial P_i} \qquad \textbf{(B2)}$$

where

h = relative head = H/H_0.

An examination of the spatial and temporal dependence of the normalized sensitivity will often yield considerable insight into the physical processes occurring during a well test.

Parameter Estimation

Sensitivity coefficients can be employed in an unweighted least squares inversing routine to estimate model parameters. McElwee (1982, 1987) describes the technique in considerable detail. The approach is an iterative procedure involving the minimization of an error functional in the form of the sum over all measurement points of the squared differences between the observed and calculated heads:

$$E = \sum_n [HO_n - HC_n]^2 \qquad \textbf{(B3)}$$

where

$HO_n = H^* + \epsilon$ = observed head at index point n;

HC_n = calculated head at index point n;

ϵ = measurement error;

n = spatial and temporal location of measurement.

The righthand side of equation (B1) is substituted for HC_i in equation (B3) and the functional minimized with respect to the parameters. This produces a system of equations with the unknown being a vector of parameter changes:

$$[A]\,\Delta P = R \qquad \textbf{(B4)}$$

where

[A] = the sensitivity summation matrix;

ΔP = vector of parameter changes, $\Delta P^{+} = (\Delta P_1, \Delta P_2, \Delta P_3)$;

R = residual vector.

The new parameter estimates are then found using

$$P_i^{m+1} = P_i^m + \Delta P_i^m \qquad \textbf{(B5)}$$

Since the outlined procedure employs a linear approximation of a nonlinear process, a number of iterations are generally required to obtain convergence to within a predefined criterion.

Sensitivity Summation Matrix

The sensitivity summation or sensitivity design matrix ([A] of equation (B4)) is a summation over time and space of products for any two sensitivity coefficients:

$$a_{ij} = [A]_{ij} = \sum_n U_i(n)\, U_j(n) \qquad \textbf{(B6)}$$

where

i,j = P_1, P_2, P_3.

The diagonal elements of the matrix are simple summations of the squares of the sensitivity coefficients with respect to the same parameter. In general, the solution to equation (B4) is well behaved if the diagonal elements are large and nearly equal and the off-diagonal elements are small. This will be the case when sensitivity coefficients are large and poorly correlated.

Sensitivity Correlation Matrix

The sensitivity summation matrix can be transformed into a "pseudo" sensitivity correlation matrix whose elements are defined as

$$c_{ij} = [C]_{ij} = \frac{a_{ij}}{\sqrt{a_{ii}a_{jj}}} \qquad \textbf{(B7)}$$

where

c_{ij} = a "pseudo" correlation between sensitivity coefficients for parameters P_i and P_j, $|c_{ij}| \leq 1$.

The elements of this matrix quantify the degree of correlation between sensitivity coefficients characterizing different parameters. By definition, the diagonal elements of the matrix will be one. If any of the off-diagonal terms are exactly one, the inverse of [A] in equation (B4) does not exist and the parameter estimation problem cannot be solved. In practice, anytime the off-diagonal elements of the sensitivity correlation matrix get above .9 the [A] matrix becomes ill-conditioned rather rapidly and the parameter estimates become more unreliable.

Parameter Covariance Matrix

Equation (B4) shows that the inverse of the [A] matrix is employed to calculate the vector of parameter changes. The inverse of [A] is also employed to estimate the approximate covariance of the estimated parameters:

$$cov(P) = [B] = [A]^{-1}s^2 \qquad \textbf{(B8)}$$

where

[B] = covariance matrix;

$s^2 = \sum_n [HO_n - HC_n]^2/(N-M)$;

N = total number of measurements;

M = total number of parameters.

The estimated standard error of parameter P_i is given by the $\sqrt{b_{ii}}$ element of the covariance matrix. Note that the form of the parameter covariance matrix is based on some simplifying assumptions about the measurement error. These assumptions include that the measurement error is additive, of a zero mean and constant variance, and uncorrelated with the measurement error at another location.

Equations (B7) and (B8) indicate that correlation between sensitivity coefficients will affect the reliability of parameter estimates. Butler and McElwee (1990) present a demonstration of the design of well testing procedures to reduce the correlation between sensitivity coefficients and therefore increase the reliability of parameter estimates. Section II.C of this report describes a sensitivity analysis of slug tests in which observation wells other than the stressed well are employed to improve the reliability of parameter estimates.